T-3005

A GRAVITY STUDY OF THE GEOLOGIC BOUNDARY SEPARATING THE KLAMATH MOUNTAINS AND CASCADE RANGE PROVINCES IN NORTHERN CALIFORNIA

by

Brett Smith

ProQuest LLC.
789 East Eisenhower Parkway
P.O. Box 1346
Ann Arbor, MI 48106 – 1346

T-3005

A thesis submitted to the Faculty and the Board of Trustees of the Colorado School of Mines in partial fulfillment of the requirements for the degree of Master of Science in Geophysics.

Golden, Colorado

Date 11-30-84

Signed: Brett Smith
Brett Smith

Approved: Doug O'Brien
Doug O'Brien, Thesis Advisor

Golden, Colorado

Date 12-7-84

P R Romig
Phillip Romig, Head
Department of Geophysics

ABSTRACT

During August, 1983, 133 gravity stations were occupied along traverses crossing the contact between the Eastern Klamath Mountains and the Cascade Range. Station elevations were established by elevation surveying or by occupying locations with existing vertical control.

The observed data were reduced to complete Bouguer gravity, using the terrain correction methods of Sandberg, Krohn and Plouff, where estimated errors of 7% were found. Data from this study and previous studies were combined to produce a complete Bouguer anomaly map at a 2-milligal contour interval.

Seismic refraction data (from another study) reveal the upper and lower boundaries of the Western Paleozoic and Triassic plate to be at 10 km and 38 km below sea level, respectively. Via modeling, the gravity effect of this deep body was calculated to determine the regional Bouguer anomaly.

Modeling of residual Bouguer profiles provided the following principal conclusions. The Trinity ophiolite (ranging in thickness from 6 km - 10 km) and the subjacent Central metamorphic plate, comprise an antiformal structure that extends northward beneath early Paleozoic

sediments. An unmapped listric normal(?) fault delineates the boundary between the Klamath Mountains province and the Cascade Range province, and probably extends down to or beyond 10 km below sea level. The Trinity ophiolite, and probably the subjacent Central metamorphic belt, occur beneath the Cenozoic volcanics of the Cascade Range, with subsidence of the latter contributing to the gravity low over Mt. Shasta. A sizeable cylindrically shaped silicic intrusive may also exist ~2 km beneath Mt. Shasta's summit and extend downwards to 10 km below sea level.

TABLE OF CONTENTS

LIST OF FIGURES

Page

Page

LIST OF TABLES

T-3005

ACKNOWLEDGEMENTS

I wish to thank Dr. Thomas R. LaFehr for suggesting this study. His much needed assistance in planning the field surveys is also appreciated. Special thanks is extended to Xiaomu Wang and Nick Josten, who assisted the author in the fieldwork; without whose help this project would have been impossible. Elevations for eleven stations were provided by Mike Harbin and John Zink, surveyors for the cadastral engineering office, United States Forest Service, Mt. Shasta, California.

Drs. Douglas O'Brien and Thomas L.T. Grose are due special thanks for their continued suggestions and advice throughout this study. Appreciation is extended to Colin Wagoner, who improved the program of Barnett such that the modeling of complex bodies was made possible. I very much appreciate the capable work of Peggy Ballard and Marietta Cunningham, who had the challenging task of translating my cryptic script into a well-typed thesis.

I deeply appreciate the strong, unyielding, moral support offered me by my in-laws, Robert (O.H.) and Roberta (B.B.) Tucker. Of course, my deepest thanks and

appreciation goes to my wife, Lucy. Without her support and tolerance of a less than ideal lifestyle, my graduate career would have indeed been short-lived.

Funding for this study was provided by the sponsors of the Center for Potential Field Studies, Department of Geophysics, Colorado School of Mines.

INTRODUCTION

The study area, located in northern California between 122.24° and 122.75° West and between 41.33° and 41.58° North (Figure 1), lies entirely within the 1:250,000 Weed Sheet of the Geological Map of the State of California.

A significant Bouguer gravity gradient exists in Northern California between the Eastern Klamaths and Mt. Shasta. This gradient generally coincides with the geologic boundary separating the Klamath Mountains from the Cascade Range. Previous geologic interpretations of this anomalous feature are based on a low density of gravity stations. The objectives of this project are 1) to better define the gravity gradient, by substantially improving the number and quality of stations, 2) to adequately reduce the data, especially with regard to terrain corrections, and 3) to determine, through forward modeling, a geologic model that best fits the gravity data and the regional geologic framework.

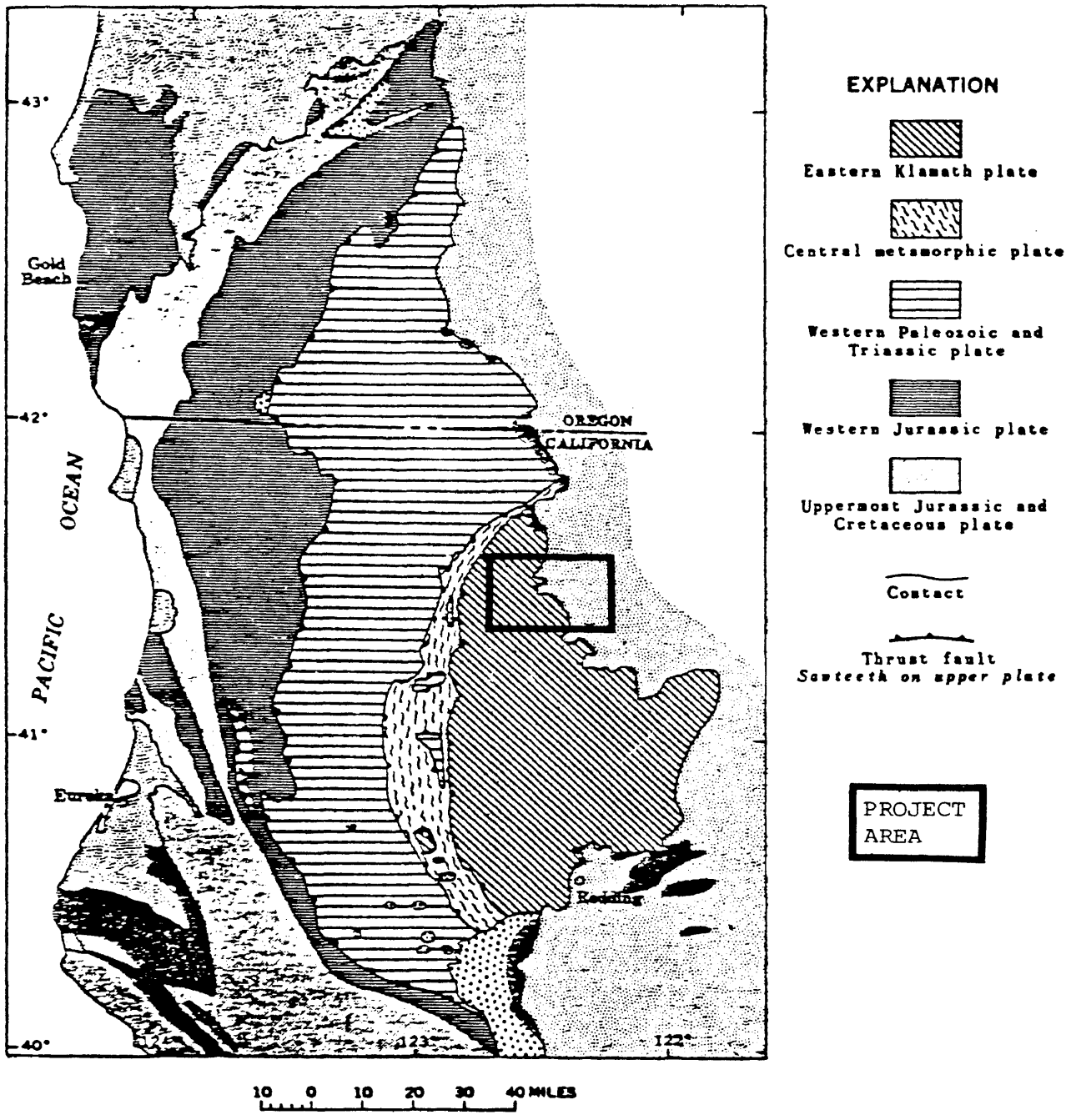

Figure 1. Regional geology (after Irwin, 1966) with project area outlined.

GEOLOGIC BACKGROUND

Klamath Mountains Province

The geology of this area is complex and a subject of continued study among contemporary geologists such as Coney (1981), Davis (1969), Dickinson (1981), Ernst (1979), Irwin (1966), and Potter, and others (1977). They describe the area's geologic history as follows.

During the Antler (Devonian-Missisippian) and Sonoma (Permian-Triassic) orogenies, the continental crust of the North American plate underwent to a minor depth, westward subduction beneath the island arc sequences of the Farallon plate, resulting in eastward overthrusting of the latter onto the craton, as shown in Figure 2a. Reversal of subduction zone polarity (Figure 2b) occurred during the Triassic, so that, in Jurassic time, the Nevadan orogeny involved eastward subduction of oceanic crust beneath continental. Repeated Nevadan underthrusting of successively younger oceanic plate created the configuration of plates shown in Figures 1 and 3. These plates or lithic belts (Irwin, 1966), southern Oregon and northern California, compose the structurally complex Klamath Mountains province, and are described below.

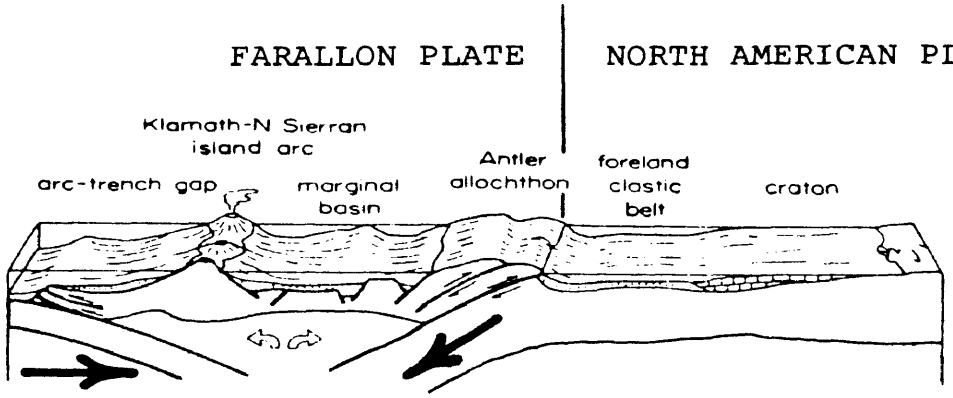

DEVONIAN - TRIASSIC

Figure 2a. Schematic view of Antler-Sonoma orogenies (after Poole and Sandberg, 1977).

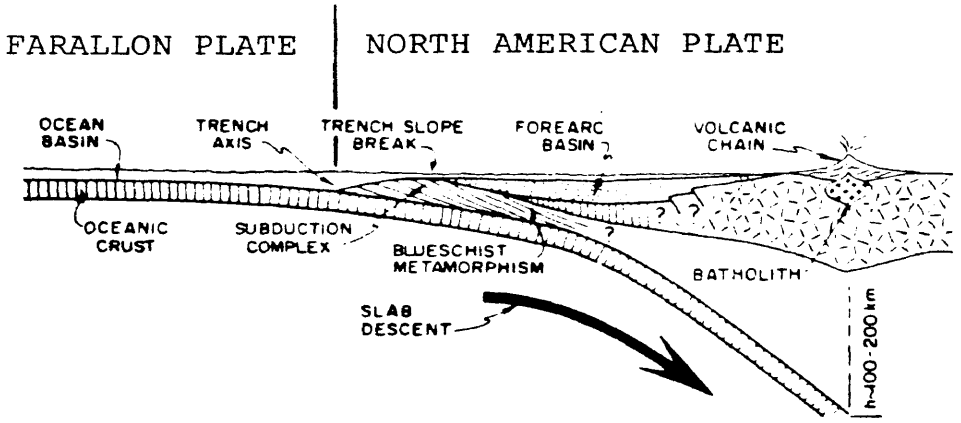

JURASSIC

Figure 2b. Schematic view of Nevadan orogeny (after Dickinson, 1981).

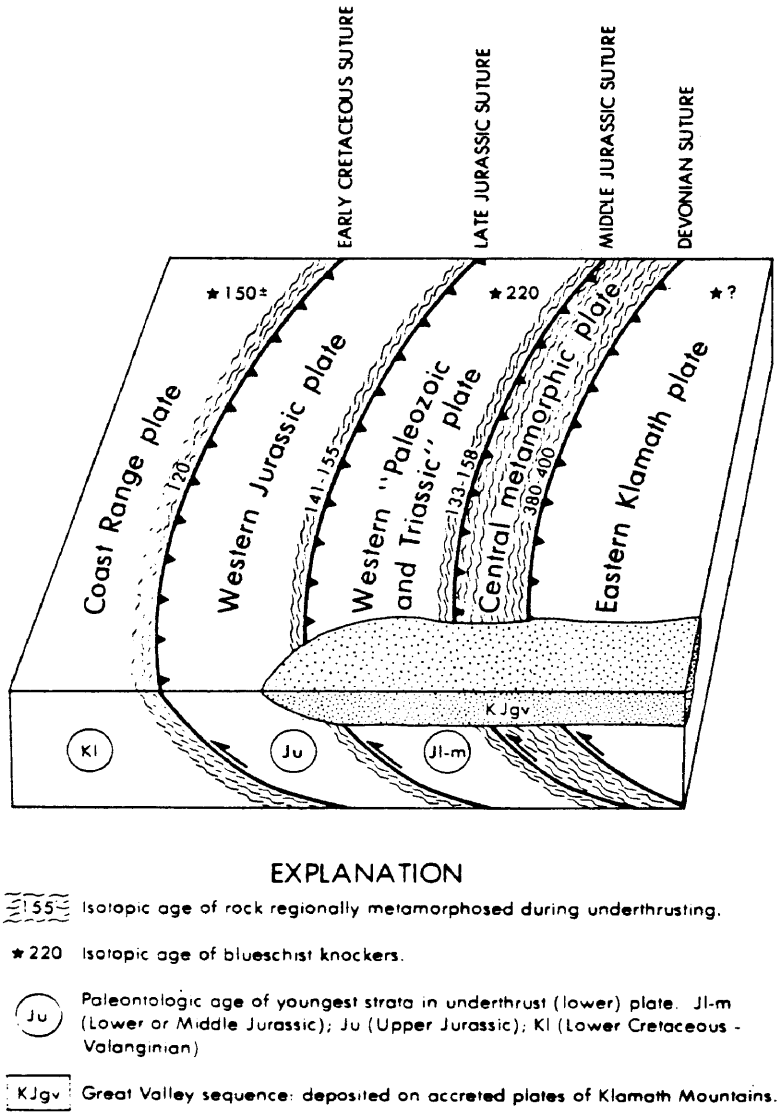

Figure 3. Schematic diagram showing sequential ages of suturing of accretionary plates of the Klamath Mountains and adjacent Coast Ranges (after Irwin, in Ernst, 1981).

The Western Jurassic belt is best represented by the Galice formation, which in the area of interest, is primarily composed of a lower metavolcanic unit and an upper metasedimentary unit. The lower unit is primarily meta-andesite flows and breccias and is probably at least 7,000 feet thick (Irwin, 1966). The metasedimentary unit consists mainly of slaty mudstones and interbedded graywackes and attains thicknesses of up to 3,000 feet (Irwin, 1966). Rocks of the Western Paleozoic and Triassic Belt are characterized as eugeosynclinal, consisting of thin-bedded radiolarian chert, phyllitic detrital rocks, coarse crystalline limestone lenses, and mafic volcanics.

Hornblende and mica schists of problematic age comprise the majority of rocks within the Central metamorphic belt. Average K-Ar isotopic ages of 300 m.y.b.p. for the hornblende and the muscovite indicate a Carboniferous age of metamorphism (Lanphere and Irwin, 1965), whereas Rb-Sr age dating of the schists yielded a much greater Devonian age of 380 m.y.b.p. (Lanphere et al., 1968). Progressive regional metamorphism (upper greenschist and amphibolite facies) followed by retrogressive metamorphism (lower greenschist facies

typifies the metamorphic history. Present day rocks reveal complete recrystallization and elimination of the primary textures (Davis, 1966).

The Eastern Klamath belt consists of an east-dipping homoclinal sequence that terminates against ultramafic rocks to the west. The stratigraphic column represents time from Ordovician to Jurassic, but, in the specific area covered by this report, only Ordovician to Silurian strata are present (Irwin, 1966). These sediments were laid down in a marine environment.

A subject of considerable debate is the origin of the Trinity ultramafic complex (Trinity ophiolite). This sheet-like ultramafic body is structurally above the Central metamorphic belt and is presumed to continue beneath the Cretaceous and younger Great Valley sediments to the southeast (Irwin, 1966). Prior to 1972, the Trinity ophiolite was considered to be a sill-like intrusive resulting from the intersection of a steeply dipping Benioff zone with the upper mantle during Mesozoic time (Davis, 1969). This theory was tenuous however, because gabbroic rocks are <u>older</u> than the Trinity body into which they intrude (Lanphere and others, 1968)! Thinking in favor of an oceanic plate origin for

this ultramafic sheet finally resulted, with the designation of an Ordovician age to best fit the age date values. Having an Ordovician (vs. Mesozoic) sheet structurally atop the Devonian Central metamorphic belt is much more plausible in light of the area's history of underthrusting. (Lanphere and others, 1968).

Cascade Range Province

The formation of this province occurred during Cenozoic time when the subducted Gorda plate reached sufficient depth to become molten and migrate upwards through the crust, resulting in pluton emplacement and the associated formation of stratovolcanoes above.

The Cascade Range is divided into the Western Cascade and High Cascade Ranges (Callaghan, 1933; Peck and others, 1964), which are described below. Early eruptions in the High Cascades were primarily mafic, yielding low viscosity lava flows that created many small shield volcanoes that later coalesced to form a broad, gently sloping ridge. With time, the silica content increased, thus enhancing the conditions for explosive eruptions. Eventually, impressive stratovolcanoes formed atop the pre-existing lava flows. Mount Shasta, the largest (with respect to

relief) of the Cascade volcanoes, is such a structure. To the south and west, the lava flows of Mount Shasta partially rest atop High Cascades andesites, Western Cascades volcanics and partially atop the rocks of the Klamath Mountains province.

Mount Shasta began to erupt about 100,000 years ago (Grose, personal communication) and has retained most of its structure. Recently in its history, a fissure opened on the west flank of the volcano, creating Mount Shastina. Previously, about 300,000 years ago, tremendous quantities of avalanche debris (derived from the presumed ancestor of Mt. Shasta) were spread out onto the valley floor to the northwest, creating impressive mound-like forms (Crandell, and others, 1984).

The Western Cascades volcanics reached thicknesses of up to 15,000 feet near the present day California/Oregon state boundary. These volcanics consist of lava flows and explosion derived fragmental deposits. The flows consist mainly of pyroxene andesite, averaging about 20 feet in thickness, and form a nearly continuous belt along the western foothills of the Cascades for about 45 miles (Williams, 1949).

At the close of the Miocene, the entire Cascade Range was uplifted, perhaps as a result of arching and high angle north-south faulting. Subsequent fissures formed on or near the crest of the range, where new magma rose to the surface. The formation of the High Cascades stratovolcanoes during Pliocene to Recent time was the result of these faults and related crestal fissures (Williams, 1949).

PREVIOUS GEOPHYSICAL WORK

Geophysical studies important to the present study are:

Gravity in the Eastern Klamath Mountains, California (LaFehr, 1966):

-- 65 gravity stations within the study area were occupied, with the following elevation accuracy: 50% at bench marks (± 0.2 Feet), 16% at vertical angle bench marks (± 2 feet), and 34% at controlled map elevations (± 2 feet).

-- terrain corrections were made using templates from the station out to the standard radius of 166.7 km. However, all of LaFehr's terrain corrections were re-calculated by computer (Plouff, 1966) from 2.29 or 28.8 km out to the standard radius of 166.7 km (Kim and Blank, 1973). These recalculated data were used in the present study.

-- LaFehr reduced the data to complete Bouguer values, subsequently removed the regional (LaFehr, 1965) and derived a positive residual anomaly of about 50 mgal over the Eastern Klamath Mountains.

-- modeling of the data enabled LaFehr to interpret the causative source as a large ultramafic sill-like intrusion with a maximum possible depth of 4 km.

A Gravity Investigation of the Weed Sheet, Northwestern California (Kim, 1974).

-- 13 gravity stations within the study area were occupied with the following elevation accuracy: 91% at vertical-angle bench marks (± 2 feet), bench marks (± 0.2 feet), and other controlled map elevations (± 2 feet), 5% determined altimetrically (± 20 ft), 3% photogrammetrically (± 10 ft), and 1% using lake levels (± 5 ft).

-- terrain corrections were made using templates from the station out to 2.29 km and using the computerized method of Plouff (1966) from 2.29 km to 166.7 km.

-- Kim reduced the data to complete Bouguer values and determined (through modeling) the causative source to be less than 3 km thick and of a depth and shape similar to that determined by LaFehr.

Unpublished gravity data, Weed Sheet, Northwestern California (Evernden, 1963)

-- 17 gravity stations within the study area were occupied; no elevation control specifications given.

-- terrain corrections were re-calculated via the same method applied to LaFehr's data.

Principal facts for gravity stations near Medicine Lake and Mt. Shasta California (Finn, C., 1981).

-- 6 gravity stations within the study area were occupied; all elevations determined photogrammetrically with a probable accuracy of ± 10 feet.

-- terrain corrections were made from the station to 166.7 km, using "Bouguer" (unpublished program by R.H. Godson, U.S.G.S., which is a modification of Plouff, 1977).

-- Because 5 stations reside within an area where the gravity gradient is only 0.76 milligals/mile, and because the elevation errors would contribute to gravity errors as great as 0.60 milligals, these data were not used.

Principal facts for seventy-four gravity stations in the northern California Cascade Mountains (Finn and Spydell, 1982).

-- 3 gravity stations within the study area were occupied; 2 were surveyed in with a laser theodolite and presumed accurate to ±0.10 feet, 1 was determined photogrammetrically with a probable accuracy of ±10 feet.

Tectonic setting of the southern Cascade Range as interpreted from its magnetic and gravity fields (Blakely, and others, in press).

-- interpretations of magnetic and gravity data yielded the following conclusions:

1. The Trinity ophiolite has a shallow eastward dip and probably continues in the subsurface as far as 10 km east of Mt. Shasta.
2. Mt. Shasta, Lassen Peak, and Medicine Lake volcanoes occur within a magnetic low which is probably the result of an upwarping of the Curie isotherm.
3. The axis of the High Cascades (upon which Mt. Shasta is situated) is coincident with a residual gravity low, indicating a possible graben structure at depth.

A Geologic Interpretation of Seismic-Refraction Results in Northeastern California (Fuis and others, in press)

-- three seismic refraction lines were shot in 1981, traversing the project area as shown in Figure 4.

-- interpretation of seismic P-wave velocities yielded the following conclusions:

1. The base of the Trinity ophiolite occurs at about 7 km depth.
2. The Trinity ophiolite is layered into zones of serpentinization, shear, pore-pressure change, and/or composition change.
3. The crust beneath the Modoc Plateau (east of the Cascades) is different from that beneath the Klamaths.
4. The Klamath Mountains are underlain by an imbricated stack of oceanic plates.

The work of LaFehr (1966) and Kim (1974) formed the basis for the 1973 Weed sheet (Kim and Blank, 1973), but the density of their stations within the study area is quite low, as shown in Figure 5. In some places, more than 20 mgals of the gradient is defined by only two stations.

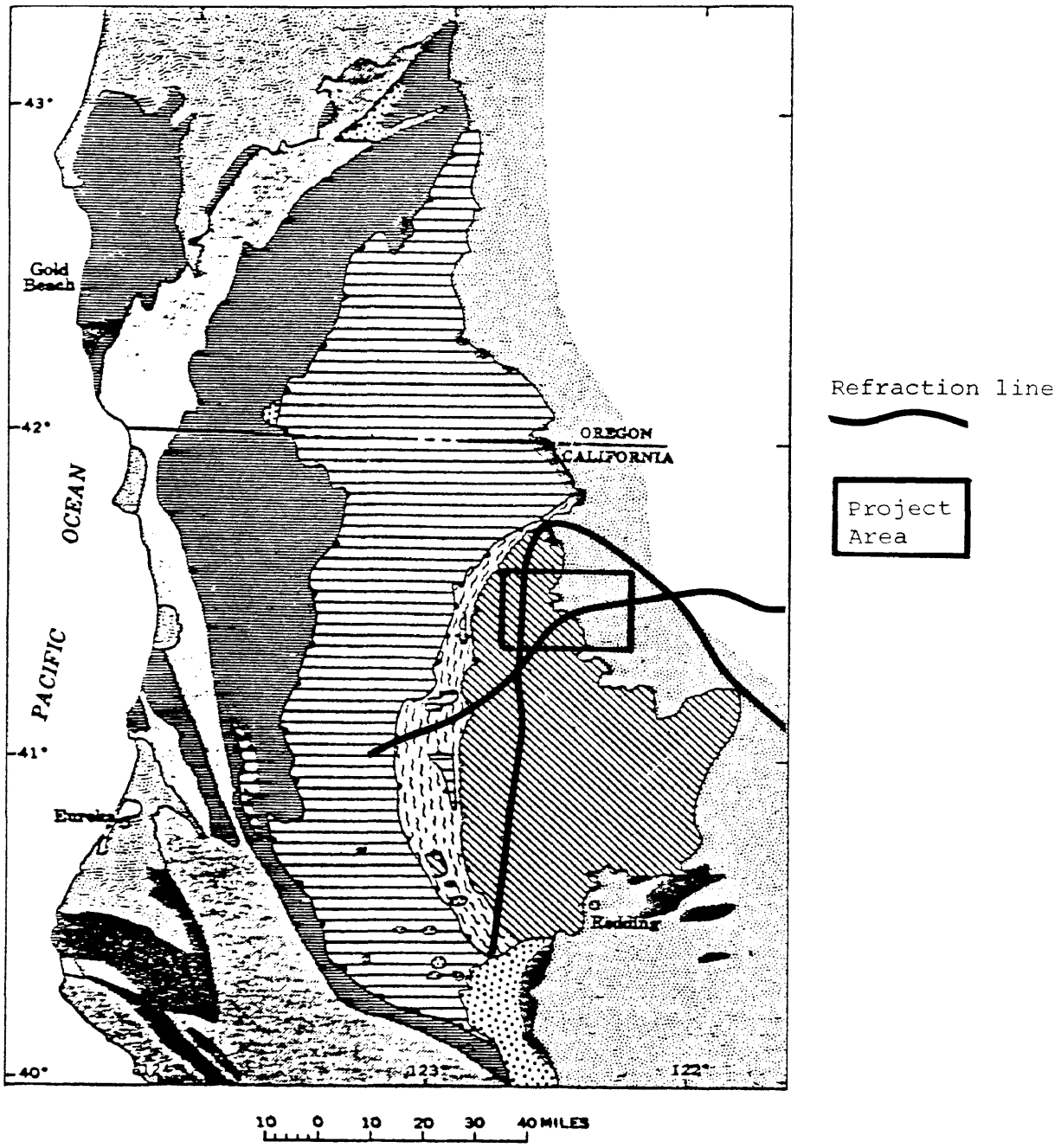

Figure 4. Location of seismic refraction profiles shot during the summer of 1981 by the U.S.G.S. (Fuis and others, in press).

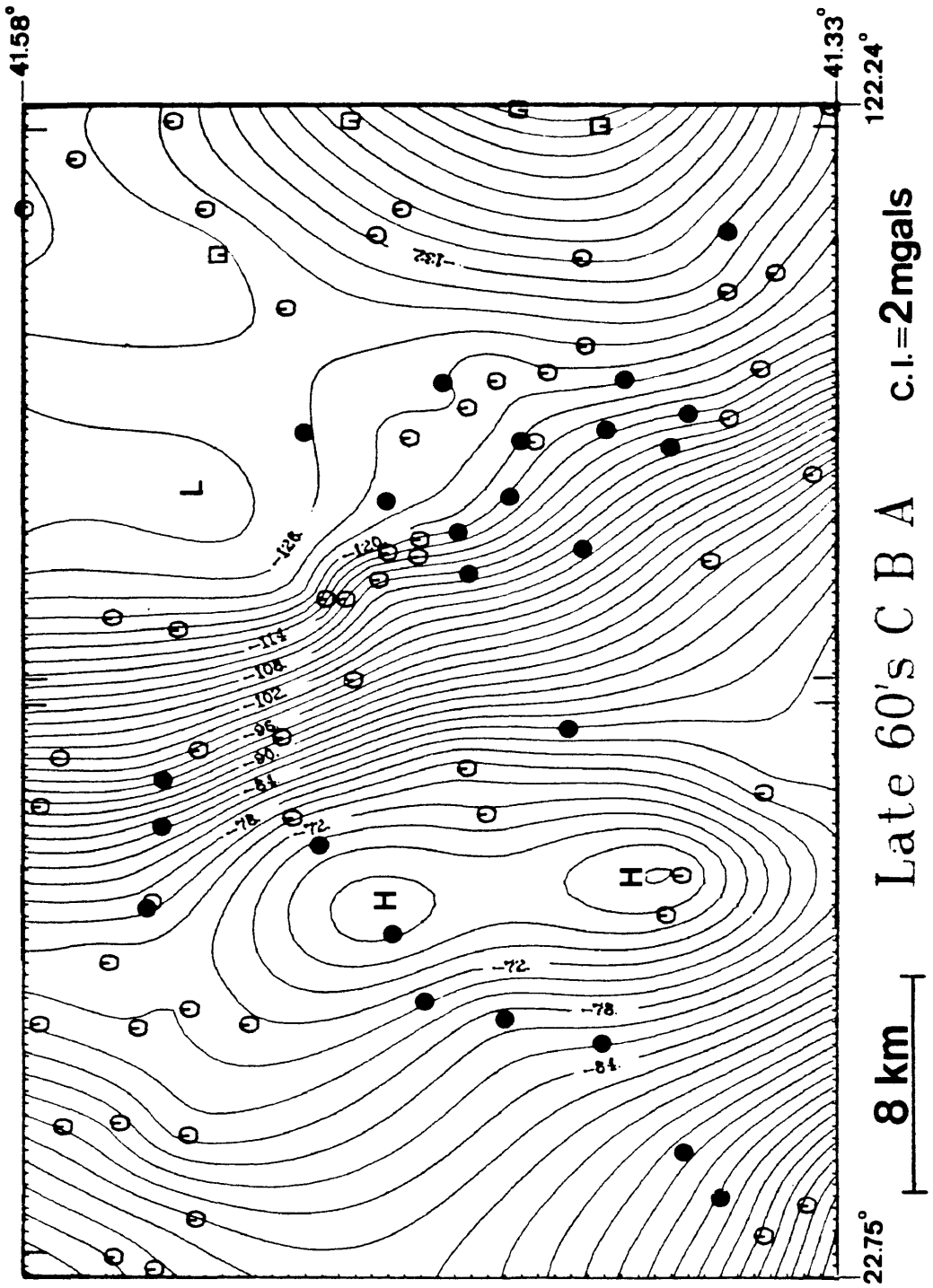

Figure 5. Complete Bouguer anomaly map (Woollard/Rose datum, 1930 Theoretical Gravity Formula) based upon all available data prior to the present study. Gravity stations are represented by open and closed circles, the latter of which denote stations reoccupied during the 1983 survey.

DATA ACQUISITION

A search for existing data led to the acquisition of a magnetic tape of the Weed sheet gravity data, provided by Carter Roberts of the USGS. Proprietary data for the study area also exists (Eureka Resources & Associates), but permission to use such was not granted. All gravity stations occurring within the study area were computer plotted and transferred onto topographic maps, to determine the optimal locations for additional stations.

During August 1983, 133 gravity stations were occupied. Using a Leitz theodolite/electronic distance meter, 92 stations were surveyed with respect to elevation; of which 90 were referenced to bench marks, and two to vertical-angle bench marks.

Location Accuracy

Whenever possible, stations were occupied at known map features; namely road intersections, curves, and stream crossings. All the above were later double checked using slope distances from the survey notes. As only 1:62,500 scale topographic maps were available, the possible maximum error attributable to simply misplacing a 0.02 inch sized dot on the map could be as much as 100 feet. Coupled with the fact that multiple slope distance

measurements were made to locate 29 stations, I believe the maximum associated error to be ~ 0.05 inches on the map, which translates into ~ 250 feet.

The remaining gravity stations were at the following location types: 17 at bench marks, 5 at bench marks not found, 3 at vertical-angle bench marks, 3 at hilltops (black map elevations), 2 at road intersections (black map elevations), and 11 at quarter section and section corners. The latter station locations were surveyed by the U.S. Forest Service, using either a Zeiss Delta 2 or AGA models 110,112 for the slope distances, and a Wild model T-2 for the vertical angles. These instruments have a rated accuracy of $\pm$1 arc-second. The maximum location error, would be associated with the 5 stations occupied at the non-verifiable bench mark locations, where a probable uncertainty of about 250 feet exists.

Latitude and longitude coordinates were determined by computer digitization of the locations referred to above. The digitizing error, determined by digitizing coordinates of known map locations, ranged from 15 feet to 112 feet . The combination of hand-plotting errors and digitizing errors yields a maximum possible error in the determination of latitude and longitude of ~ 350 feet; equivalent to a 0.06 milligal error in the theoretical gravity value.

Elevation Accuracy

Elevation accuracy of the 92 surveyed station locations is reflected by the closures of nine bench mark to bench mark loops, which range from ±0.25 to ±2.17 feet, as shown in Figure 6. Seventeen stations, occupied at bench marks, have an elevation uncertainty of ±0.20 feet. Ten U.S. Forest Service surveyed stations have an uncertainty of ±0.50 feet, with one station having a possible ±3.00 feet elevation error. The remaining thirteen stations, located at good black map elevations, lost benchmarks, or vertical-angle benchmarks, all have an elevation uncertainty of ±2.00 feet.

Gravity Meters

LaCoste and Romberg gravity meter G-491 and Worden gravity meter 27 were used in the reading of the 133 gravity stations in this study. Conversion factors used to convert scale readings to milligals are shown in Table 1.

Table 1

Meter	Calibration Factor
L&R G-491	~1.025 mgal/div.
Worden 27	0.0895 mgal/div.

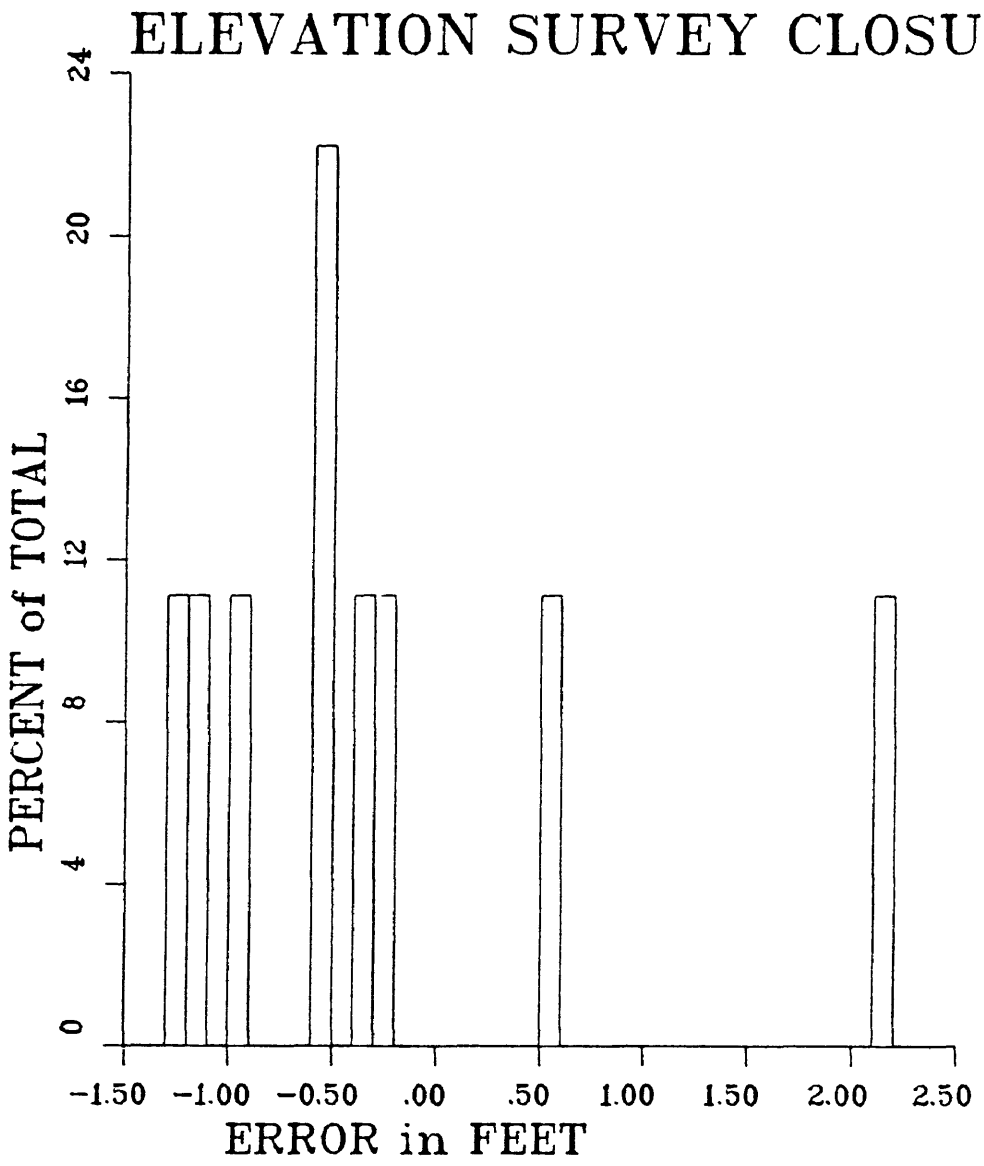

Figure 6. Frequency versus error distribution of closures for nine elevation survey loops.

Gravity Base Station

All observed gravity values for the 1983 survey are based upon the observed gravity of 979.97741 gals at the Weed gravity base station, Weed, California (California Division of Mines and Geology gravity base station network, station number 6, Chapman, 1966). The CDMG network ties satisfactorily with that of Woollard and Rose (1963), with a base station difference (former-latter) of only +0.05 milligals occurring at the Redding, California station 60 miles south of the Weed base. When using the L&R meter, the Weed base was occupied only at the beginning and end of each loop, spanning a maximum period of 12 hours. More frequent base station readings were made when using the Worden meter, with nine loops spanning 3 hours time or less, and three loops spanning 6 to 7 hours of time.

ACCURACY OF GRAVITY DATA

Internal and external repeats comprised 16 percent and 12 percent of all readings, respectively. Eleven percent of all readings represented repeats of stations occupied by Evernden (1963) and/or LaFehr (1966). Both internal and external repeats with the L&R meter had a mean error of 0.10 milligals, while such repeats with the Worden meter had mean errors 0.06 milligals and 0.12 milligals, respectively. A frequency versus error distribution of all internal and external repeats is shown in Figure 7. Repeats between the two meters had an absolute mean error of 0.19 milligals, as shown in Figure 8. Repeats between the 1983 survey and the previous surveys had an absolute mean error of 0.19 milligals, as shown in Figure 9.

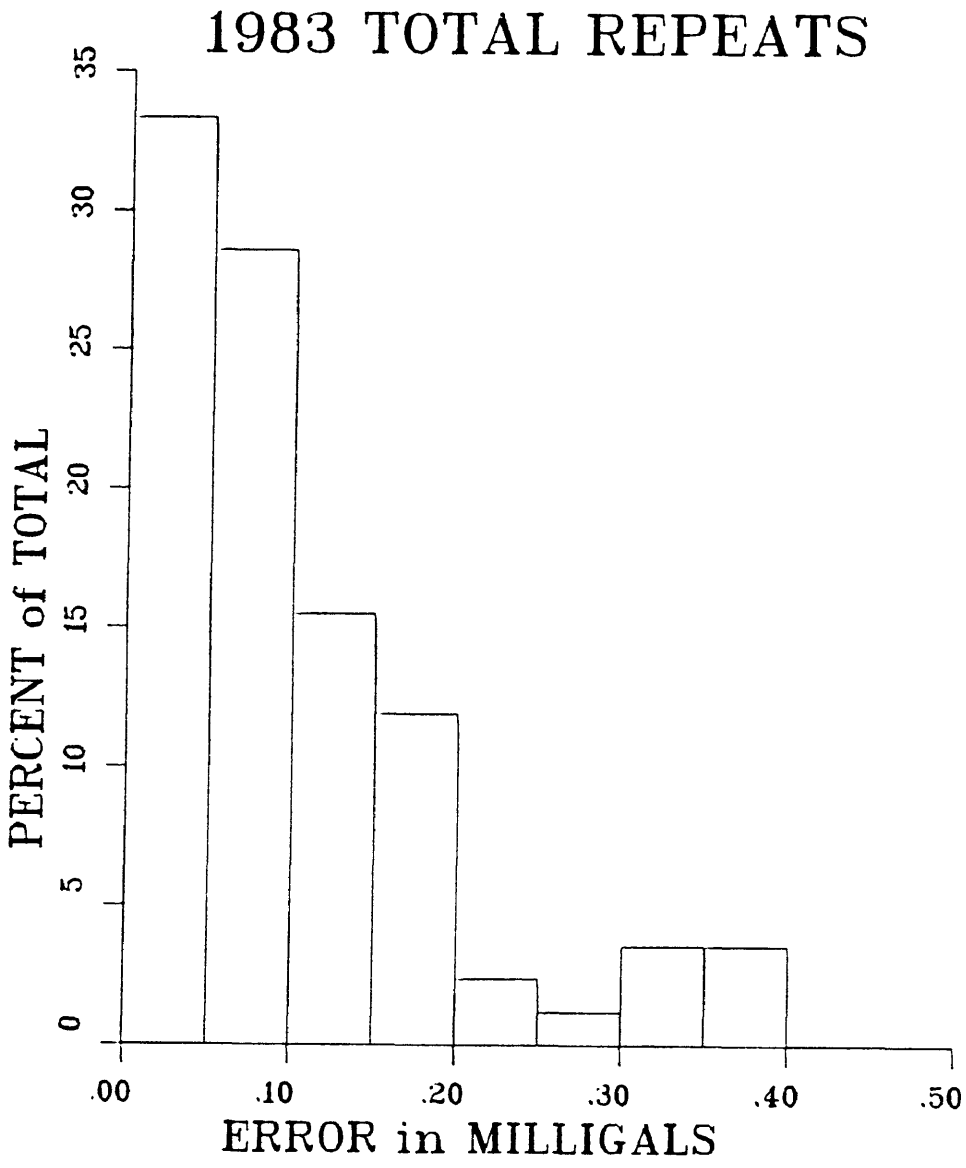

Figure 7. Frequency versus error distribution of all internal and external repeat readings. Regarding external repeats, all possible combinations were made, yielding a full range of possible repeat errors. Of these, 92 percent were less than 0.30 mgals, 88 percent less than 0.20 mgals, 61 percent less than 0.10 milligals, and 33 percent less than 0.05 mgals.

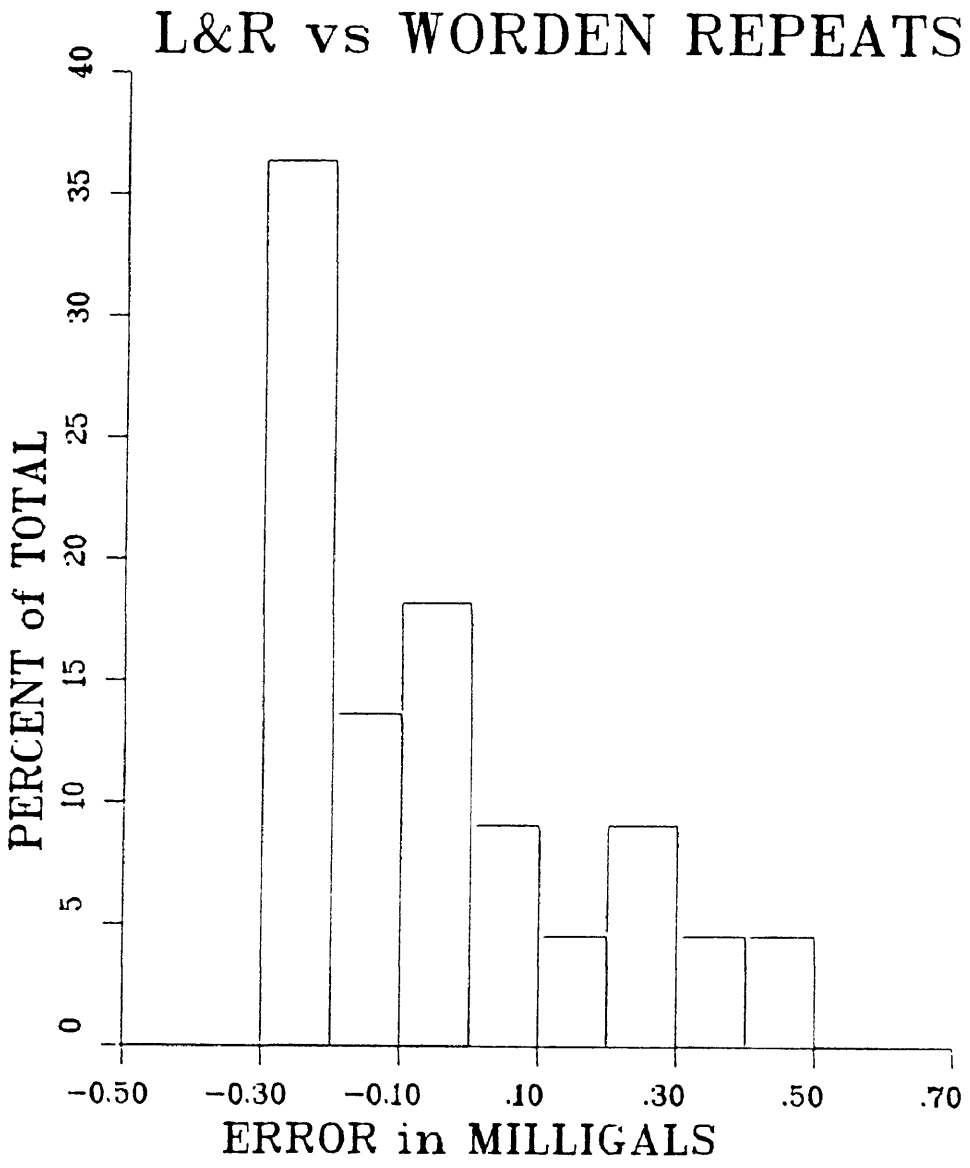

Figure 8. Frequency versus error distribution of L&R readings with those of the Worden meter. All possible combinations were made, yielding a full range of possible repeat errors. Of these, 91 percent were less than $\pm$0.30 mgals, 46 percent less than $\pm$0.20 mgals, and 27 percent less than $\pm$0.10 mgals.

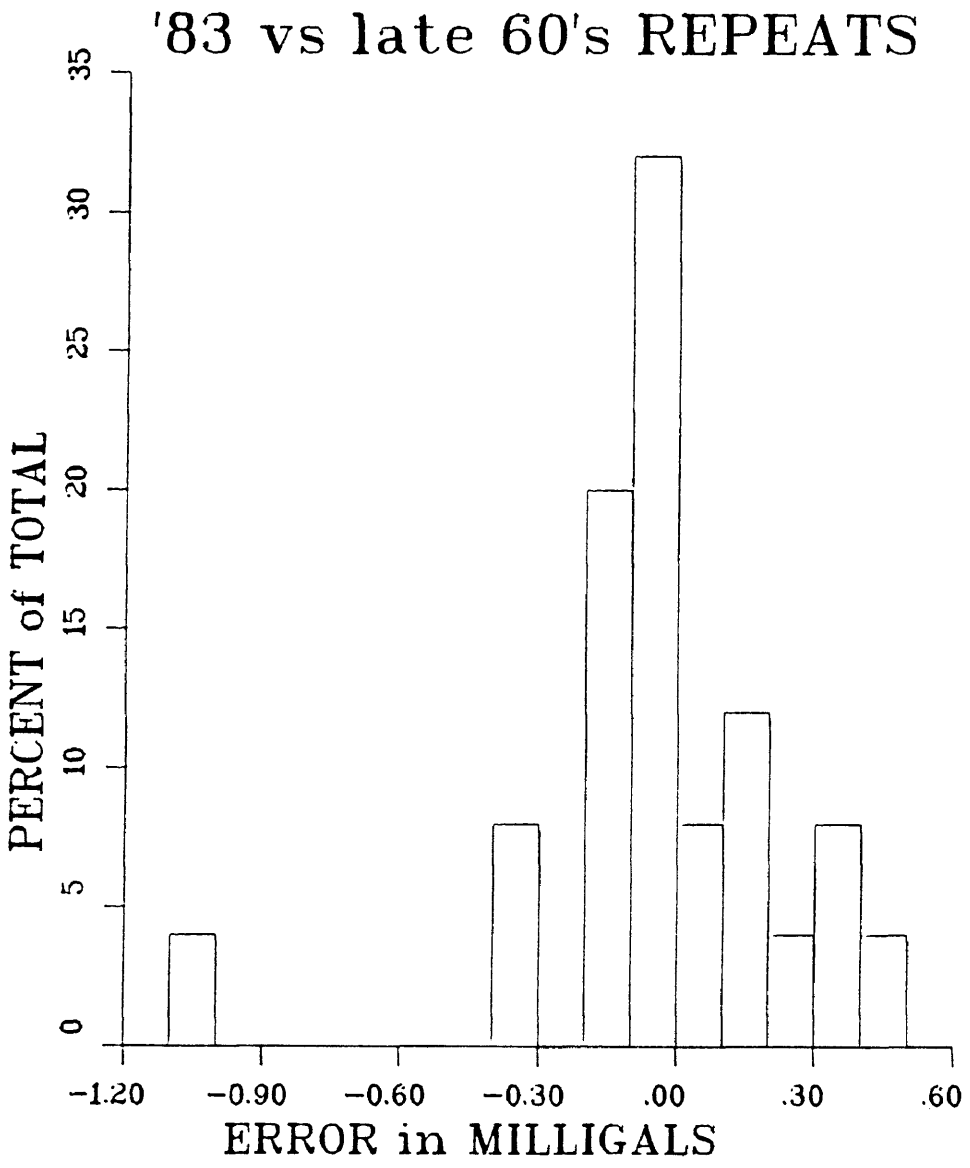

Figure 9. Frequency versus error distribution of repeat readings between the 1983 survey and previous surveys. Of these, 84 percent were less than ±0.30 mgals, 72 percent less than ±0.20 mgals, and 40 percent less than ±0.10 mgals.

REDUCTION OF DATA

The 1967 International Gravity Formula for theoretical gravity, a sea-level datum, and a constant density of 2.67 g/cc were used to reduce the observed data to simple Bouguer gravity values. The tidal variation of the earth's gravity field was computed (Rudman and others, 1977) and removed from all readings. The assumed linear instrument drift was then determined for each gravity loop and corrected for accordingly. All observed gravity values were reduced to the datum of the 1971 International Gravity Standardization Net (IGSN-71) of Morelli (1971). The conversion from the Woollard-Rose datum (1963) to the IGSN-71 datum was made by subtracting 14.46 milligals from the former. This constant was determined from comparisons of the two networks at common points nearby the study area, namely Dunsmuir and Yreka, where differences of 14.45 milligals and 14.47 milligals respectively were found.

Terrain corrections for all 1983 gravity stations were corrected from the station out to the standard radius of 166.7 km. The manual method of Sandberg (1958) was used to determine the attraction of the nearby terrain from the station out to 558 feet (Hammer rings A-D).

From 558 feet to 2,936 feet (Hammer rings E and F), the computerized method of Krohn (1976) was employed. The computer program of Plouff (1977) determined the terrain effects occurring from the Hammer G ring out to 166.7 km.

The above methods all utilize a sloping surface; either directly, as in Sandberg and Krohn, or indirectly via the line elements used by Plouff. A sloping surface accurately defines the nearby terrain, whereas the flat-topped prisms used in Hammer's manual method tend to overestimate the terrain effect upon the gravity meter.

SANDBERG'S MANUAL METHOD (HAMMER RINGS A-D)

The most accurate topographic maps available for the study area, have a 1:62,500 scale. Hence, an accurate estimation of the topography within rings A-C (0-175 feet) is not possible because the template would only be 0.03 inches in diameter. Because of this limitation, the slope for ring D (175-558 feet) was assumed to be representative of the slope from 0 to 558 feet. This method, as employed in this project, had the following sources of error: 1) rings A-C were assumed to be represented by the same plane(s) as estimated in ring D, 2) elevations read from maps were accurate to within $\pm$40 feet (contour interval of 80 feet), and 3) the topography was approximated by a simple plane or set of planes. An empirical analysis of the accuracy of this method relative to the Hammer (1939) method is shown in Figure 10. With the exception of two cases, the Hammer corrections were higher than those obtained by the Sandberg method. One would expect these results since Hammer's method defines the terrain as flat topped rectangular prisms, whereas Sandberg uses annular prisms with sloping surfaces.

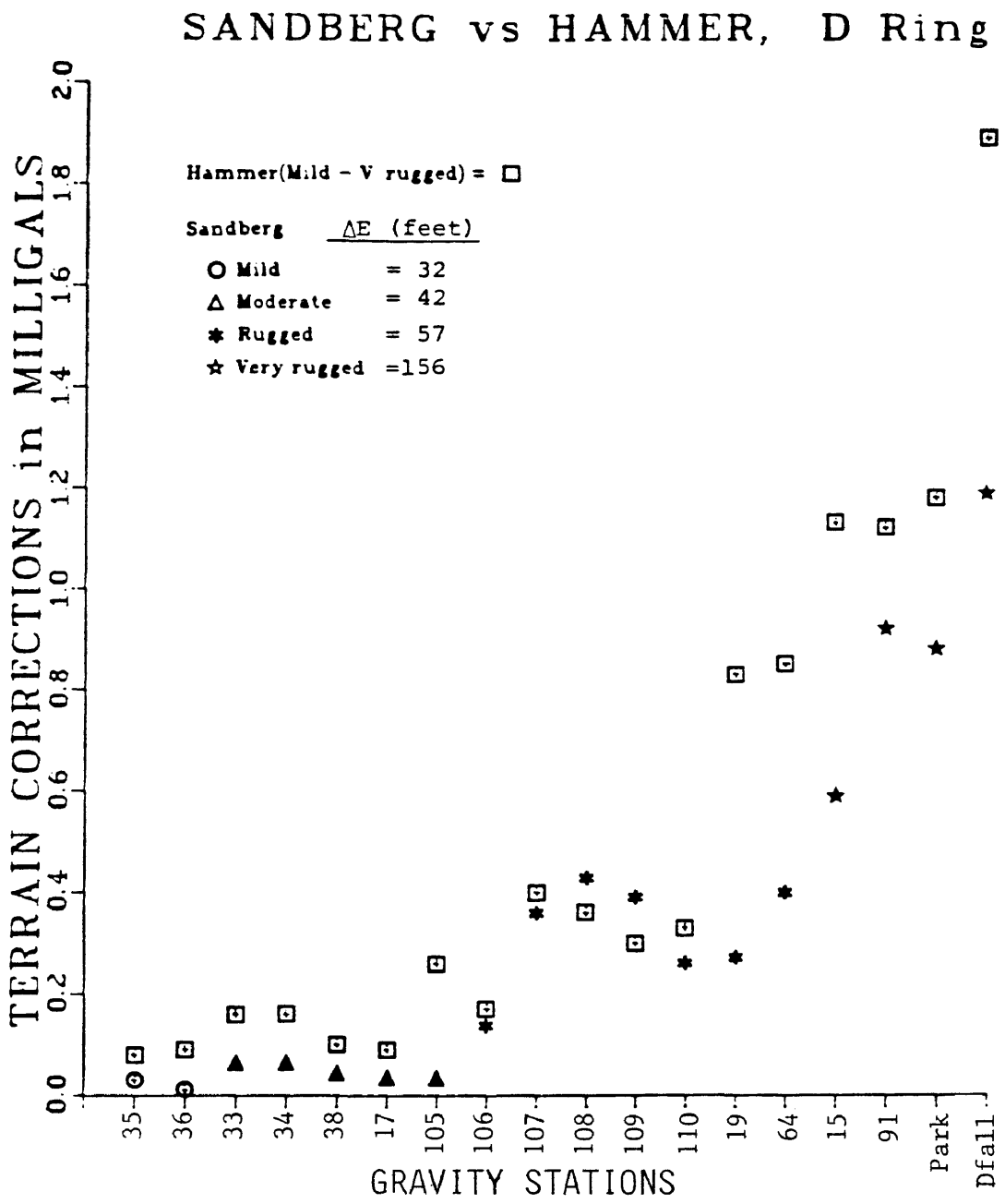

Figure 10. Comparison of terrain corrections obtained by the methods of Sandberg and Hammer. A maximum units difference of 0.70 mgals is found in the above comparison. Percentage differences were not calculated, due to the small-valued numbers involved. ΔE is the difference between the station elevation and the average elevation of the D ring.

PLOUFF'S COMPUTERIZED METHOD (HAMMER RINGS G-166.7 km)

Terrain corrections from .895 km (2,936 feet) to 166.7 km were obtained using the computerized method of Plouff (1977). This method requires a vast data base of digital elevation values, and is therefore only as good as the number and quality of elevation values used to represent the surrounding terrain. Plouff assigns a line element of mass to each elevation value, creating a model with an attraction closely approximating that of a mass bounded by a sloping surface passing through the station (Plouff, 1966).

The Defense Mapping Agency has prepared extensive data bases of digitized elevation values, obtained via computer scanning of 1:250,000 scale topographic contour plates. Scanning of these plates occurs at 3 arc-second intervals. Resampling of the 3-second data is also done, in order to provide 15-second, 30-second, 1-minute, and 3-minute sampled elevation data, as needed for varying definitions of the topography.

Originally, 30-second sampled elevation data were used from .895 km to 4.47 km (rings G-I), 1-minute sampled elevation data from 4.47 km to 21.94 km (rings J-M), and 3-minute sampled elevation data from 21.94 km to 166.7 km. Comparisons of 30 second digital elevation data with

elevations at corresponding locations on 1:62,500 topographic maps were made, as shown in Figure 11. Inaccurate elevations will obviously lead to errors in the determination of the line elements used in Plouff's terrain correction program. The effect of such line element errors will be greatest in the inner rings and least in the outer rings. The estimation of the effects of line element errors was made by reference to Hammer's charts. Though rectangular prisms generally have an attraction slightly greater than line elements of similar height (Plouff, 1966), the assumption that the two are equal is satisfactory regarding the following error analysis.

Gravity effects associated with elevation errors (ΔE) were determined by 1) adding ΔE to the average ring compartment elevation, 2) reading the corresponding attraction, and 3) subtracting from the former the attraction associated with the proper elevation. Average compartmental elevations for Hammer rings E-M were obtained from worksheets used in determining terrain corrections (via Hammer's method) for selected 1983 gravity stations. In the error analysis, two terrain types were considered: 1) the mild relief of the Shasta Valley, and 2) the very rugged relief associated with Park

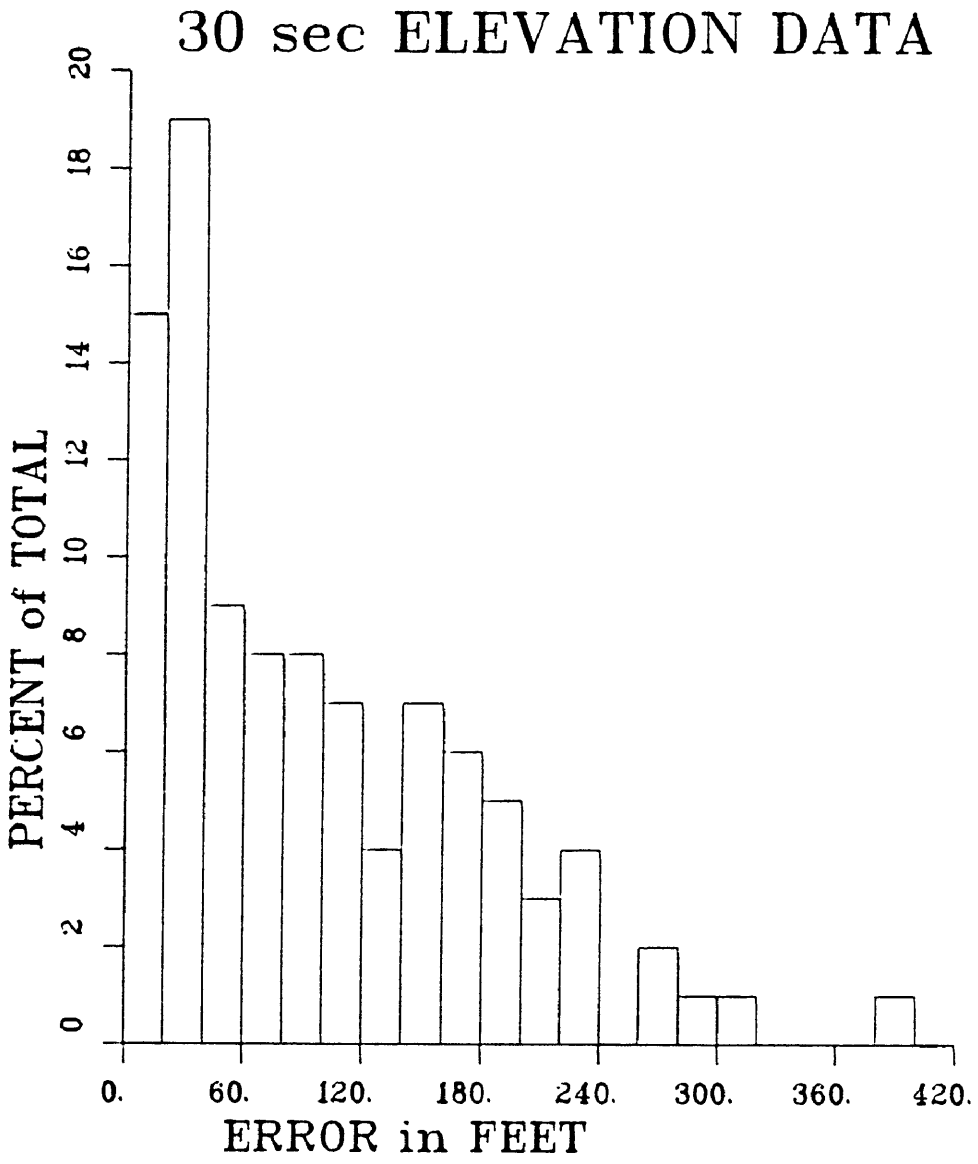

Figure 11. Frequency versus error distribution of discrepancies between 30-second sampled elevation values and corresponding topographic map elevations (read with a maximum error of ±40 feet). One hundred comparisons were made.

Peak in the eastern Klamath Mountains. The results of the above study are shown on Figures A-1 through A-6 in Appendix A. Inspection of these figures leads to the following conclusions: 1) in both mild and very rugged topography, terrain corrections (using 30-second data) could be significantly inaccurate if calculated within Hammer rings E and F, and 2) assuming no aliasing, terrain corrections are probably of sufficient accuracy within the area bounded by Hammer ring G and 166.7 km, when made in mild or even very rugged topography.

In lieu of detailed statistical analyses, an empirical test of the accuracy of Plouff's method was made by simply comparing terrain corrections (in rings G-M) with those calculated via Hammer's manual method. Because the Hammer method uses topographic maps and was found reproducible to within about 5 percent, it was considered a good standard of accuracy. A comparison of the two methods is shown in Figure 12.

One would expect the Hammer values to be consistently higher than those obtained via Plouff's method yet only one case (Figure 12) reveals this. However, if the topography is not accurately defined by the 30-second

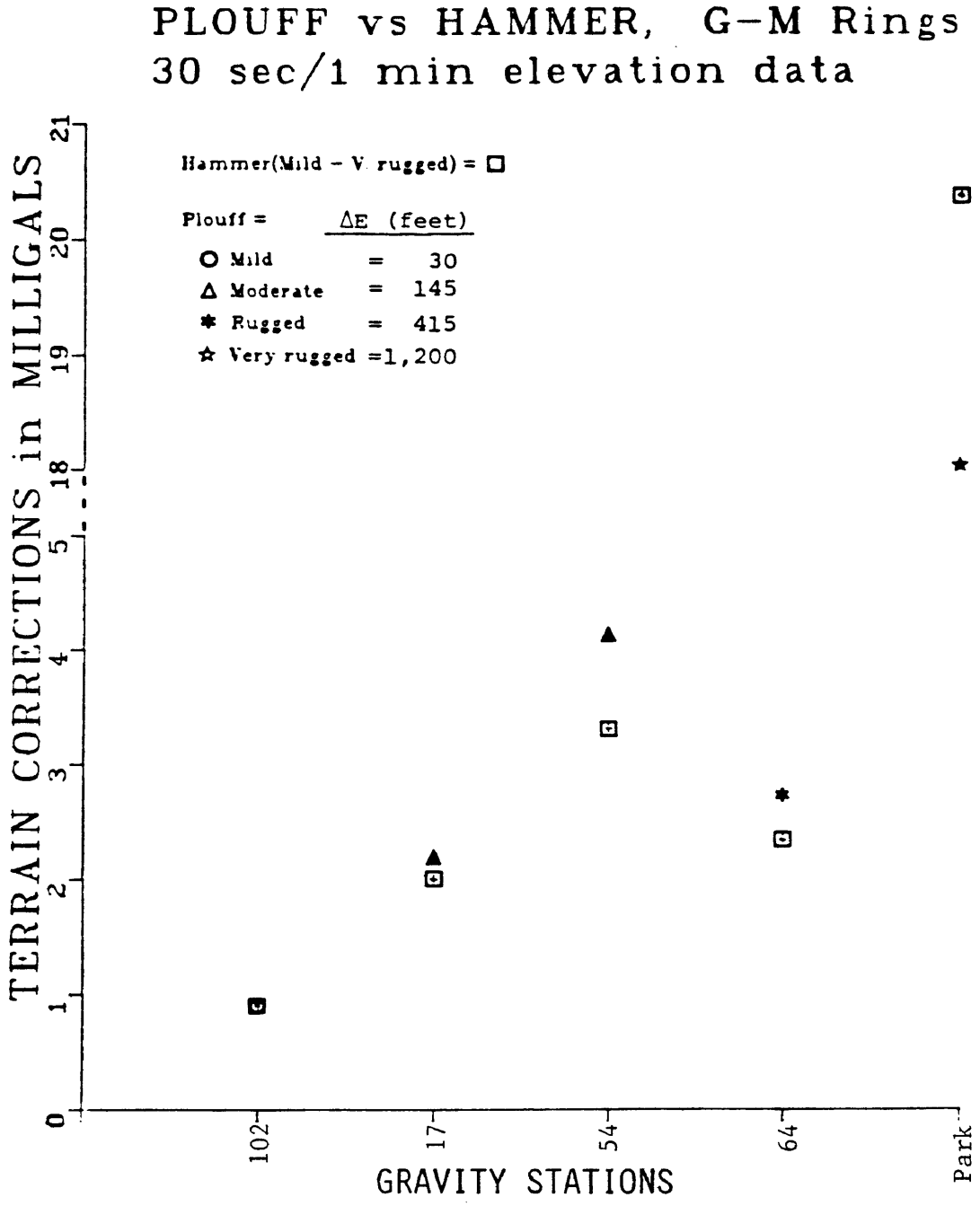

Figure 12. Comparison of terrain corrections obtained by the methods of Plouff and Hammer. A maximum proportional difference of 23 percent, and a maximum units difference of 2.34 mgals is found in the above comparison. ΔE is the difference between the station elevation and the average elevation of the G ring.

elevation data, it is conceivable that terrain corrections obtained by the Plouff method could be greater than those of Hammer, as shown in Figure 12.

The accuracy of these data appears to be adequate, but what of their sampling interval? In the location of the study area, a 30-second (longitude) by 30-second (latitude) grid cell equals .70 km by .92 km respectively. At this sampling interval, 0.8, 2.0, and 5.3 elevation values occur in each compartment of the Hammer G, H, and I rings, respectively. It is therefore apparent that within the G and possibly the H ring(s) 30-second elevation data is of an insufficient sampling interval to adequately define a rapidly changing topography. This aliasing problem may well account for the unexpected differences (Figure 12) occurring between the methods of Plouff and Hammer.

To minimize possible aliasing effects, 15-second average elevation data (supplied by R.H. Godson, U.S.G.S., Denver) were used from .895 km to 21.94 km, replacing the original 30-second and 1-minute data. From 21.94 km to 166.7 km, the previously mentioned 3-minute data were again used. The original and improved digital elevation

models are shown on Figure 13. To test the accuracy of the 15-second average elevation data, comparisons with elevations at corresponding locations on 1:62,500 topographic maps were made, as shown in Figure 14. A comparison of Figure 14 with Figure 11 shows the accuracy of the 15-second average data to be superior to that of the 30-second data.

Inspection of Figures A-7 through A-12 reveals the much lower gravity errors associated with the 15-second data (vs. 30-second data). Further inspection of these figures leads to the following conclusion: In terrain ranging from mild to very rugged, terrain corrections (using 15-second data) are probably of sufficient accuracy within the area bounded by Hammer ring E and 166.7 km, assuming that no aliasing effects exist. Noting that 15-second data provides .5, and 1.5 elevation values per compartment of the E and F rings, respectively, it is apparent that aliasing of the topography does occur within these rings. Therefore, in spite of its accuracy, 15-second data cannot be used in rings E and F, as its sampling interval aliases the topography. In rings G, H, and I, 2.7, 7.5, and 15 elevation values, respectively, occur in each compartment using 15-second data. This is

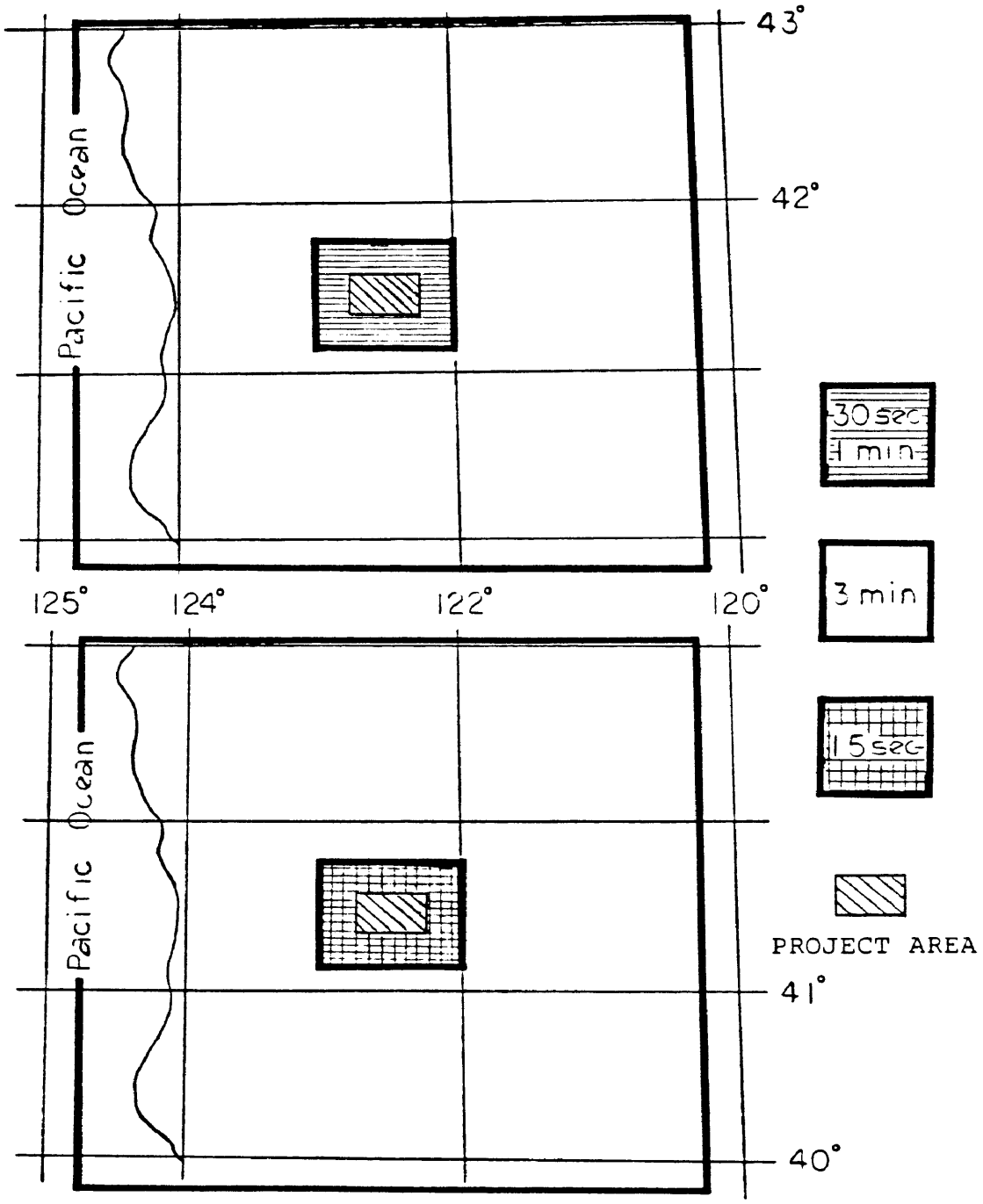

Figure 13. Index maps of digital elevation models used as input into the terrain correction program of Plouff. The original model (top of page) was later replaced by the much improved model below it.

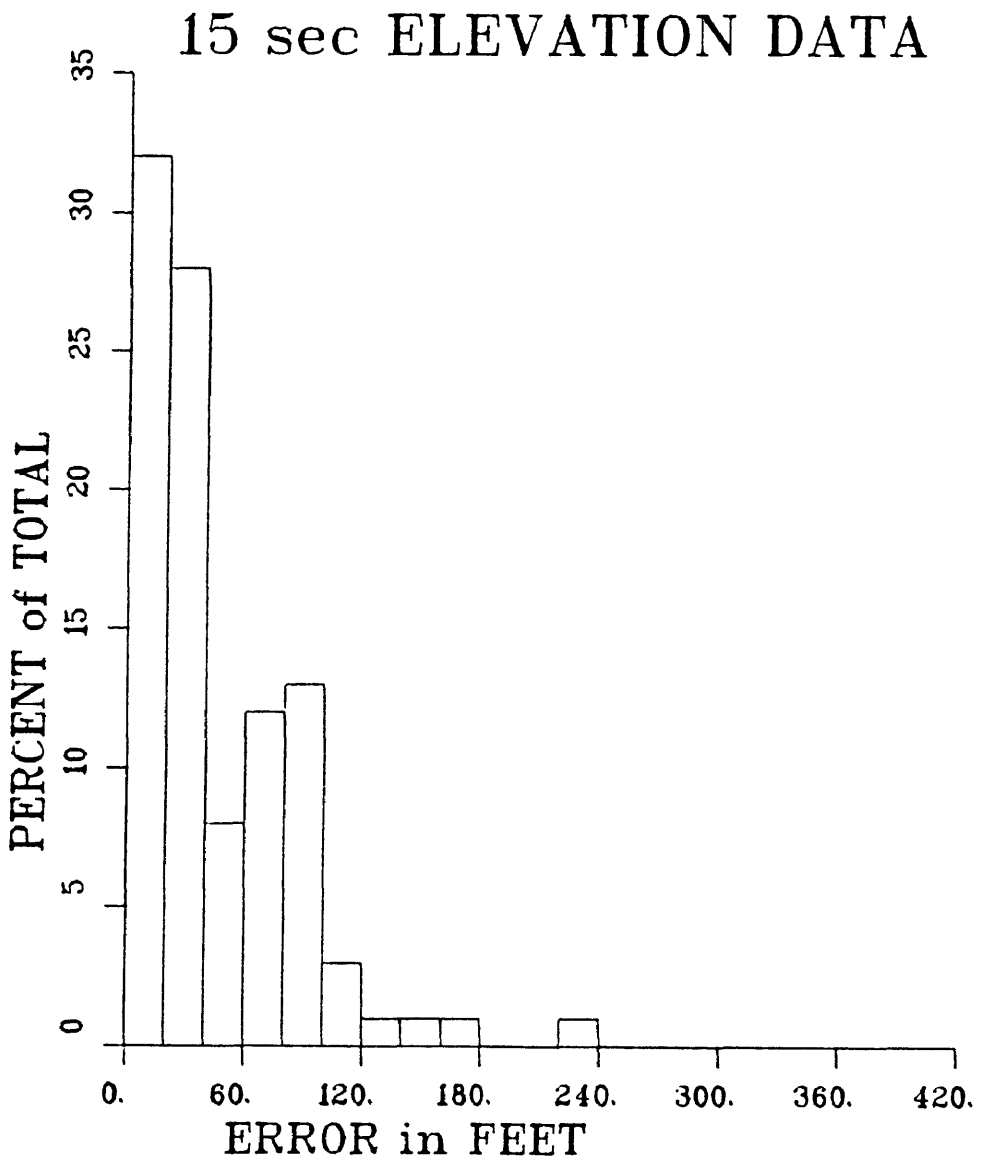

Figure 14. Frequency versus error distribution of discrepancies between 15-second average elevation values and corresponding topographic map elevations (read with a maximum error of ±40 feet). One hundred comparisons were made.

about a 3-fold sampling increase over the 30-second data, and thus represents a significant improvement.

Again, Plouff's terrain corrections were compared with those obtained by the Hammer method, as shown in Figure 15. Inspection of this figure reveals a significant reduction in the discrepancies between the two methods, and now shows the Hammer corrections to be about equal to or greater than those obtained by the Plouff method, as one would expect. The mean percentage differences between Hammer chart corrections and those of Plouff is only 6 percent.

All terrain corrections (calculated by Plouff's method) for the pre-existing gravity data, excluding those obtained by Finn (1981) and Finn and Spydell (1982), were recalculated using the improved 15-second data. The gravity data of Finn and Spydell already include corrections calculated with 15-second data (Finn, personal communication).

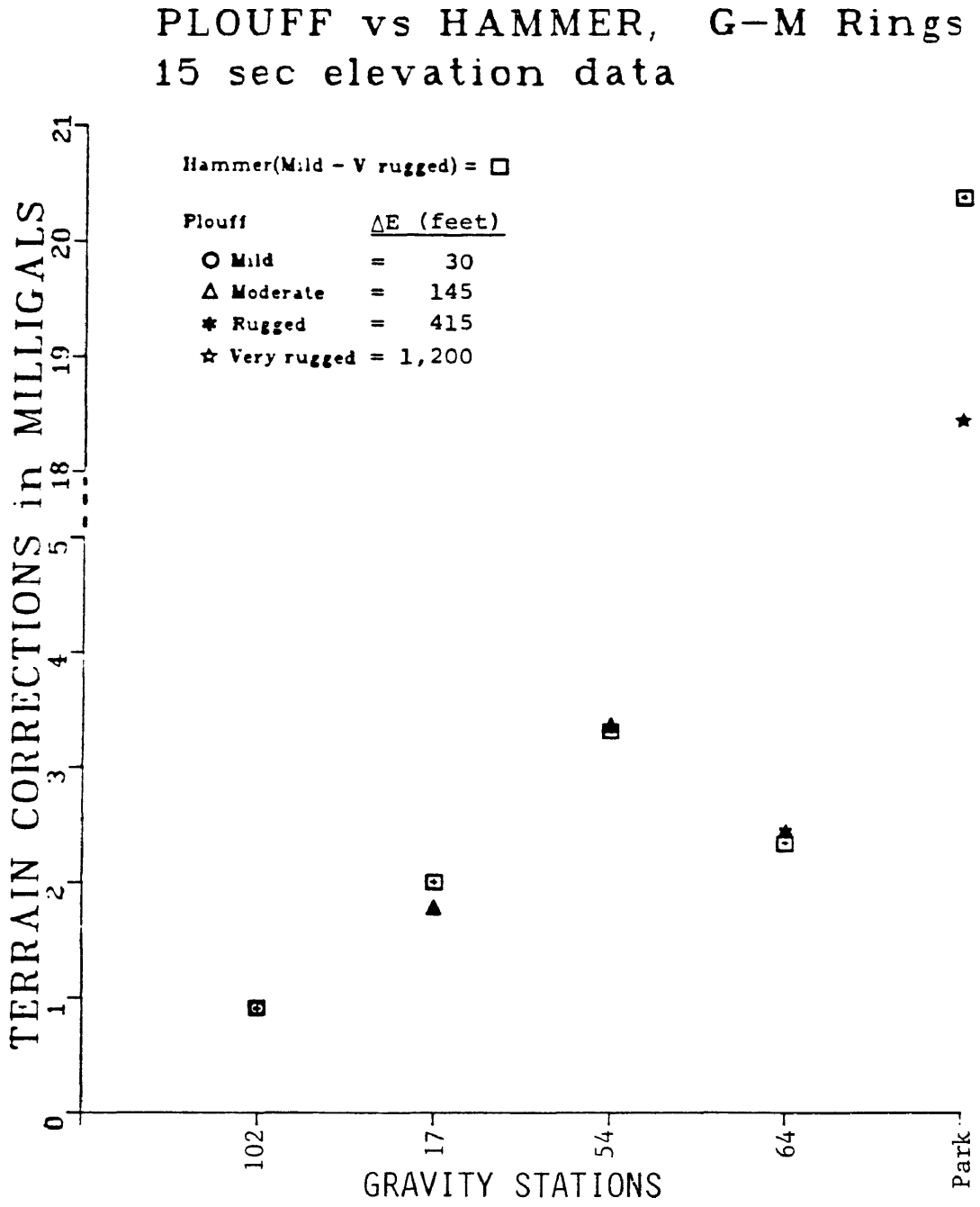

Figure 15. Comparison of terrain corrections obtained by the methods of Plouff and Hammer. A maximum proportional difference of 14 percent, and a maximum units difference of 1.93 mgals is found in the above comparison. ΔE is the difference between the station elevation and the average elevation of the G ring.

KROHN'S COMPUTERIZED METHOD (HAMMER RINGS E-F)

Because of aliasing problems with the elevation data, a method other than that of Plouff had to be used for rings E and F; the computerized method of Krohn (1976) was chosen. His program also requires as input a digital elevation file of the topograhy surrounding the station and, accordingly, square grids, 1.8 km on a side, consisting of 81 cells (9x9), 49 cells (7x7) or 25 cells (5x5), were constructed, with the finer grids used for those stations occurring in the most rugged topography.

A 5x5 grid provides .5 and 2.5 elevation values per compartment in rings E and F, respectively. However, such grids were adequate for 91 of the gravity stations, as the minimum wavelength of the surrounding terrain was adequately sampled by the grid cells (.36 km x .36 km). This sampling is only slightly better (0.5/E ring, 1.5/F ring) than that obtained by Plouff's method using 15-second data. Recalling that the accuracy of 15-second data is adequate regarding rings E and F, then in such mild terrain, either method could have been utilized with minimal aliasing effects; however, for the sake of consistency, Krohn's method was used. For the remaining

stations, 7x7 grids (.26 km x .26 km cell) adequately sampled the surrounding terrain, so that in rings E and F, there were 1 and 5 elevation values (per compartment), respectively.

Krohn's program fits a quadric equation of a cone to each grid cell elevation and then sums these equations to produce a multiquadric surface that passes through all the elevation points. When an unaliased elevation file is entered into this program, the resulting multiquadric surface closely resembles the original topography, as shown in Figures 16 and 17. Krohn then takes this surface and divides it into a ring/compartment system analogous to that employed by Hammer (1949). Using Hammer's equation for the gravitational attraction, Krohn calculates such for all compartments and then sums them together to obtain the terrain correction.

A comparison of terrain corrections (rings E-F) calculated by the methods of Krohn and Hammer is shown in Figure 18. As expected, Hammer chart corrections are higher than those obtained by Krohn's method, with a mean percentage difference of 21 percent. This is attributed to the fact that Hammer's method sums mass attractions

ACTUAL TOPOGRAPHY

MULTIQUADRIC SURFACE

5x5 input grid

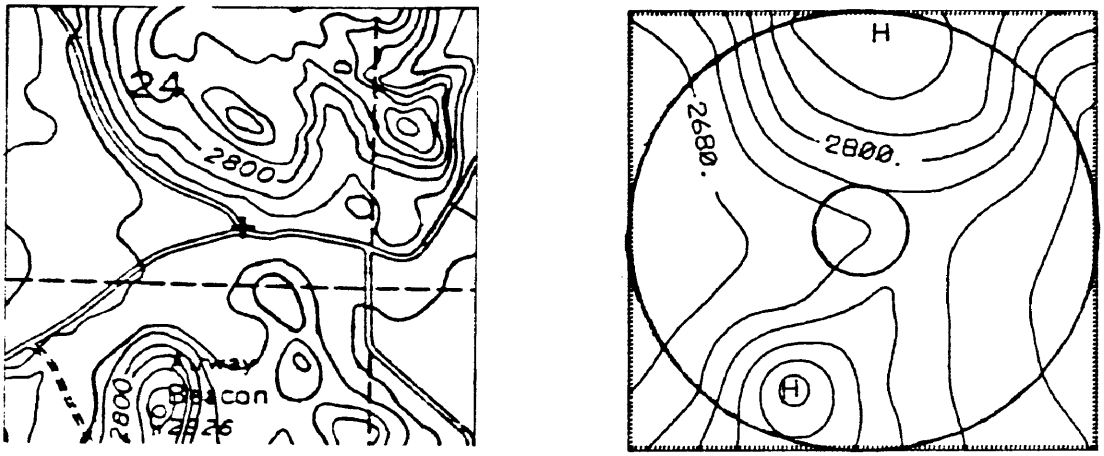

station G-84

C.I.= 40 feet

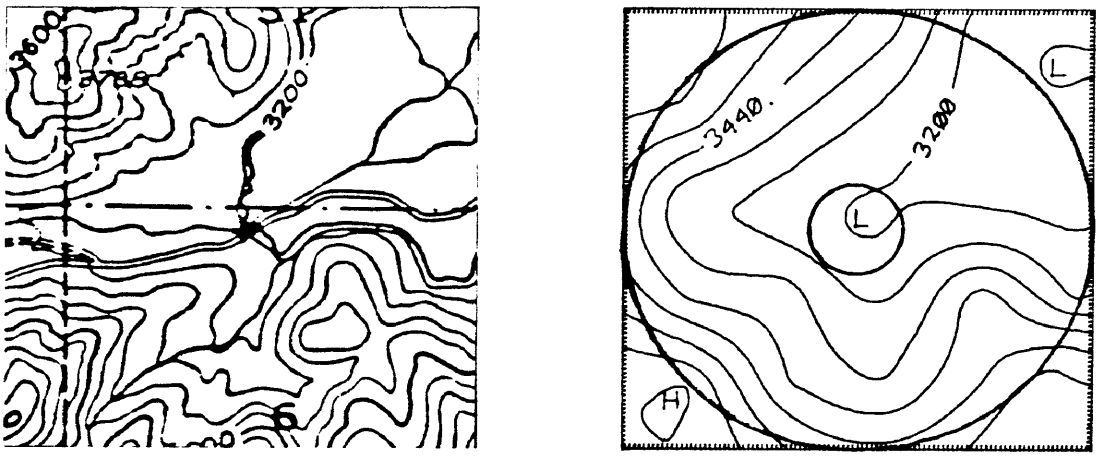

station G-21

C.I.= 80 feet

1 km

Figure 16. Comparison of actual topography with multiquadric surfaces generated from input of 5x5 elevation grids into Krohn's program. The area bounded by the circles is that for which terrain corrections are calculated.

ACTUAL TOPOGRAPHY

MULTIQUADRIC SURFACE

7x7 input grid

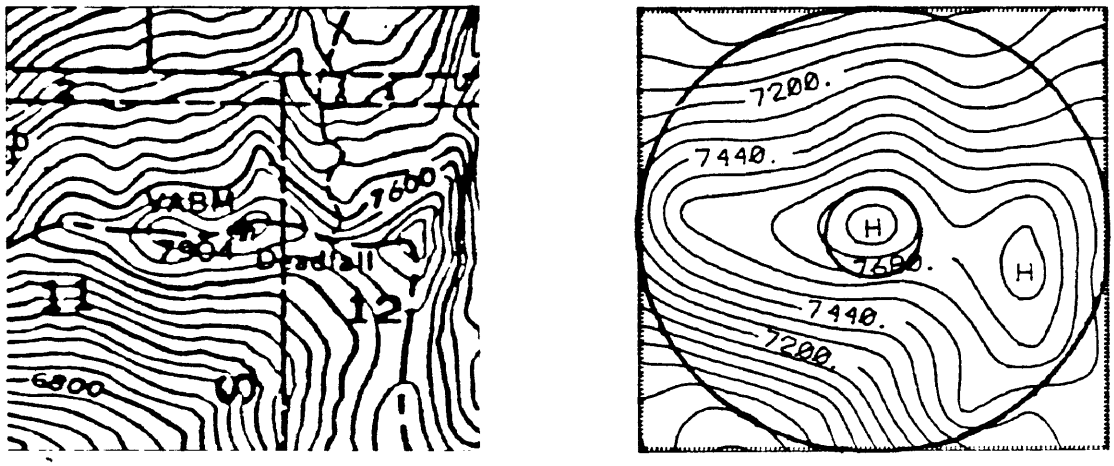

station Deadfall

C.I.= 80 feet

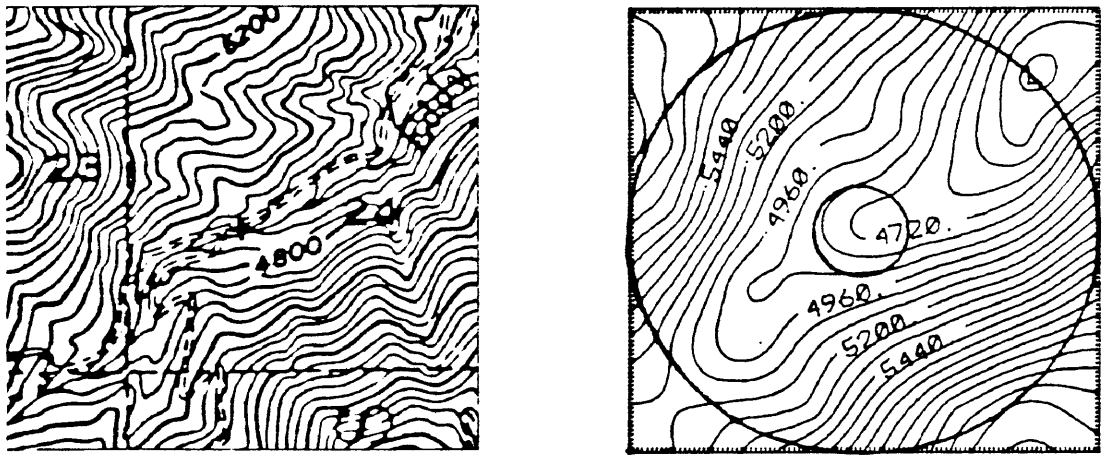

station G-110

C.I.= 80 feet

1 km

Figure 17. Comparison of actual topography with multiquadric surfaces generated from input of 7x7 elevation grids into Krohn's program. The area bounded by the circles is that for which terrain corrections are calculated.

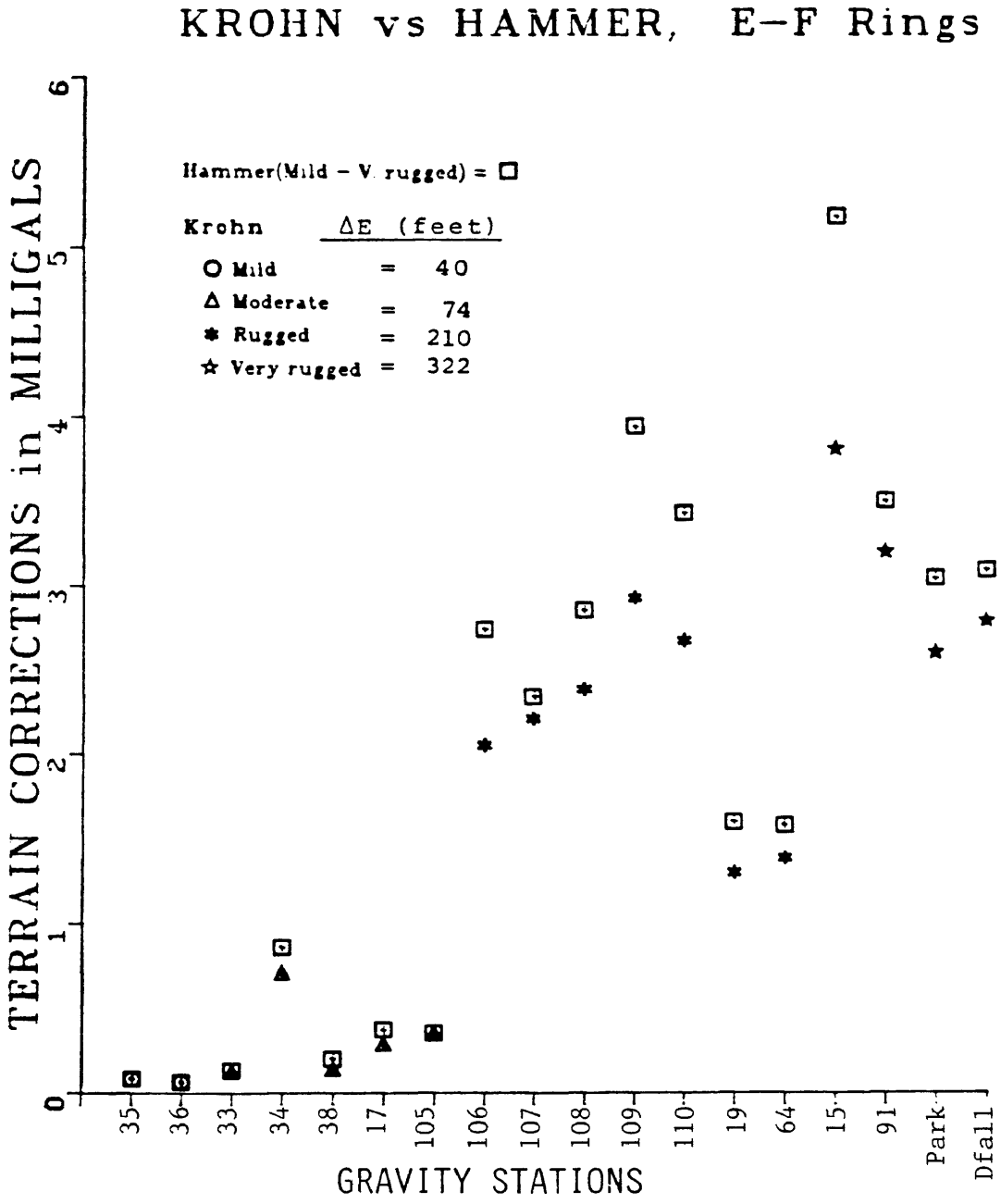

Figure 18. Comparison of terrain corrections obtained by the methods of Krohn and Hammer. A maximum proportional difference of 54 percent, and a maximum units difference of 1.37 mgals is found in the above comparison. ΔE is the difference between the station elevation and the average elevation of the E ring.

over only 16 compartments (rings E-F), whereas 975 much smaller compartments are summed in Krohn's program.

Krohn's method was not utilized for rings A-D because given the elevation grids used, aliasing of the near station terrain would inevitably result. In order for this method to better define the near station terrain, a much finer grid would be necessary, thus becoming much more labor intensive, and in turn more prone to error. It should be noted that the 1:62,500 scale topographic maps used in this project do not allow accurate sampling of the near station terrain, regardless of the terrain correction method used. Because of these problems, I consider the method of Sandberg to be best suited for calculating terrain corrections in rings A-D.

ACCURACY OF TERRAIN CORRECTIONS

An analysis of Figures 10, 15, and 18 led to the following observation: the mean percentage difference between Hammer chart corrections and the composite corrections calculated by Sandberg, Krohn, and Plouff, is about 10 percent, with the composite corrections being systematically smaller.

Krohn (1976) found that Hammer's method overestimates the attractions of a cone and a sloping surface by about 17%. Since cones and sloping surfaces more adequately define rugged topography than Hammer's prisms, the terrain corrections calculated in the present study are more accurate than those obtained via Hammer's method. The estimated error, represented as the difference between Hammer's overestimation error of 17% and the 10% discrepancy between the two methods, is therefore about 7%. Approximately 67 percent of the stations have total terrain corrections between 0 and 5 milligals, 23 percent between 5 and 10 milligals, 8 percent between 10 and 15 milligals, 1 percent between 20 and 25 milligals and 1 percent between 25 and 30 milligals. Given the range (1.29-26.36 milligals) of corrections calculated in this

study, actual errors of 0.09 to 1.85 milligals are possible. However, the large majority (67%) of errors range from only 0.09 to 0.35 milligals.

Terrain corrections were also calculated (using Plouff's program and 15-second elevation data) from .295 km (inner limit of program) to 166.7 km and compared with the complete corrections of this study. The extent and proportion of errors that result from neglecting the inner zones are shown in Figure 19. In most cases, partial terrain corrections are within $\pm$0.20 milligals of the complete terrain corrections. Nevertheless, a sufficient number (29%) of partial corrections have errors greater than $\pm$0.20 milligals, thus confirming the need for corrections all the way into the station.

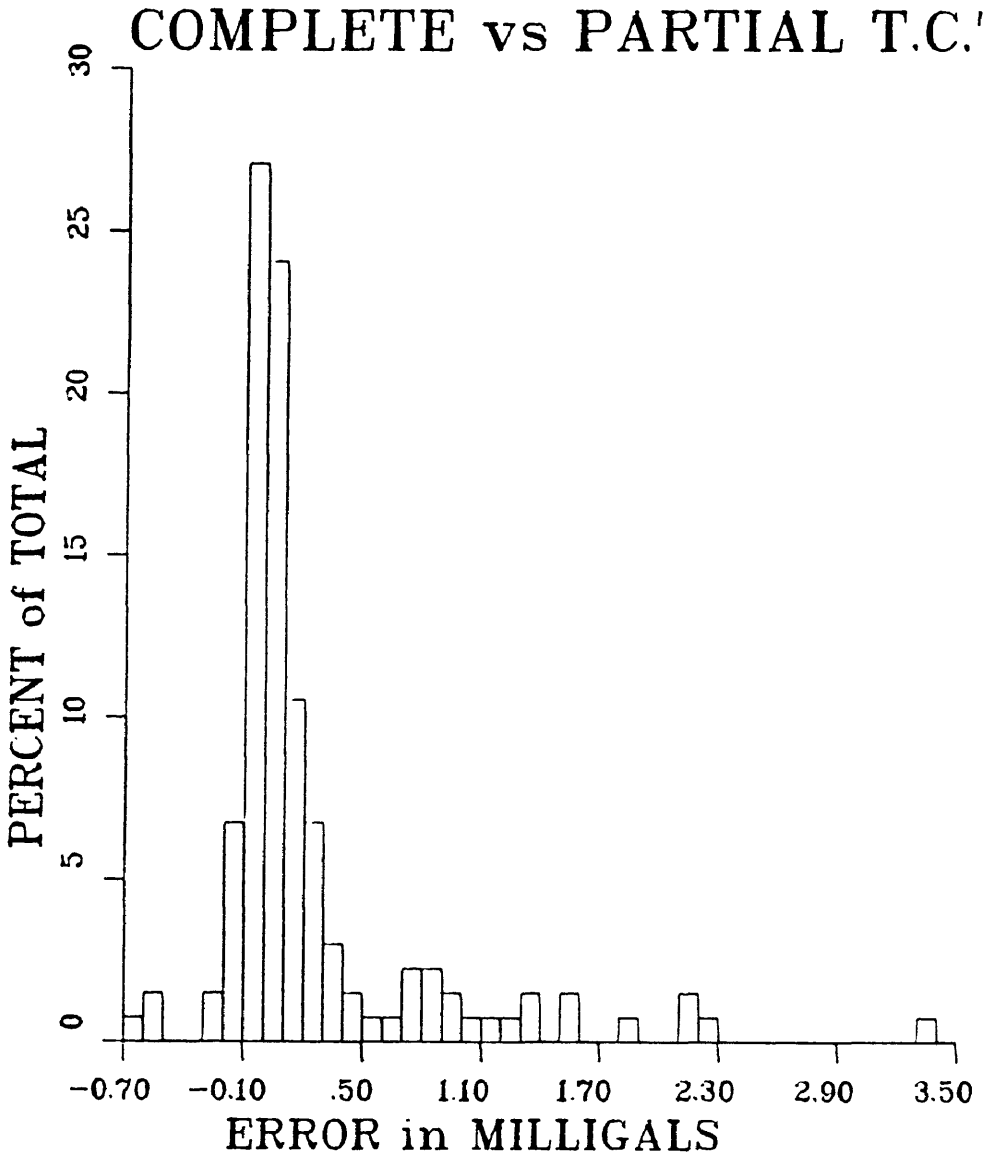

Figure 19. Comparison of complete terrain corrections (this study) with partial corrections (.295 km - 166.7 km) calculated by Plouff's program and 15-second elevation data. Note that 71 percent of all discrepancies fall within $\pm$0.20 mgals.

STANDARDIZATION OF DATA SETS

The data of LaFehr (1966), Kim (1974), and Evernden (1963) were referenced to the datum of Woollard and Rose (1963) and reduced using the 1930 International Gravity Formula for theoretical gravity. As part of this study, these data were referenced to the IGSN-71 datum, and theoretical gravity was recalculated using the 1967 Gravity Formula, accounting for adjustments of -14.46 and ~+11.18 milligals, respectively. As previously mentioned, terrain corrections determined by Plouff's method were re-calculated for the above data using the 15-second elevation data obtained for the present study. No adjustments of any sort were necessary regarding the data of Finn (1981) and Finn and Spydell (1982). Comparisons of terrain corrections for 18 stations common to both the late 60's surveys and 1983 survey were made and are shown in Figure 20.

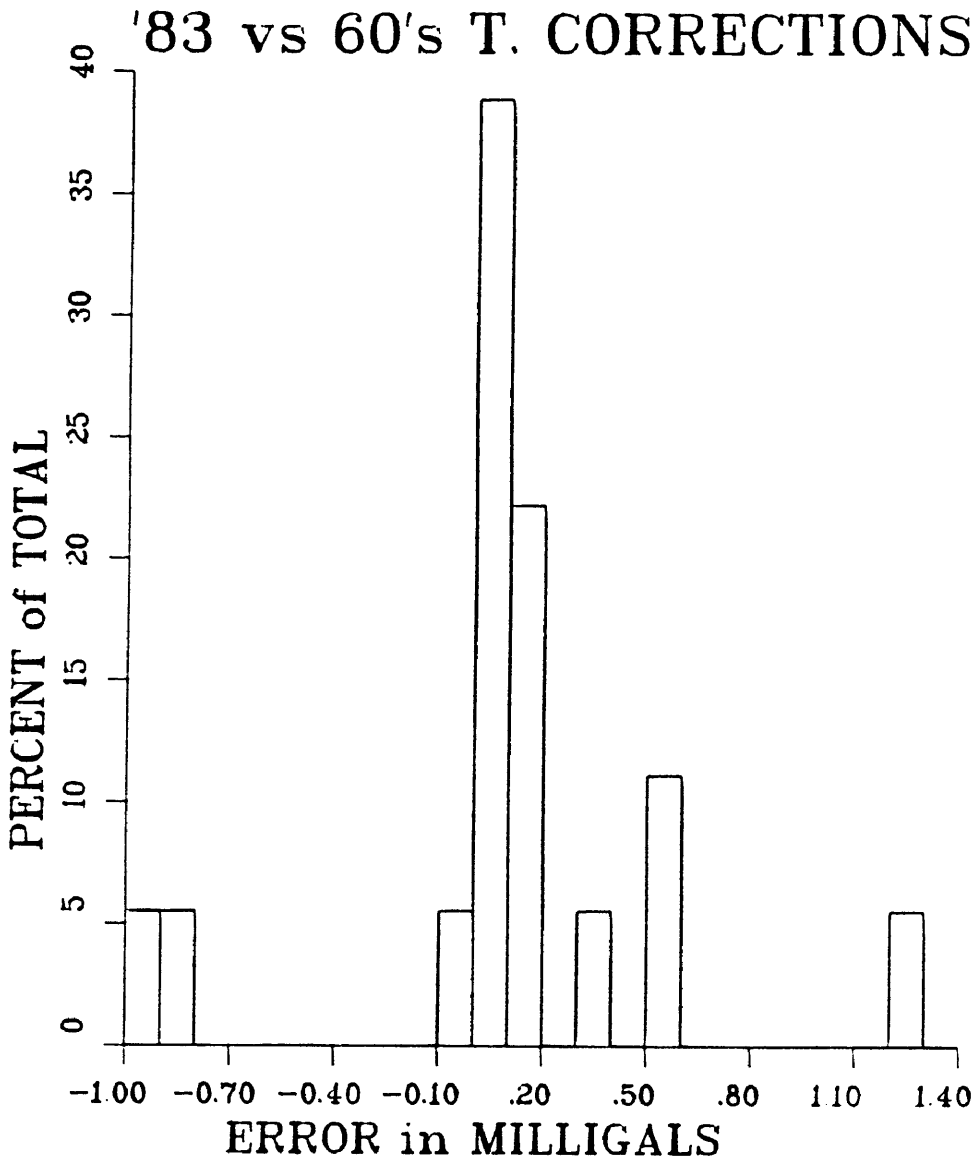

Figure 20. Comparison of total terrain corrections calculated for data of LaFehr (1965) and Evernden (1963) with those of the present study. Note that 67 percent of all comparisons are within $\pm$0.20 mgals.

COMPLETE BOUGUER ANOMALY (CBA) FIELD

Contour maps of the pre-existing CBA data and the augmented 1983 CBA data are shown in Figures 21 and 22, respectively. All data were gridded at 0.5 km spacing, using the program MINC (Webring, 1981), which is based upon the principle of minimum curvature (Briggs, 1974). The gridded data were contoured, using the program TOPO (Smith, 1982).

A comparison of these data is best shown by the profiles in Figure 23.

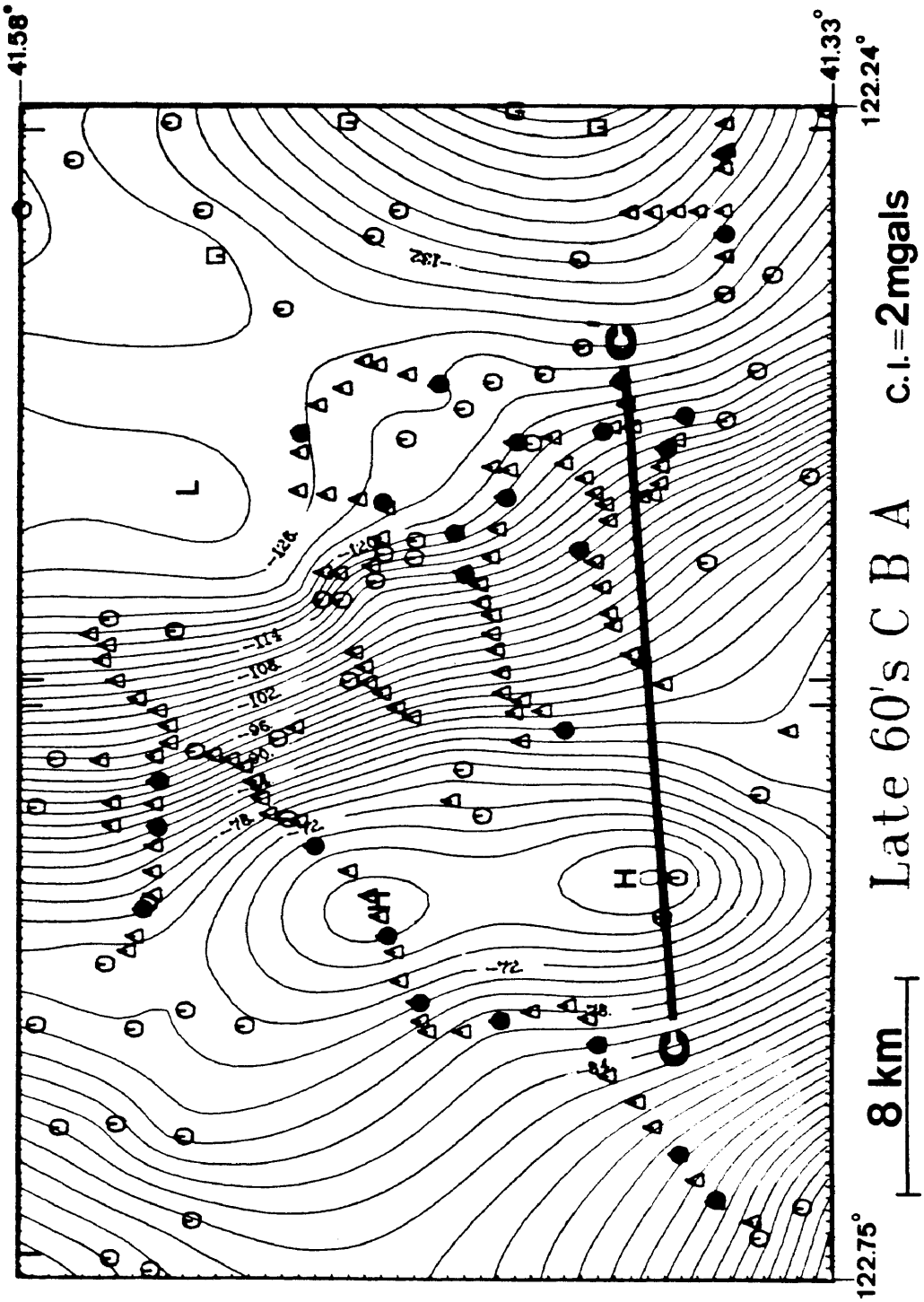

Figure 21. Complete Bouguer anomaly map (Woollard/Rose datum, 1930 Theoretical Gravity Formula), based upon all available data prior to the present study. See Figure 23 regarding profile C-C'.

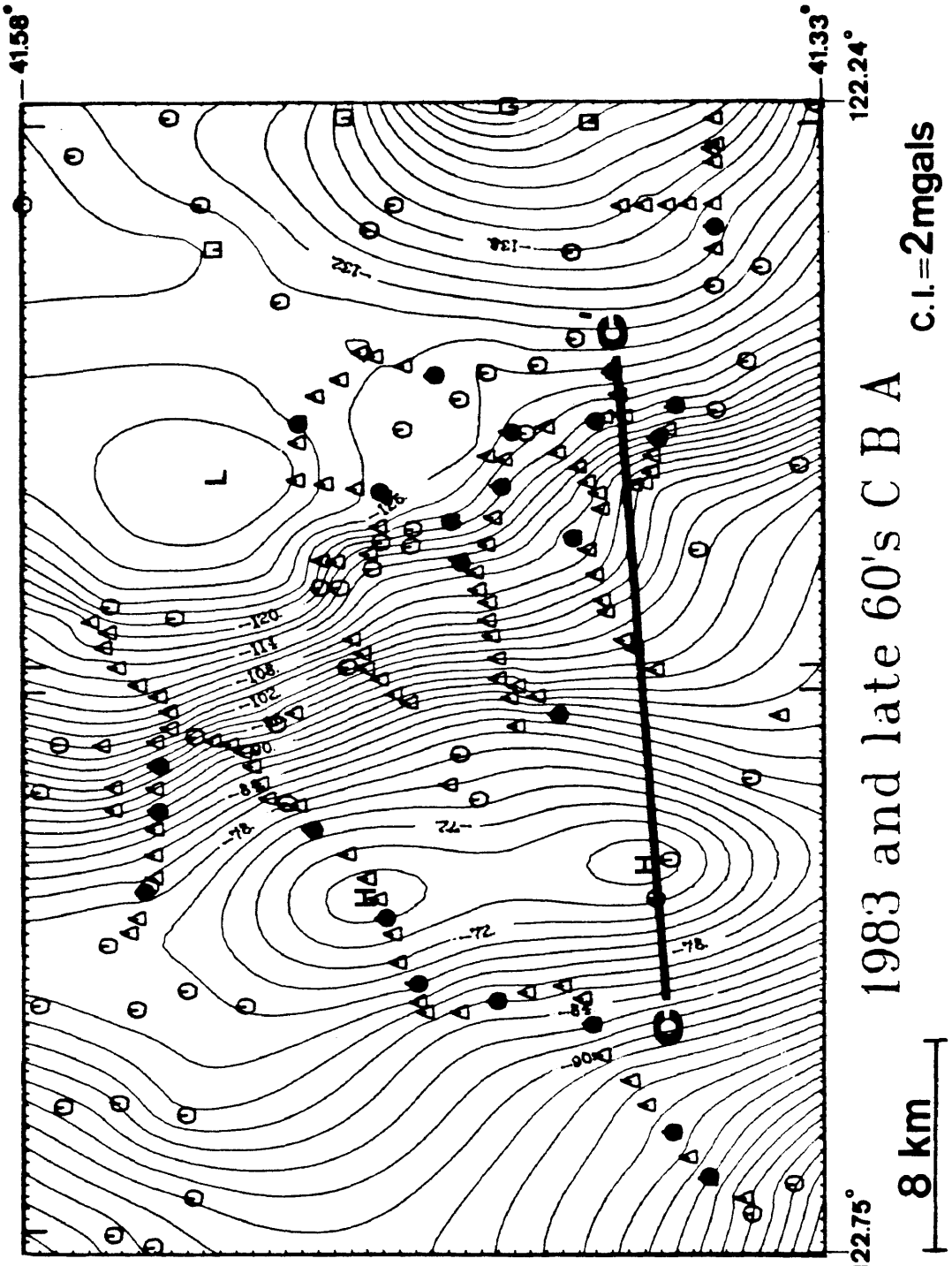

Figure 22. Complete Bouguer anomaly map (IGSN-71, 1967 Theoretical Formula) based upon pre-existing data and 1983 data. Circles represent late 60's stations, squares represent stations of Finn and Spydell, and triangles represent 1983 stations. See Figure 23 regarding profile C-C'.

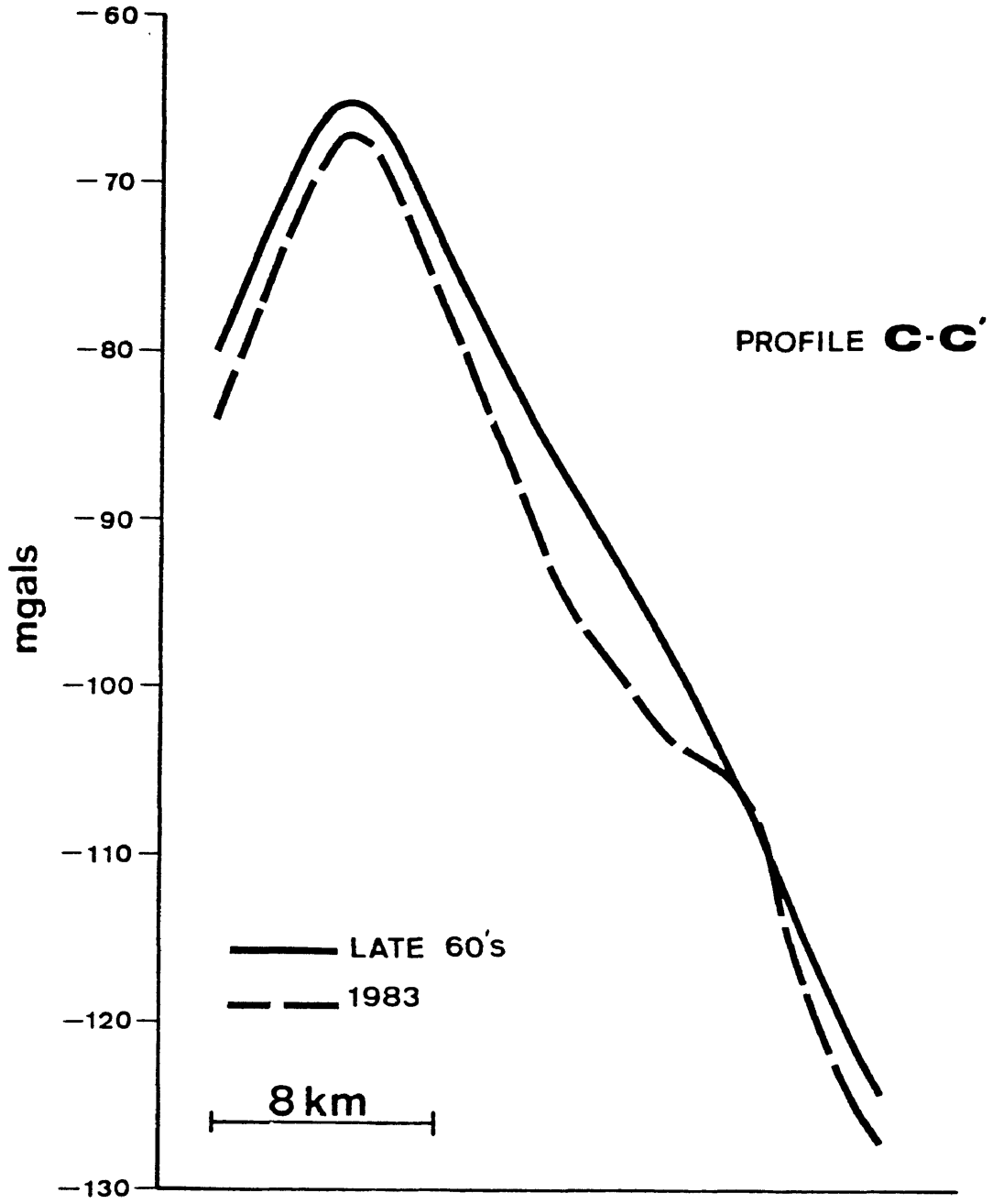

Figure 23. Comparison along profile C-C' of late 60's CBA map with CBA map containing additional 1983 data. The 3.3 mgal difference between the two profiles (best shown along gravity high) is a direct result of the different datums and Theoretical Gravity Formulas used to produce each map.

THE VARIABLE DENSITY PROBLEM

The above CBA data were derived from a constant reduction density of 2.67 g/cc. Wherever actual densities differ from such a reduction density, the CBA data will be inaccurate. The magnitude of the error will be directly proportional to the deviations from the reduction density used. Figure 24 shows a generalized density distribution for the rocks of the study area, based upon Nettleton profiling studies and actual field samples. Table 2 lists densities of various rocks which I gathered and measured.

Figure 24 clearly shows the need to account for the deviations of surface rocks from the standard reduction density of 2.67 g/cc. This can be accomplished in two ways: 1) model standard Bouguer data and account for the deviations from 2.67 g/cc with the appropriate "adjustment body" or, 2) remove from the free-air anomaly the attraction of the variable density terrain model. The latter method uses a combined terrain/Bouguer correction, modified for laterally changing densities. The former method uses "adjustment bodies" that are defined by geometric approximations less accurate than those defined by the variable density terrain model of approach 2. I

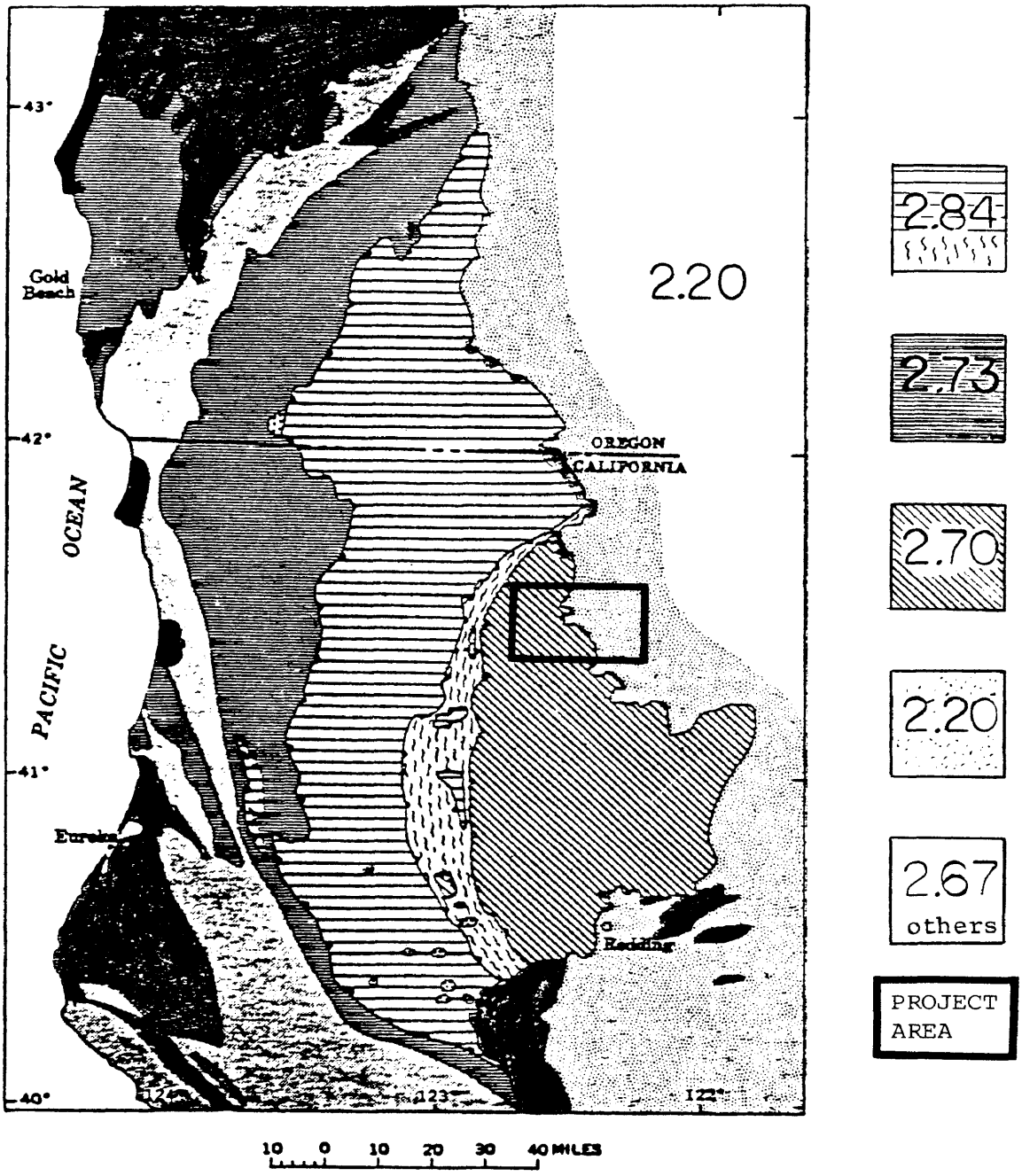

Figure 24. Generalized distribution of surface densities occurring within and around the project area. Sources of density information are: 2.84 g/cc, 2.73 g/cc (Jachens, written communication); 2.70 g/cc (LaFehr, 1966); 2.20 g/cc (Williams and Finn, in press); and 2.67 g/cc based upon the standard density assumption of the U.S.G.S.

Table 2

Rock type	Density (g/cc)	Location (°Lat., °Lon.)
Slate	2.62	41.432, 122.637
Pencil slate	2.40	41.456, 122.637
Chert pebble cgl	2.62	41.523, 122.258
Chert pebble cgl	2.59	41.456, 122.637
Chert	2.51	41.456, 122.637
Limestone (xln)	2.71	41.499, 122.556
Graywacke	2.64	41.456, 122.637
Phyllite	2.55	41.503, 122.526
Actinolite/ Tremolite schist	2.84	41.398, 122.465
Granodiorite	2.67	41.533, 122.255
Granodiorite	2.70	41.344, 122.511
Mafic pumice	1.73	41.429, 122.475
Peridotite	3.18	41.420, 122.515
Peridotite (weathered)	2.38	41.429, 122.475
Met. peridotite	2.94	41.366, 122.723
Met. peridotite	2.65	41.452, 122.505
Met. peridotite	2.58	41.447, 122.542
Met. peridotite	2.62	41.432, 122.637
Met. periodite	2.57	41.432, 122.637
Met. periodite	2.58	41.432, 122.637
Serpentinite	2.61	41.344, 122.511
Serpentinite	2.55	41.432, 122.637
Serpentinite	2.51	41.398, 122.465
Serpentinite	2.54	41.398, 122.465
Serpentinite	2.52	41.429, 122.475

Densities were determined by the following method: 1) dry samples were cored and weighed, 2) same samples were suspended in water and weighed, 3) densities (ρ) were determined, using the equation below.

$$\rho = \frac{W_1}{W_1 - W_2}$$

Where W_1 and W_2 are the weights in air and water, respectively. Weight measurements were made using a Mettler balance with accuracies of ± 0.01 g and -0.05 g for dry and wet samples, respectively.

consider the latter approach to most accurately account for laterally changing densities within the near surface.

An unsuccessful attempt to modify the three-dimensional modeling program of Barnett (1976), so that it could handle the complex bodies of the variable density terrain model, led to the previously described modeling method of approach 1.

ISOSTASY

The accuracy of the data reduced to the complete Bouguer anomaly is largely effected by how well topographic effects are accounted for. Because of this, isostasy must be considered. For instance, a significant portion of the Bouguer low over Mt. Shasta is probably attributable to isostatic compensation; or more specifically, a mass deficiency at depth compensating for the mass excess of the stratovolcano.

LaFehr (1965) used Gauss' theorem to calculate the mass deficiency of Mt. Shasta and concluded that the compensating mass probably exists within the upper 10 km of the crust, suggesting to him localized isostatic compensation.

If a compensating mass occurs at a depth greater than that accounted for in the modeling of residual Bouguer data, its effects must be accounted for elsewhere, namely in the regional trend. According to McNutt (1983), the compensation depth for the Eastern Klamath Mountains is greater than 10 km below sea level and as a result, isostatic effects would be accounted for in the regional Bouguer anomaly shown in Figure 25. Because the isostatic

effects associated with Mt. Shasta probably occur within 0 km - 10 km below sea level, and since the modeling of the residual Bouguer anomalies includes this portion of the crust (Figures 30a and 31), the root of Mt. Shasta will in turn be accounted for.

DETERMINATION OF REGIONAL BOUGUER ANOMALY

Only those bodies occurring within the upper 10 km of the crust are of interest to this study, and as a result, the gravity effects due to deeper causative bodies must be removed from the gravity field.

Using the seismic refraction results of Fuis and others (in press), a cross-section of the subsurface occurring between 10 km and 38 km depth was determined and subsequently modeled in order to calculate the regional Bouguer anomaly (Figure 25). The causative bodies, defined by a significant P-wave velocity change of 0.6 km/sec (see Figure 25), are interpreted as units within the Western Paleozoic and Triassic belt. More specifically, the upper unit is considered to be sedimentary and volcanic, while the lower unit is probably ophiolitic, with assigned densities of 2.75 g/cc and 2.85 g/cc, respectively. The upper unit correlates with a velocity reversal (~0.2 km/sec) occurring beneath the Central metamorphic belt of 2.75 g/cc density (Fuis and others, in press). The ophiolitic lower unit has been

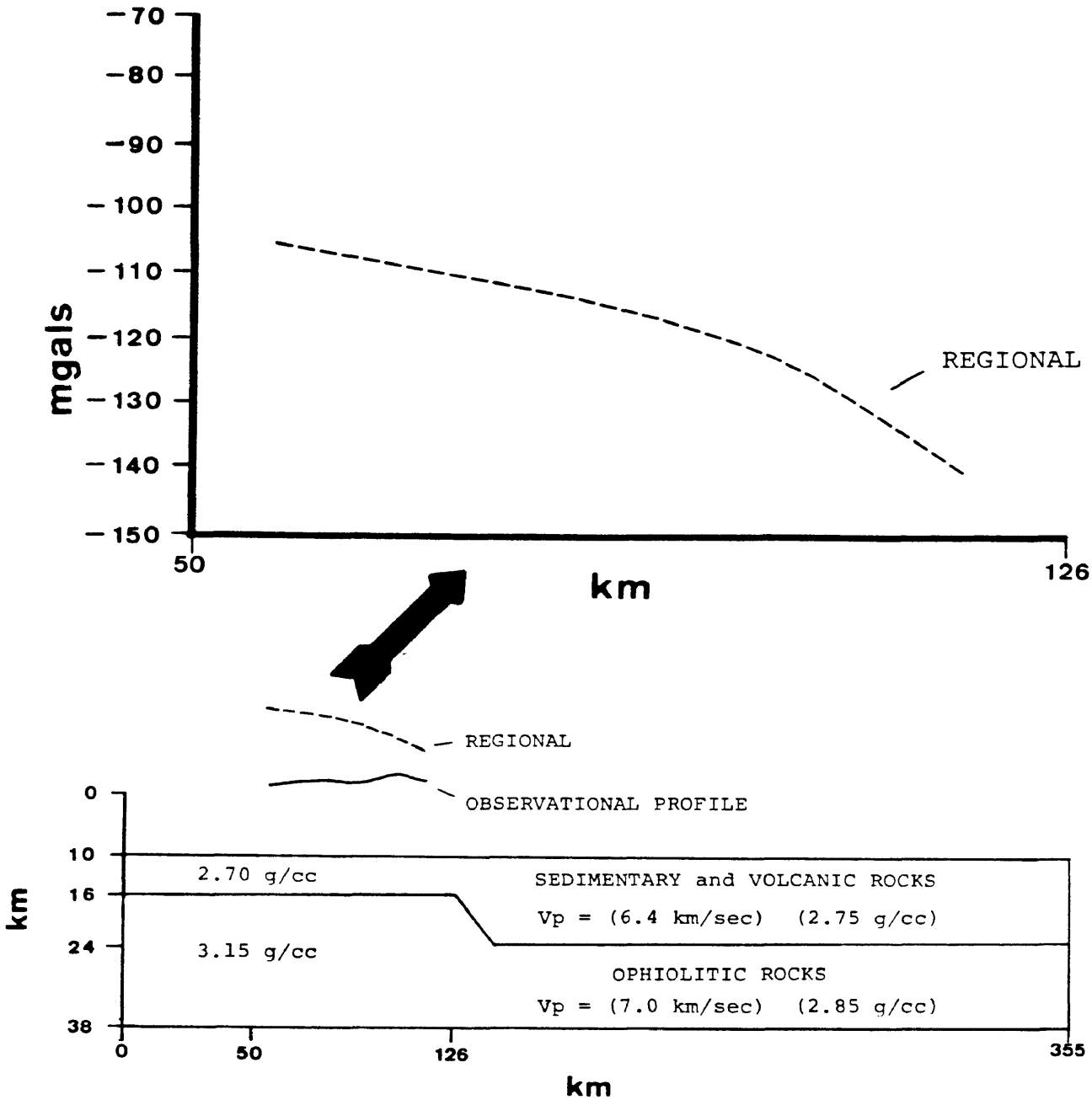

Figure 25. Seismic refraction based cross-section showing bodies that were modeled in order to determine the regional Bouguer anomaly. Density values in parentheses are those based upon P-wave velocities, Vp. Note that the top half of this figure is simply an enlargement of the regional shown below it.

determined by Ando and others (1983) to consist of gabbro, diabase, pillow basalts, and tectonic harzburgite. An average density of the ophiolitic unit could be ~3.05 g/cc (Daly, 1966), assuming equal proportions of these constituents. Obviously, this value could be higher or lower, depending upon the relative abundances of the rock types. In this study, densities of 2.70 g/cc and 3.15 g/cc were assigned to the upper and lower units, respectively, on the basis of the work by Ando and others (1983). Therefore, a density contrast of -0.45 g/cc was used to determine the regional Bouguer anomaly shown in Figure 25. Other density contrasts were also used (see Figure 26) to determine whether or not densities less than 3.15 g/cc could be assigned to the ophiolitic unit. A preliminary model with a cross-section ranging from the surface to the base (38 km) of the regional bodies was made, using the density information of Fuis and others (in press). The calculated gravity of this model was then determined, using various density contrasts for the regional bodies. The regional due to a -0.45 g/cc density contrast yielded gravity values of the same magnitude as those of the complete Bouguer field, as shown in Figure 26. For this reason, the regional Bouguer gravity based

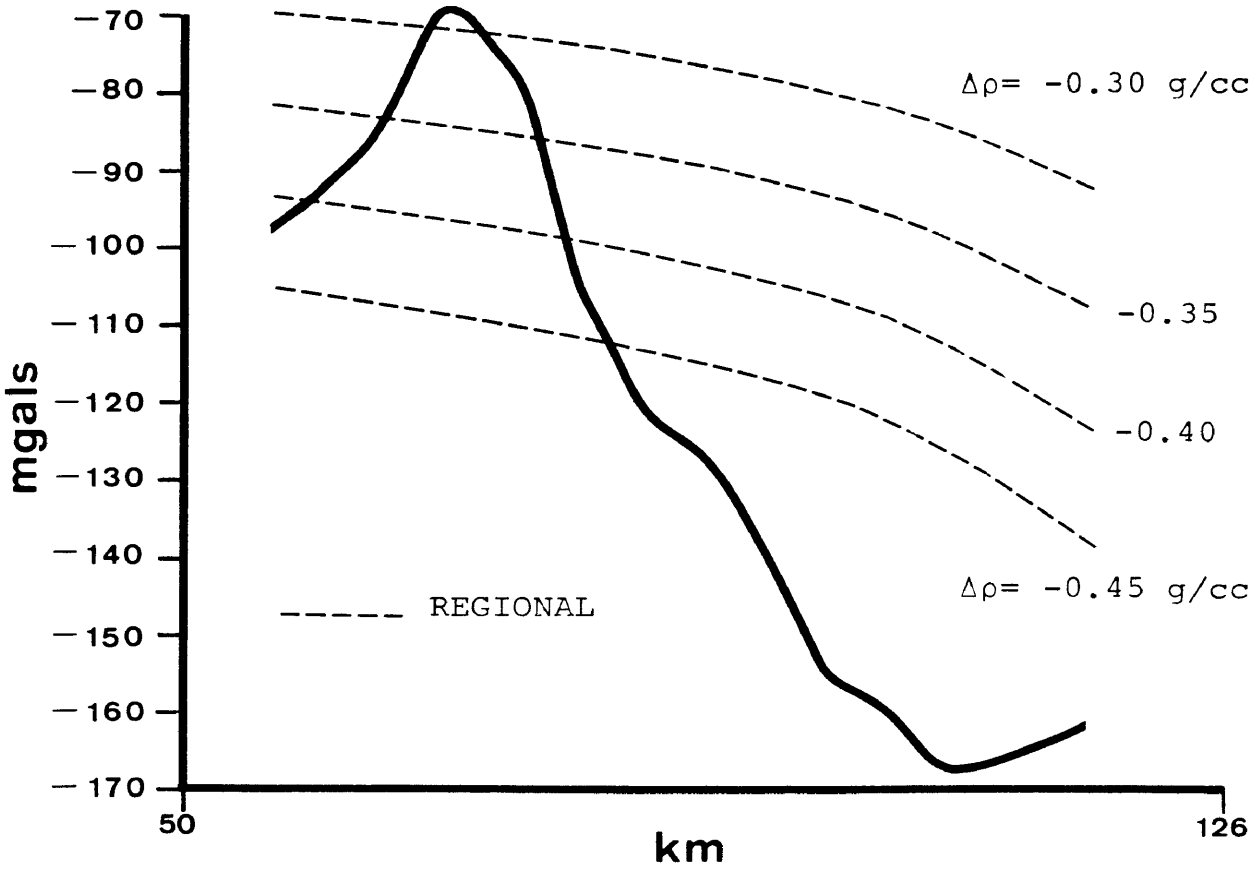

Figure 26. Complete Bouguer anomaly along profile A-A'. Regional Bouguer anomalies, at various density contrasts are shown.

upon a -0.45 g/cc density contrast was used in this study. This smoothly changing regional of deep origin was then removed from the complete Bouguer data to yield a residual Bouguer anomaly.

Two profile lines, crossing the gravity gradient between the Eastern Klamaths and the Cascades, were chosen (Figure 27). Profiles of the complete Bouguer gravity and the regional gravity for lines A-A' and B-B' are shown in Figures 26 and 28, respectively.

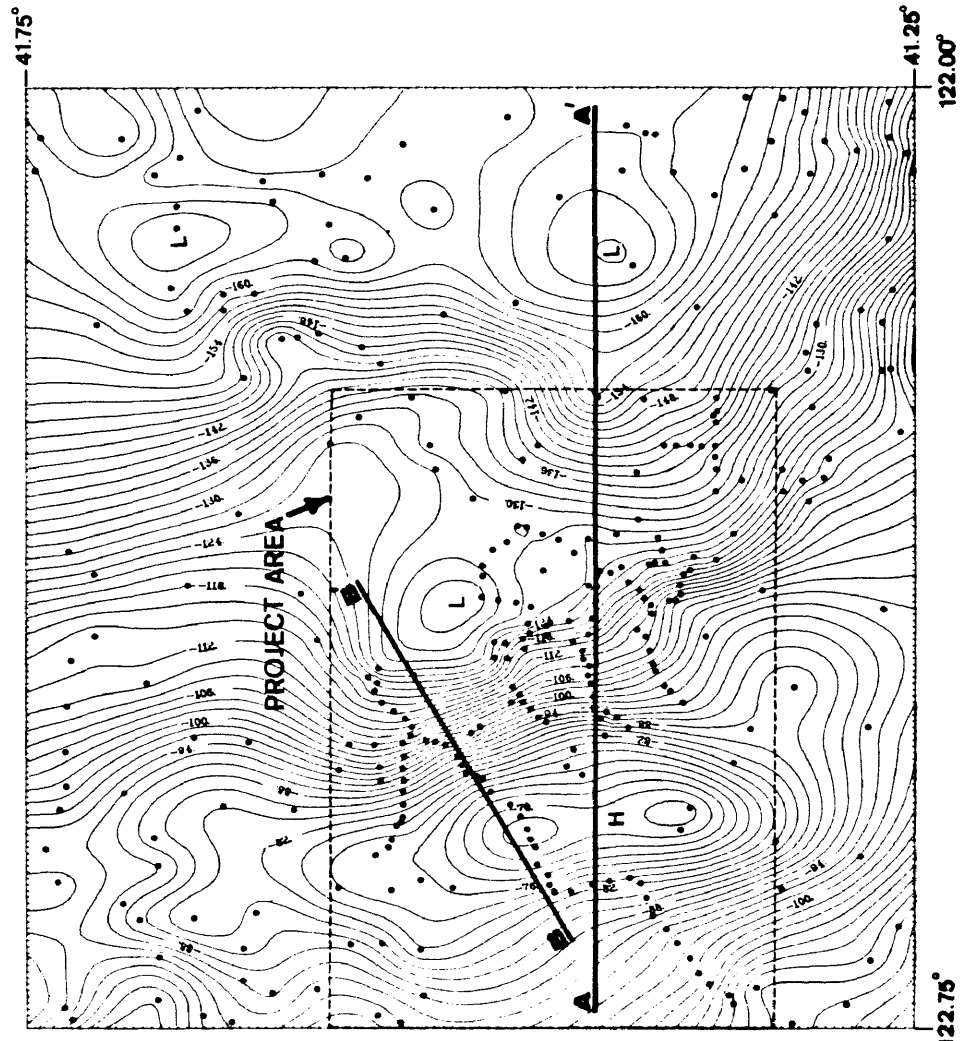

Figure 27. Lines of profile for model sections A-A' and B-B'. Gravity stations are represented by solid circles.

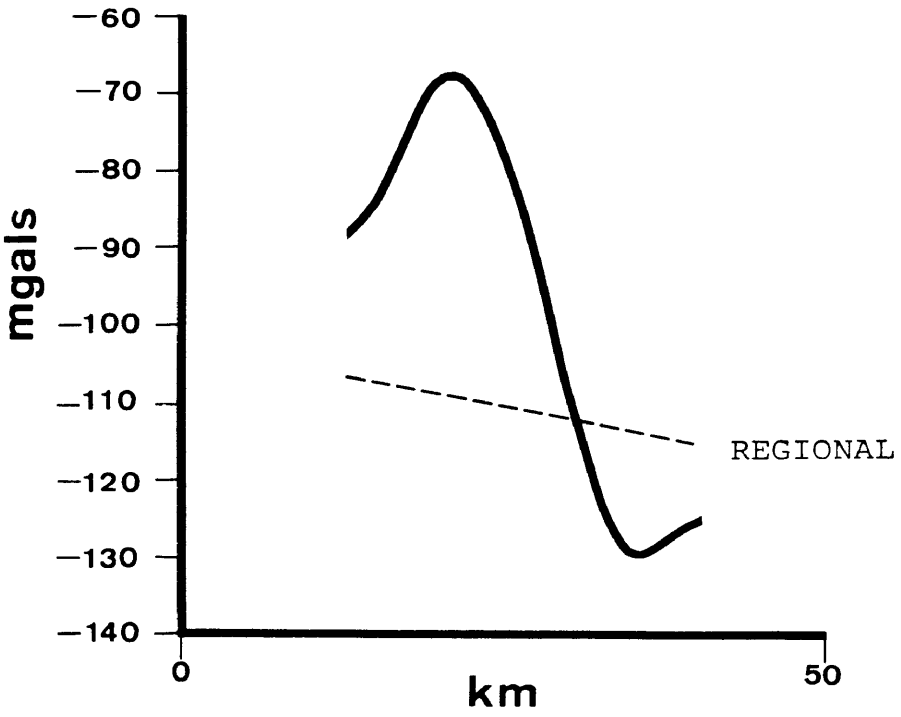

Figure 28. Complete Bouguer anomaly along profile B-B' with calculated regional Bouguer anomaly.

COMPUTER MODELING OF RESIDUAL ANOMALIES

The three dimensional modeling program of Barnett (1976) was used to determine models of the subsurface geology. Briefly, this program uses as input two or three dimensional bodies; each surface of which is divided into triangular facets. The flux of F for each facet is calculated, as shown below.

$$1) \quad \text{Flux of } F = \iint_s F \cdot \hat{n}\, ds \;, \quad F = \frac{\hat{M}}{R},$$

where s is the surface of the facet over which integration takes place, $\hat{n}$ is the outward-directed unit vector normal to the surface element ds, $\hat{M}$ is the unit vector specifying the direction of measurement of the gravity field, and R is the distance from the observation point to the surface of the triangular facet.

The fluxes of all the facets are then summed to yield the total flux (of F) for the entire closed surface of the body. The total fluxes of all bodies are then summed and finally multiplied by the gravitational constant (G) and the body density (ρ), to yield the gravitational attraction, g_m.

$$2)\ g_m = G\rho \sum_{1}^{N} B \quad , \quad B = \sum_{1}^{P} \left(\iint_s F \cdot \hat{n}\ ds \right)$$

where B is the total flux of the surface enclosing a body, N is the total number of bodies, P is the total number of facets per body, and g_m is the gravitational field component in a given direction of measurement. Since the gravity meter measures only the vertical or z-component of the earth's gravitational field, g_m always refers to g_z, the gravitational component in the z direction.

Using the divergence theorem (3), the above surface integral approach can be used to calculate the gravitational attraction of a body of a given volume.

$$3)\ \iint_s F \cdot \hat{n}\ ds = \iiint_v \nabla \cdot F\ dv \qquad \text{DIVERGENCE THEOREM,}$$

where v is the volume of a body having a closed surface s.

A useful feature of Barnett's program is that the observational surface need not be a level horizontal plane.

As with any modeling strategy, certain constraints must be determined in order to minimize the ambiguity of the modeling process. The results of the seismic

refraction study performed by Fuis and others (in press) provided such a constraint, where density information down to 38 km below sea level was provided. Compressional wave velocities were converted to densities, using the method of Birch (1960, 1961). In addition to the above density information, a geologic bias was also employed; namely that a graben bounding fault (Blakely and others, in press) separates the Klamath Mountains from the Cascades.

Two-dimensionality was assumed for the elongated rock units comprising the Klamath Mountains and Cascade Range provinces modeling of the residual Bouguer profiles. As described below, three dimensionality was otherwise required. Invariably, subsurface densities will deviate along strike from those assigned to the cross-section being modeled, thus contributing to inaccuracies in the density values assigned to the final model. Two-dimensional modeling of bodies with upper surfaces defined by the topography will also generate errors proportional to the deviation of the two-dimensional surface from the actual three-dimensional one. Consider the errors associated with the two-dimensional assumption to account for probably no more than a $\pm$0.10 g/cc uncertainty in the density values of the final model.

The occurrence of the rock types pertinent to this study are shown in Figure 29, a modification of a preliminary map recently compiled by Wagner and others (in press). Also shown are the locations of profiles A-A' and B-B'.

Profile A-A'

A model of the subsurface geology that could produce the residual Bouguer profile along A-A' is shown in Figure 30a. Seventy-seven percent of the calculated values are within 1 milligal of the actual gravity values. Of the 26 bodies used in this model, seven were three-dimensional; namely the surface bodies of Mt. Shasta, Mt. Shastina, Ash Creek Butte, Whaleback Mountain, and Black Butte, as well as the subsurface gabbroic intrusive (3.05 g/cc) in the Klamath Mountains, and the silicic intrusive (2.70 - 2.67 g/cc) beneath Mt. Shasta. A density of 2.20 g/cc was given the predominantly pyroclastic bodies of Mt. Shasta, Mt. Shastina, and Whaleback Mountain, and a density of 2.55 g/cc assigned to the more competent bodies of Ash Creek Butte and Black Butte. Each surface or topographic body was defined by two or more circular slices (representing cross-sectional cuts in plan view),

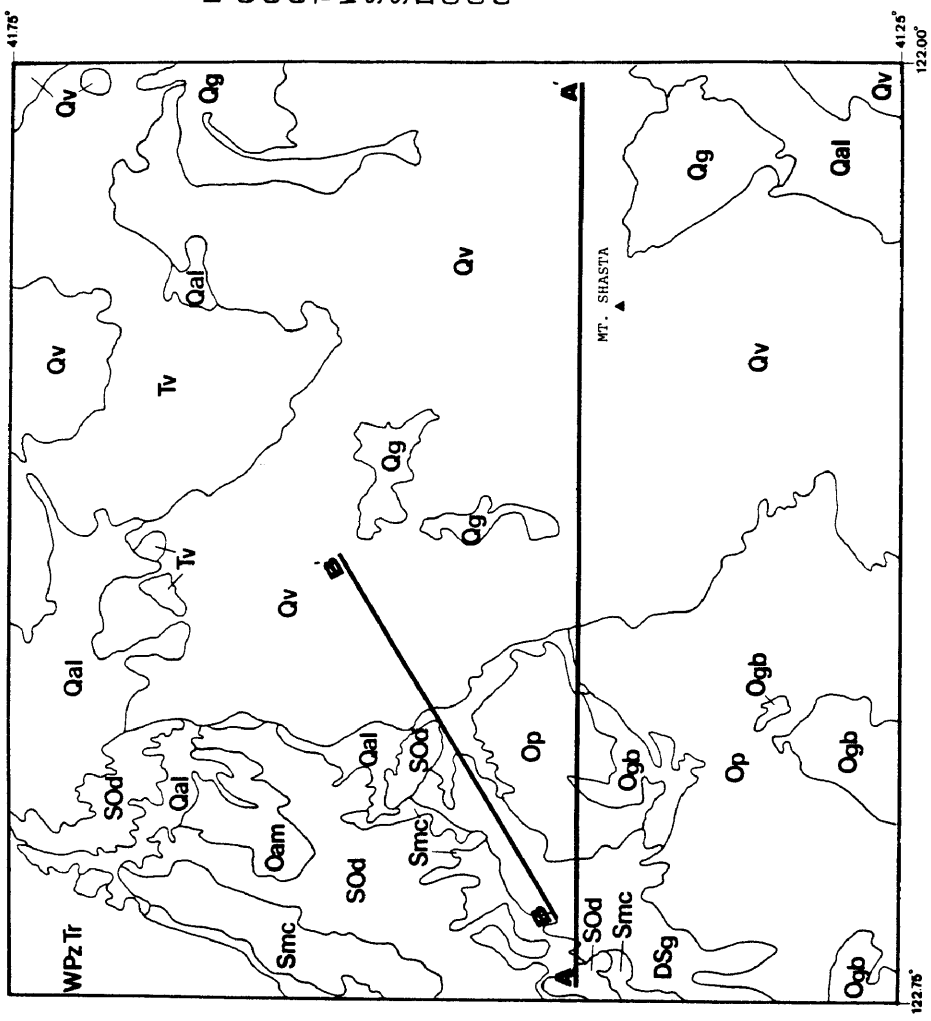

Figure 29. Generalized geologic map of project area and vicinity, with locations of profile lines A-A' and B-B'. Modified after Wagner and others (in press).

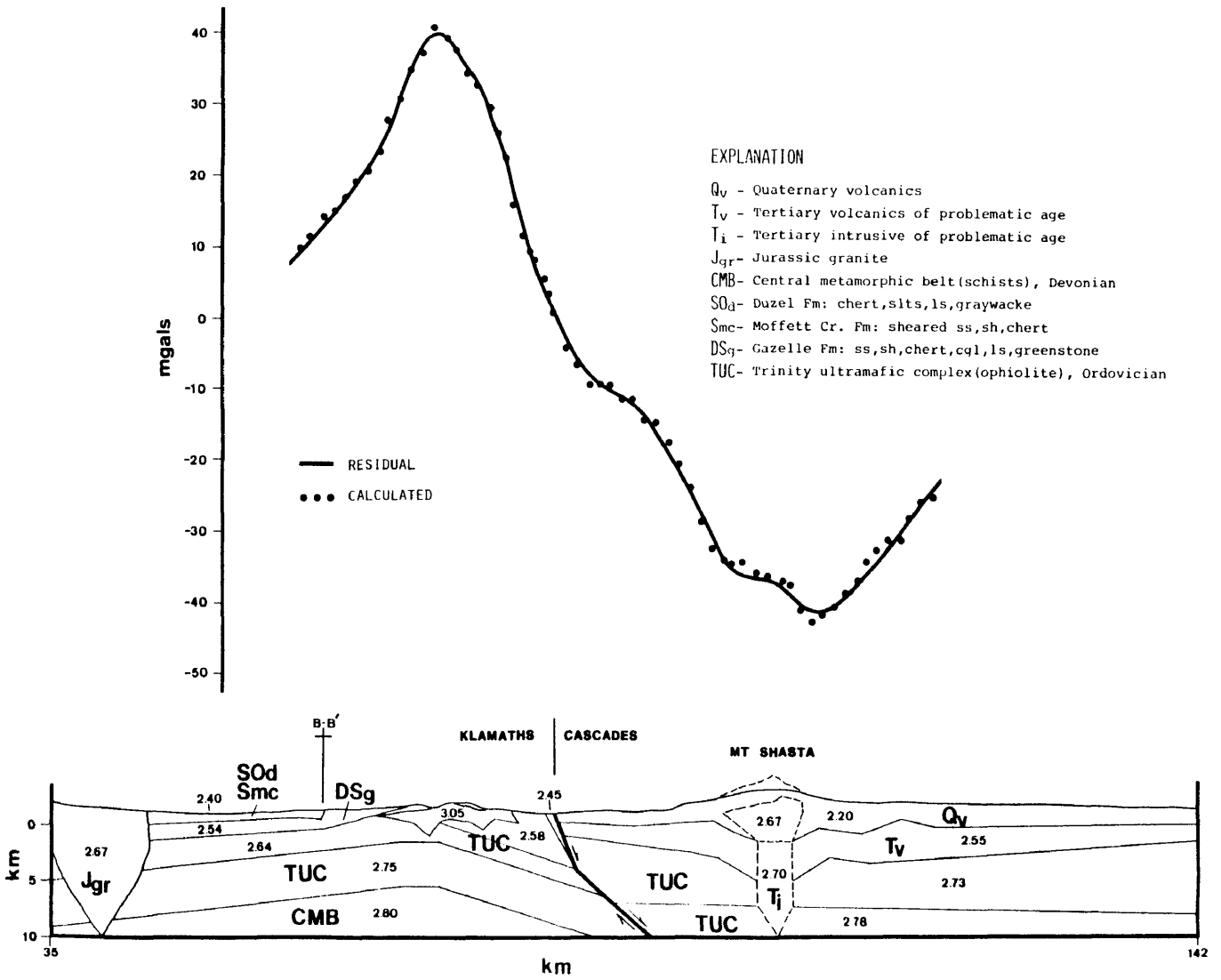

Figure 30a. Residual Bouguer anomaly along profile A-A', with associated structural model. Dashed lines represent features centered 2.5 km south of section. See Figure 30b for a plan view representation of the three-dimensional intrusive bodies.

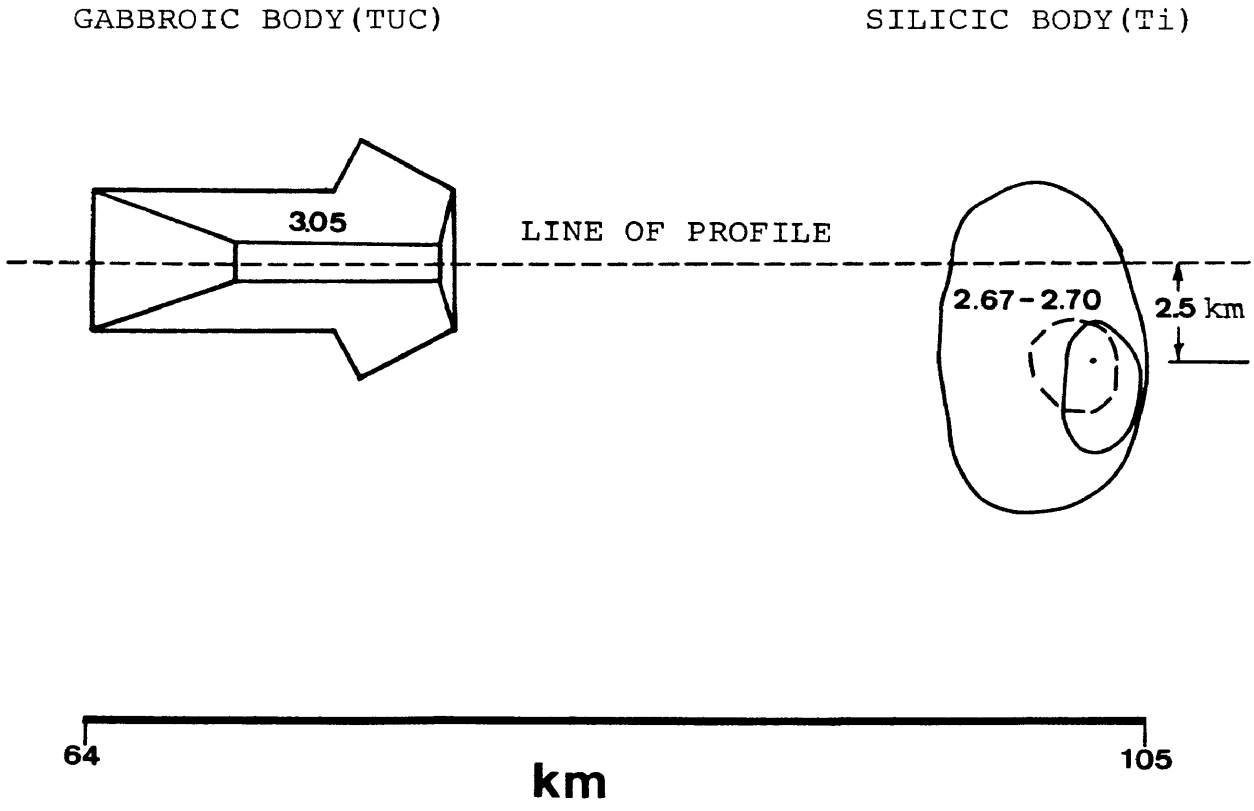

Figure 30b. Plan view of three-dimensional intrusive bodies used in the model for profile A-A'.

that when connected yielded a conical shape closely approximating the three-dimensional form of the body. These topographic bodies were modeled in order to account for the improper reduction density (2.67 g/cc) applied to them in the Bouguer and terrain corrections. Accounting for such overcorrections greatly improves modeling accuracy. For instance, the combined Bouguer/terrain corrections for a gravity station at the summit of Mt. Shasta are 352 mgals and 290 mgals, when using reduction densities of 2.67 g/cc and 2.20 g/cc, respectively. Therefore, in this case, a 62 mgals reduction error is accounted for when the topographic body of Mt. Shasta is incorporated into the model!

Profile B-B'

A model of the subsurface geology that could produce the residual Bouguer profile along B-B' is shown in Figure 31. Ninety-three percent of the calculated values are within 1 milligal of the actual gravity values. Of the 13 bodies used in this model, only one was three-dimensional; namely the gabbroic intrusive (3.05 g/cc) in the Klamath

Mtns. Three-dimensional topographic bodies were not modeled, as they occurred at sufficient distances from the profile to have negliglble effect.

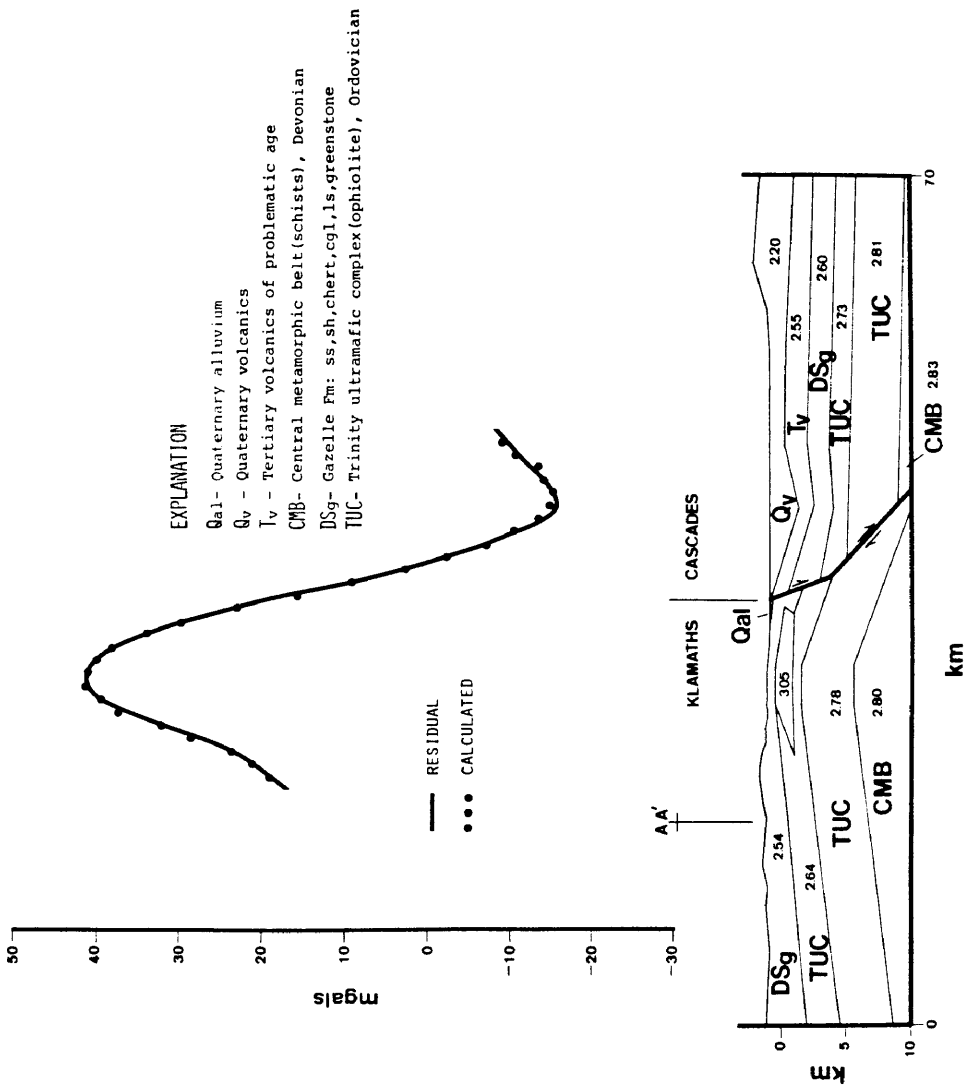

Figure 31. Residual Bouguer anomaly along profile B-B', with associated structural model. The three-dimensional intrusive body extends 5.0 km in and out of the plane of section.

INTERPRETATION OF MODELING RESULTS

Gravity data modeling and interpretation is inherently ambiguous (Skeels, 1940) because the gravitational field cannot define a unique causative mass distribution. Nettleton (1940) elucidated this point when he stated:

> "The interpretation of a gravity map in terms of a definite mass distribution below the surface is never unique on the basis of gravity information alone. This results from the fact that a given gravity distribution can be produced by a variety of mass distributions. Therefore, any mass distribution or geologic condition that is given as a solution for the cause of a given gravity distribution depends upon additional control other than gravity."

Fortunately, the recent seismic refraction study of Fuis and others (in press) provided additional control of the subsurface geology, in terms of body depth, geometry and density. In the present study, the initial model was essentially the seismic refraction model. The final model represents a best fit between the available geologic, seismic and gravity data. Because the seismic refraction study provided good subsurface control, the models of the present study are relatively complex, but justifiably so.

The following interpretations are concordant with the regional geologic framework described in the literature and explain the modeling results.

Profile A-A' (see Fig. 30a)

The subsurface section of Paleozoic units represents ophiolitic terranes, probably underthrusted by the Western Paleozoic and Triassic plate during the Nevadan orogeny. As previously mentioned, the latter unit represents the deep source producing the broad regional field that was removed to derive the residual Bouguer anomaly.

The present configuration of the ophiolitic terranes strongly suggests a history of underthrusting, since the Devonian Central metamorphic plate is shown beneath the Ordovician Trinity ophiolite. The relationship of the Trinity ophiolite with the eugeosynclinal deposits of the Ordovician-Silurian Duzel Formation, Silurian Moffet Creek Formation, and the Silurian-Devonian Gazelle Formation is probably best described as follows: Prior to subduction of the Trinity ophiolite, the Duzel and Moffett Creek sediments were shed from a volcanic arc close to the craton. With continued arc activity, sediments representing the Gazelle Formation were then deposited on

top of the Duzel and Moffett Creek Formations. Upon collison of the oceanic Trinity ophiolite with the above sequence, the Duzel and Moffett Creek Formations were thrust over the younger Gazelle Formation. The Moffett Creek Formation has been mapped as a probable tectonic melange (Wagner and others, in press) which supports the above overthrusting model. The densities of the Duzel, Moffett Creek and Gazelle Formations, as well as that of the Central metamorphic belt differ from those of Fuis and others (in press) by +0.11 g/cc, -0.10 g/cc, and +0.05 g/cc, respectively. Ultimately, the Trinity ophiolite was thrust under the lesser dense sedimentary sequence to produce the present-day configuration. The antiform nature of this structural section reflects the eastwardly directed compressional stresses that were acting upon the area at least since Nevadan time. In response to such forces, the relatively competent units of this section buckled upwards into their present form.

Emplacement of the Jurassic granite belt mapped by Wagner and others (in press) was probably related to subduction of the Western Jurassic plate beneath the western edge of the previously accreted Western Paleozoic and Triassic plate. This granitic belt was probably

formed when the subducted oceanic plate reached sufficient depth to become molten and migrate upwards through the crust. Back arc (?) extension led to normal(?) faulting, with as much as 6,500 feet of downdropping of the section east of the fault (Figure 30a). This fault has been active probably since mid-Cenozoic time.

In the upthrown section, the seemingly low densities of the Trinity ophiolite, 2.64 g/cc, 2.58 g/cc, and 2.45 g/cc, are primarily due to hydration (metamorphism) of peridotite into serpentinite, with the latter having considerably lower densities (see Table 2). The densities of 2.64 g/cc, 2.58 g/cc, and 2.45 g/cc differ from those of Fuis and others (in press) by +0.06 g/cc, -0.13 g/cc, and -0.26 g/cc, respectively. According to Bowen's reaction series, Ophiolitic rocks occur first and in turn erode rapidly. It is therefore conceivable that fracturing does occur to a significant degree within the Trinity ophiolite, and may have contributed significantly to the reduction of its bulk density, as best evidenced by the 2.45 g/cc sliver adjacent to the fault zone (Figure 30a).

The 3.05 g/cc density of the gabbroic body was based upon values in Daly (1966), with the assumption that the gabbroic rocks underwent little or no hydration. Since

they were mapped (Wagner and others, in press) as non-serpentinized gabbro, this assumption is probably a valid one. I think that the gabbroic body formed within a steady-state magma chamber associated with the early Paleozoic spreading center that produced the ophiolites discussed in this section. Therefore, this body, probably of Ordovician age, was passively transported along with the Trinity ophiolite to its present location.

The downthrown section reveals the entirely different and much later Cenozoic activity of the Cascade Range province. At the close of the Miocene (Williams, 1949), upward migrating magma (associated with the subducting Gorda plate) reached the location of the intrusive body beneath Mt. Shasta (Figure 30a). It is thought by Blakely and others (in press) that a fault similar to the one in the model (Figure 30a) may extend to even greater depths, and in turn provide an avenue of least resistance through which upward migrating magma could rise. Early eruptions produced low viscosity mafic lava flows that coalesced to form a broad, gently sloping terrain. With ongoing time, the silica content increased, leading to the explosive eruptions that ultimately created the Cascades stratovolcanoes, such as Mt. Shasta about 100,000 y.b.p.

The units with densities of 2.20 g/cc and 2.55 g/cc probably represent interlayered flows and pyroclastics, with the lower unit more compacted and therefore of higher density. The density of 2.20 g/cc differs from that of Fuis and others (in press) by -0.05 g/cc, whereas no difference exists regarding 2.55 g/cc. A study by Williams and Finn (in press) using Nettleton profiling, yielded a 2.20 g/cc density for Mt. Shasta.

The overall geometry of the downthrown section (Figure 30a) is in marked contrast with that of the upthrown section. First, the orientation of the Trinity ophiolite is near level, as opposed to the 17^{o} eastward dip of its upthrown counterpart. This could be attributable to 1) normal faulting that dropped the ophiolitic section down, and 2) subsequent Miocene uplift of the Cascade Range (Williams, 1949) that rotated and raised the downthrown section to its present attitude. Finally, a broad volcanic basin, with a much smaller superimposed basin, exists on top of the down-dropped ophiolitic section. The small volcanic basin (centered about the intrusive) is likely to be the shallow compensating mass beneath Mt. Shasta, and is interpreted to be a collapse caldera (O'Brien, personal communication).

It is conceivable then that the avalanche debris deposits described by Crandell and others (1984) were associated with the tremendous eruptions that ultimately caused collapse of the magma chamber beneath ancestral Mt. Shasta.

The down-dropped equivalent of the 2.58 g/cc and 2.64 g/cc section of the Trinity ophiolite was assigned a density of 2.73 g/cc, representing a maximum increase of +0.15 g/cc. The down-dropped equivalent of the 2.75 g/cc section of the Trinity ophiolite was assigned a density of 2.78 g/cc, or a +0.03 g/cc increase. In lieu of the inevitable compaction of these down-dropped units by the overyling volcanic section, it is conceivable that highly metamorphosed peridotites could have increased in density by 0.15 g/cc or 6 percent. The relatively smaller (1 percent) density increase in the lower half of the Trinity ophiolite is plausible, since a rock less affected by metamorphism could be less affected by compaction.

Fault Orientation (see Fig. 32)

The orientation of the normal (?) fault shown in the model yields calculated gravity values that best fit the actual gravity gradient. When the upper part of the fault

is made vertical, the calculated gravity values agree less favorably with the actual data. The better fitting fault orientation (shown in left half of Figure 32) strongly suggests listric normal (?) faulting. Determining the most plausible model to account for this steep gravity gradient is one of the primary goals of this study.

Profile B-B' (see Figure 31)

The cross-sectional model for this profile very closely parallels the model for profile A-A', except for the following significant differences: 1) the sedimentary section entirely overlies the ophiolitic section throughout the extent of the model and in turn is found on the downthrown side, 2) other than the passively emplaced gabbroic body, no igneous intrusives occur, 3) the normal (?) fault in the B-B' model occurs ~6 km closer to the crest of the antiformal structure, and 4) the Trinity ophiolite in the B-B' model has a constant thickness of ~6 km, whereas in the A-A' model its thickness varies from ~6 km to ~10 km.

All correlative units between the two models have the same densities, with the exception of the lower half of the Trinity ophiolite, where a difference of +0.03 g/cc is

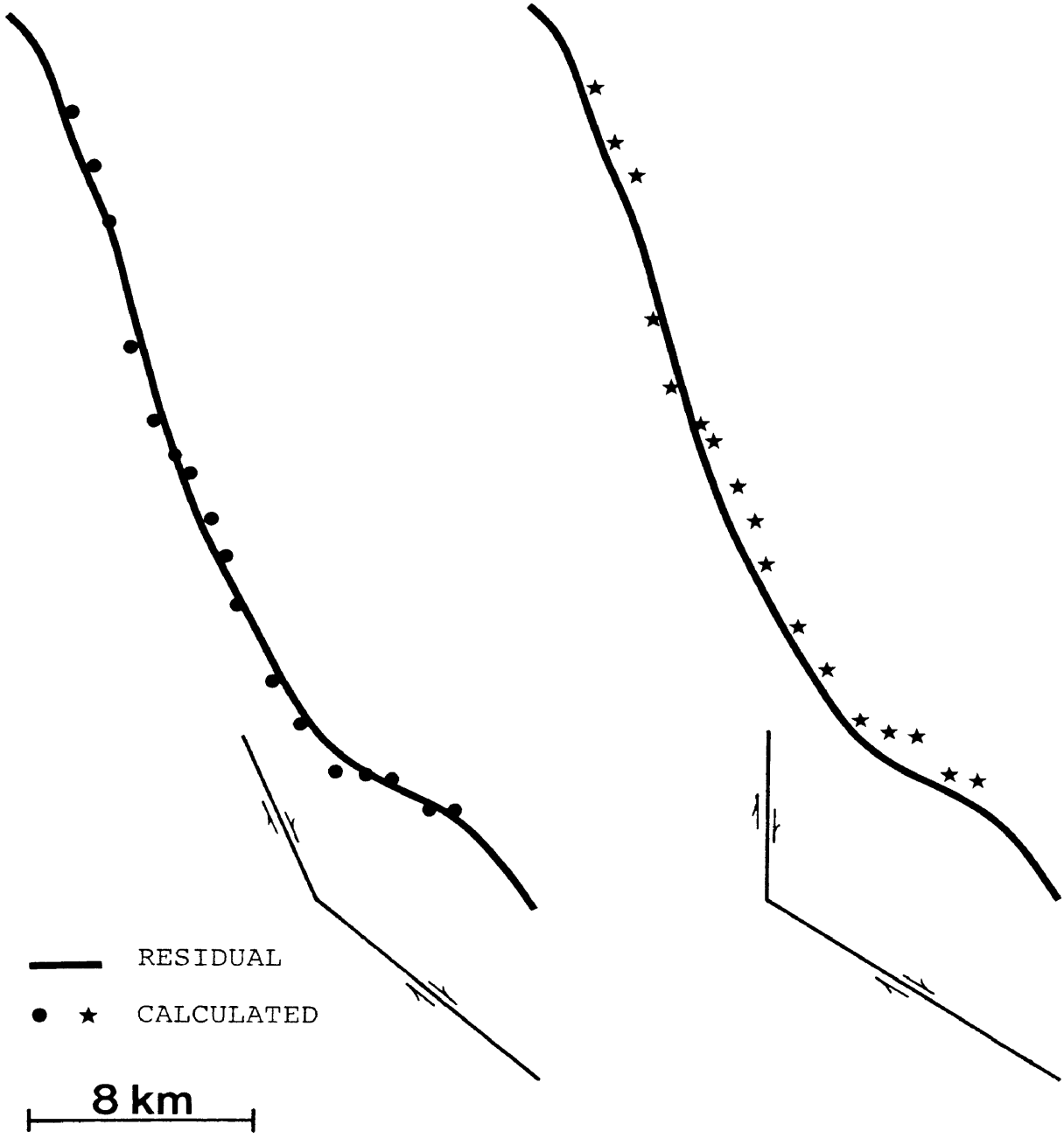

Figure 32. Comparison of effects of different fault angles upon calculated gravity. The configuration on the left of this figure was used in the structural models.

found. The downthrown counterpart of the sedimentary section also underwent compaction (in the same manner as the other units), with a density increase of 2.5 percent.

A prominent structural low occurs in the downthrown side of the model (Figure 31), and is more than likely a remnant of the previously described broad volcanic basin. The geomorphological expression of this structural low might be related to the topographic low occupied by Lake Shastina directly above.

CONCLUSIONS

In areas of rugged topography, terrain corrections are more accurately calculated when using methods other than the traditional approach of Hammer (1939). Terrain effects within Hammer zones A-D and E-F, are best determined using the manual method of Sandberg (1958) and the computerized method of Krohn (1976), respectively. The outer zones (.895 km - 166.7 km) are more accurately determined using the computerized method of Plouff (1977), when an accurate digital elevation model is used. These methods yield complete terrain corrections with an estimated 7% error, whereas the manual method of Hammer is estimated to have a 17% error. Additionally, the Sandberg/Krohn/Plouff approach to terrain corrections is considerably faster and less labor intensive than that of Hammer.

Partial terrain corrections (2.95 km - 166.7 km), using an accurate, unaliased digital elevation model and the program of Plouff, appear to be of sufficient accuracy if 1) the desired contour interval of the data is coarse (i.e., 5 milligals or greater), and/or 2) the anomalies of interest are deeper, broader features, unaffected by errors as great as 3.50 milligals. The savings in time,

when using this partial terrain correction approach, is significant and warrants its consideration.

Analyses of the models presented in this study enable the following principal conclusions. The Trinity ophiolite ranges in thickness from 6 km - 10 km, and has undergone (throughout the body) increasing amounts of serpentinization with depth. Beneath the Eastern Klamath Mountains, the Trinity ophiolite and the underthrusted Central metamorphic belt comprise an antiformal structure with a maximum dip (eastward) of 17^{o}. Within this structure, the minimum depth to the base of the Trinity ophiolite is ~6 km below sea level. This antiformal structure, the source of the gravity high occurring over the Eastern Klamath Mountains, probably extends northward beneath the early Paleozoic sedimentary section.

Though it has not been mapped, a major listric normal (?) fault probably exists, delineating the boundary between the Klamath Mountains province and the Cascade Range province. This fault decreases in dip from 68^{o} (upper 5 km) to 40^{o}, and may extend to depths greater than 10 km below sea level.

The Trinity ophiolite, and probably the subjacent Central metamorphic belt, extend northward, southward, and

eastward beneath the Cascade Range at a minimum depth of ~1 km below sea level. The gravity low occurring over Mt. Shasta is primarily due to subsidence of low density volcanic rock within the denser country rock of the Trinity ophiolite. A sizeable silicic intrusive of roughly cylindrical shape, probably occurs ~2 km beneath the summit of Mt. Shasta, and extends to 10 km below sea level.

Deeper than 10 km below sea level, the more recently underthrust rocks of the Western Paleozoic and Triassic plate probably occur as basement, and extend downward to 38 km depth, beyond which is mantle.

REFERENCES CITED

Barnett, C.T., 1976, Theoretical modeling of the magnetic and gravitational fields of an arbitrarily shaped three- dimensional body: Geophysics, v. 41, no. 6, p. 1353.

Birch, F., 1960, The velocity of compressional waves in rocks to 10 kilobars, para 1: Journal of Geophysical Research, v. 65, no. 4, p. 1083-1102.

_____, 1961, The velocity of compressional waves in rocks to 1 to kilobars, part 2: Journal of Geophysical Research, v. 66, no. 7, p. 2199-2224.

Blakely, R.J., Jachens, R.C., Simpson, R.W., and Couch, R.W., in press, Tectonic setting of the southern Cascade Range as interpreted from its magnetic and gravity fields: Bull., Geol. Soc. Amer., submitted 9/8/83.

Briggs, I.C., 1974, Machine contouring using minimum curvature, Geophysics, v. 39, no. 1, p. 39-48.

Callaghan, E., 1933, Some features of the volcanic sequence in the Cascade Range in Oregon: Am. Geophys. Union Trans., 14th Ann. Mtg., p. 243-249.

Chapman, R.H., 1966, The California Division of Mines and Geology Gravity Base Station Network: California Division of Mines and Geology Special Report 90, 49 p.

Coney, P.J., 1981, Accretionary tectonics to western North America, in relations of Tectonics to ore deposits in the Southern Cordillera, Dickinson and Payne, editors, Ariz. Geol. Soc. Digest, v. 13, p. 23-38.

Coney, P.J., Jones, D.L., and Monger, J.W.H., 1980, Cordilleran suspect terranes: Nature, v. 288, p. 329-333.

Crandell, D.R., Miller, C.D., Glicken, H.S., Christiansen, R.L., and Newhall, C.G., 1984, Catastrophic debris avalanche from ancestral Mount Shasta volcano, California: Geology, v. 12, p. 143-146.

Davis, G.A., 1966, Metamorphic and granitic history of the Klamath Mountains: In Bailey, E.H., ed., Geology of northern California, California Div. Mines Geol. Bull. 190, 507 p.

_____, 1969, Tectonic corrections, Klamath Mountains and western Sierra Nevada, California: Bull., Geol. Soc. Amer., v. 80, p. 1095-1108.

Dickinson, W.R., 1981, Plate tectonics and the continental margin of California, in Ernst, W.G. Editor, The geotectonic development of California (W.W. Rubey Volume No. 1), Prentice-Hall, New York, p. 1-18.

Ernst, W.G., 1977, California and plate tectonics: California Geology, September, p. 187-196.

Evernden, J.F., 1963, Unpublished gravity data in Kim, C.K., and Blank, H.R., Jr., 1973, Bouguer gravity map of California, Weed Sheet: California Division of Mines and Geology, map and 8 p. text, scale 1:250,000.

Finn, C., 1981, Principal facts for gravity stations near Medicine Lake and Mount Shasta, California: U.S.G.S. Open File Report 81-427.

Finn, C., and Spydell, D.R., 1982, Principle facts for seventy-four gravity stations in the northern California Cascade Mountains: U.S.G.S. Open File Report 82-1080.

Fuis, G.S., Zucca, J.J., Mooney, W.D., and Milkerett, B., in press, A geologic interpretation of seismic reraction results in northeastern California.

Hamilton, W., 1969, Mesozoic California and the underflow of Pacific mantle: Bull., Geol. Soc. Amer., v. 80, p. 2409- 2430.

Hamilton, W., 1981, Plate tectonic mechanism of Laramide deformation, contributions to Geology, Univ. of Wyoming, v. 19, no. 2, p. 87-92.

Hammer, S., 1939, Terrain corrections for gravimeter stations: Geophysics, v. 4, p. 184.

Irwin, W.P., 1966, Geology of the Klamath Mountains province in Geology of Northern California, Bailey, E.H., ed., California Division Mines Geology Bull. 190, p. 17-38.

Irwin, W.P., 1981, Tectonic accretion of the Klamath Mountains, in Ernst, W.G., Editor, The geotectonic development of California (W.W. Rubey volume no. 1) Prentice Hall, New York, p.30-49.

Kim, C.K., 1974, A gravity investigation of the Weed sheet, northwestern California: Doctoral Thesis, Univ. of Oregon, 168 p.

Kim, C.K., and Blank, H.R., Jr., 1973, Bouguer gravity map of California, Weed Sheet: California Div. Mines and Geology map and 8 p. text, scale 1:250,000.

Krohn, D.H,. 1976, Gravity terrain corrections using multi-quadric equations: Geophysics, v. 41, p. 266.

LaFehr, T.R., 1965, Gravity, isostasy and crustal structure in the southern Cascade Range: Jour. Geophys. Res., v. 70, p. 5581-5597.

_____, 1966, Gravity in the eastern Klamath Mountains, California: Bull. Geol. Soc. Amer., v: 77, p. 1177-1190.

Lanphere, M.A., and Irwin, W.P., 1965, Carboniferous isotopic age of metamorphism of the Salmon Hornblende Schist and Abrams Mica Schist, southern Klamath Mountains, California: U.S. Geol. Surv. Prof. Paper 525-D, p. D27-D33.

Lanphere, M.A., Irwin, W.P., and Hotz, P.E., 1968, Isotopic age of the Nevada orogeny and older plutonic and metamorphic events in the Klamath Mountains, California: Bull. Geol. Soc. Amer., v. 79, no. 8, p. 1027-1052.

MacDonald, G.A., 1966, Geology of the Cascade Range and Modoc plateau: in Bailey, E.H., ed., Geology of northern California: California Div. Mines Geol. Bulletin 190, 507 p.

McNutt, M.K., 1983, Influence of plate subduction on isostatic compensation in northern California: Tectonics, v. 2, no. 4, p. 399-415.

Morelli, C., ed., 1974, The International gravity Standardization Net 1971: International Association of Geodesy Spec. Pub. no. 4, 194 p.

Peck, D.L., Griggs, A.B., Schlicker, H.G., Wells, F.G. and Dole, H.M., 1964, Geology of the central and northern parts of the western Cascade Range in Oregon: U.S. Geol. Surv. Prof. Paper 449, 56 p.

Plouff, D., 1977, Preliminary documentation for a Fortran program to compute gravity terrain corrections based on topogrphy digitized on a geographic grid: U.S. Geol. Surv. Open File Report 77-535.

Poole, F.G. and Sandberg, C.A., 1977, Mississippian paleogeography and tectonics of the western United States: Paleozoic Paleogeography of the western United States: in Stewart, J.H., Stevens, C.H., and Fritsche, A.E., Pacific section Soc. Expl. Dal. Min., Pacific Coast Paleogeography Symposium 1, p. 67-86.

Potter, A.W., Hotz, P.E. and Rohr, A.M., 1977, Stratigraphy and inferred tectonic framework of lower Paleozoic rocks in the eastern Klamath Mountains, northern California, Paleozoic Paleogeography of the western United States: in Stewart, J.H., Stevens, C.H., and Fritsche, A.E., editors, Pacific section, Soc. Expl. Dal. Min., Pacific Coast Paleogeography Symposium 1, p. 421-454.

Rudman, A.J., Ziegler, R. and Blakely, R.F., 1977, Fortran program for generation of earth tide gravity values: Department of Natural Resources, U.S. Geol. Surv., Occasional paper 22.

Sandberg, C.H., 1958, Terrain corrections for an inclined plane in gravity computations: Geophysics, v. 23, no. 4, p. 701-711.

Smith, D., 1982, TOPO: A contouring program using gridded data as input, Colorado School of Mines computer center.

Wagner, D.L., and Saucedo, G.J., in press, Geologic map of the Weed quadrangle, California, 1:250,000: California Division of Mines and Geology Regional Geologic Map Series.

Webring, M., 1981, MINC: A gridding program based on minimum curvature, Geophysics, v. 39, no. 1, p. 39-48.

Williams D.L., Finn, C., in press, Analysis of gravity data in volcanic terrain and gravity anomalies and subvolcanic intrusions in the Cascade Range, U.S.A. and at other selected volcanoes: Geophysics, submitted 2/21/81.

Williams, H., 1949, Geology of the Macdoel quadrangle California: California Div. Mines Geol. Bulletin 151, p. 7-60.

APPENDIX A

GRAVITY ERRORS ASSOCIATED WITH DIGITAL ELEVATION DATA

The gravity errors shown in the following twelve figures are the errors associated with the 30-second and 15-second digital elevation models used in the computer program of Plouff (1977). Both subdued and very rugged topography were considered in order to generate a complete range of errors. The gravity errors were determined by

1) adding the elevation error to the average ring elevation and then ascertaining the associated gravity effect from Hammer charts.
2) ascertaining the gravity effect associated with the average ring elevation.
3) subtracting the latter from the former (i.e., 1-2).

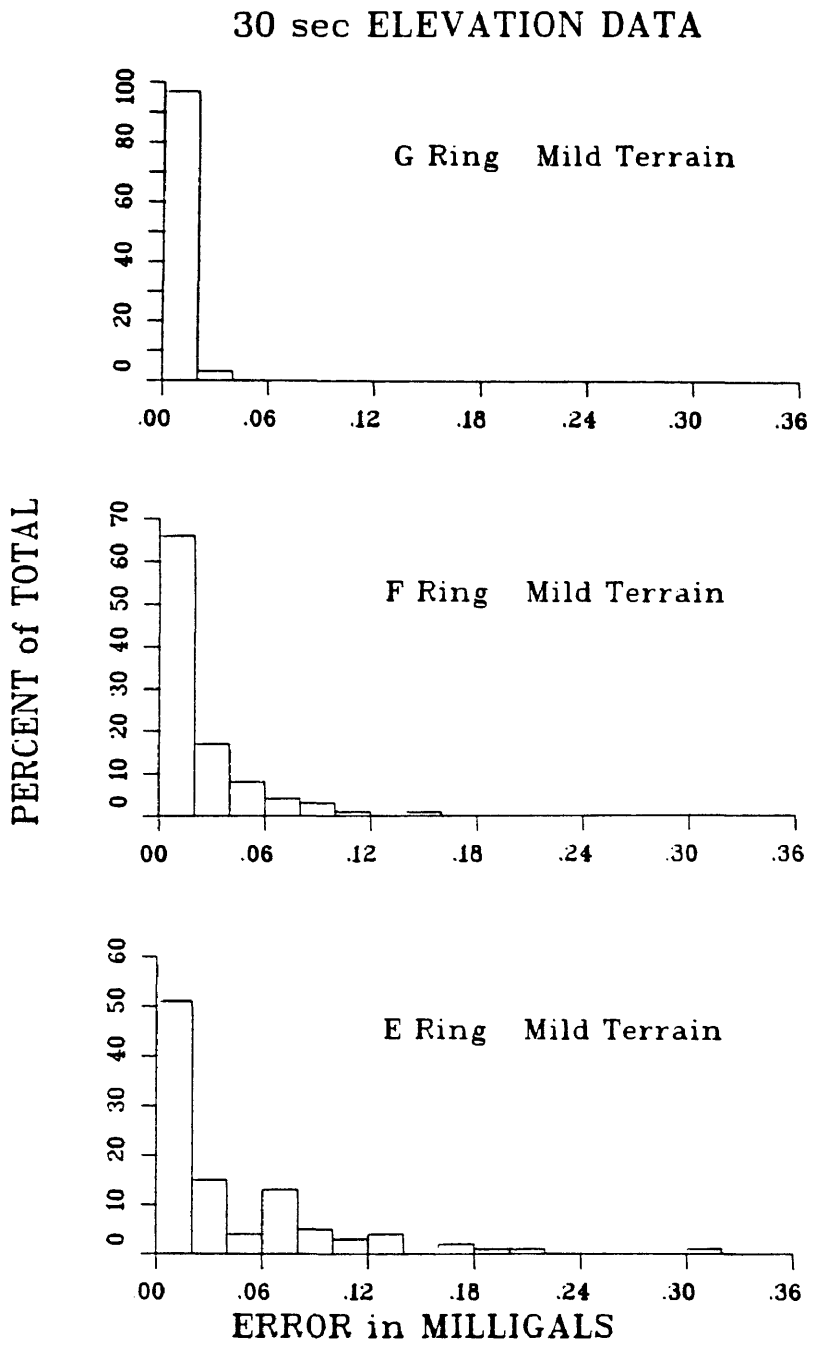

Figure A-1. Frequency versus error distribution of gravity effects associated with elevation errors occurring within a given ring. Average elevations per ring are 1) 15 feet in the E ring, 2) 20 feet in the F ring, and 3) 30 feet in the G ring.

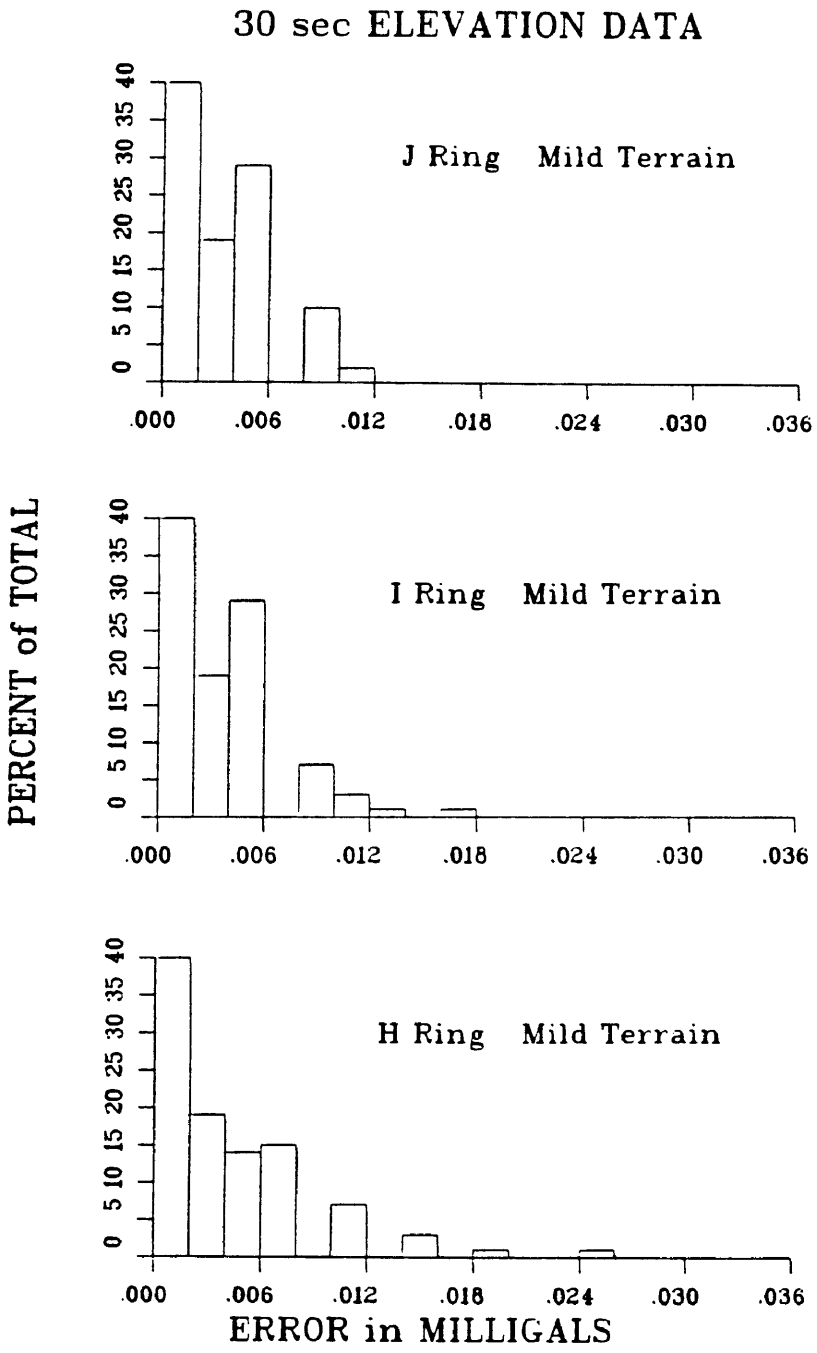

Figure A-2. Frequency versus error distribution of gravity effects associated with elevation errors occurring within a given ring. Average elevations per ring are 1) 50 feet in the H ring, 2) 100 feet in the I ring, and 3) 400 feet in the J ring.

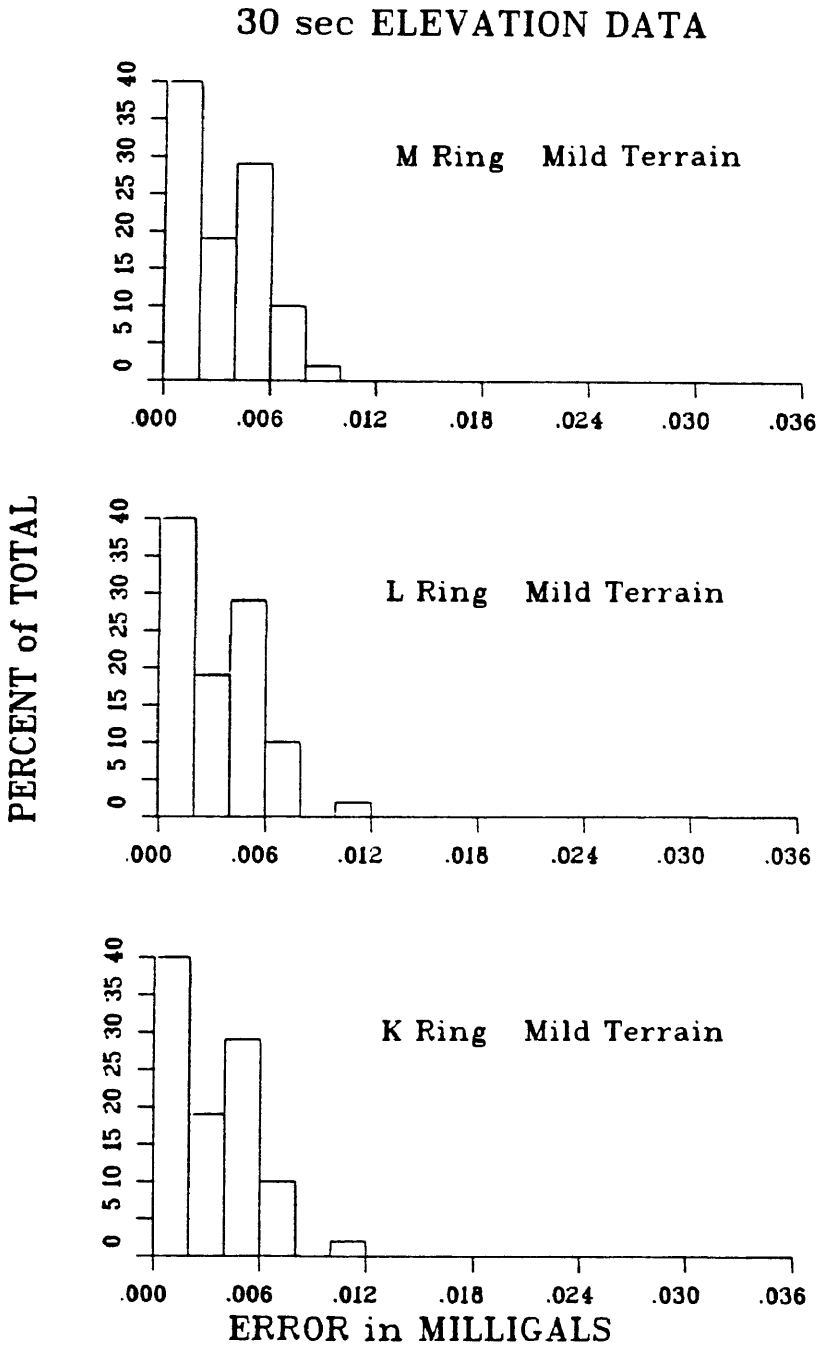

Figure A-3. Frequency versus error distribution of gravity effects associated with elevation errors occurring within a given ring. Average elevations per ring are 1) 600 feet in the K ring, 2) 1,000 feet in the L ring, and 3) 1,100 feet in the M ring.

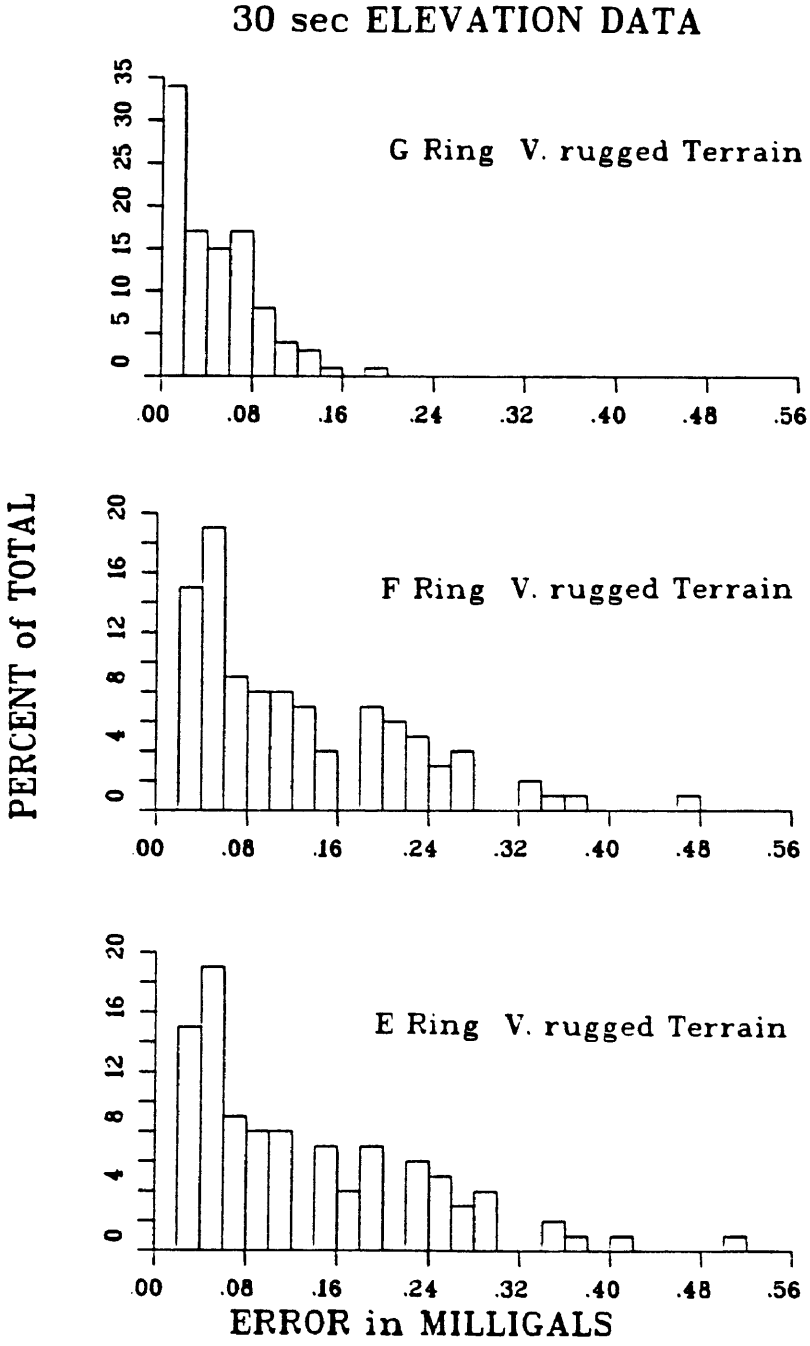

Figure A-4. Frequency versus error distribution of gravity effects associated with elevation errors occurring within a given ring. Average elevations per ring are 1) 330 feet in the E ring, 2) 710 feet in the F ring, and 3) 1,200 feet in the G ring.

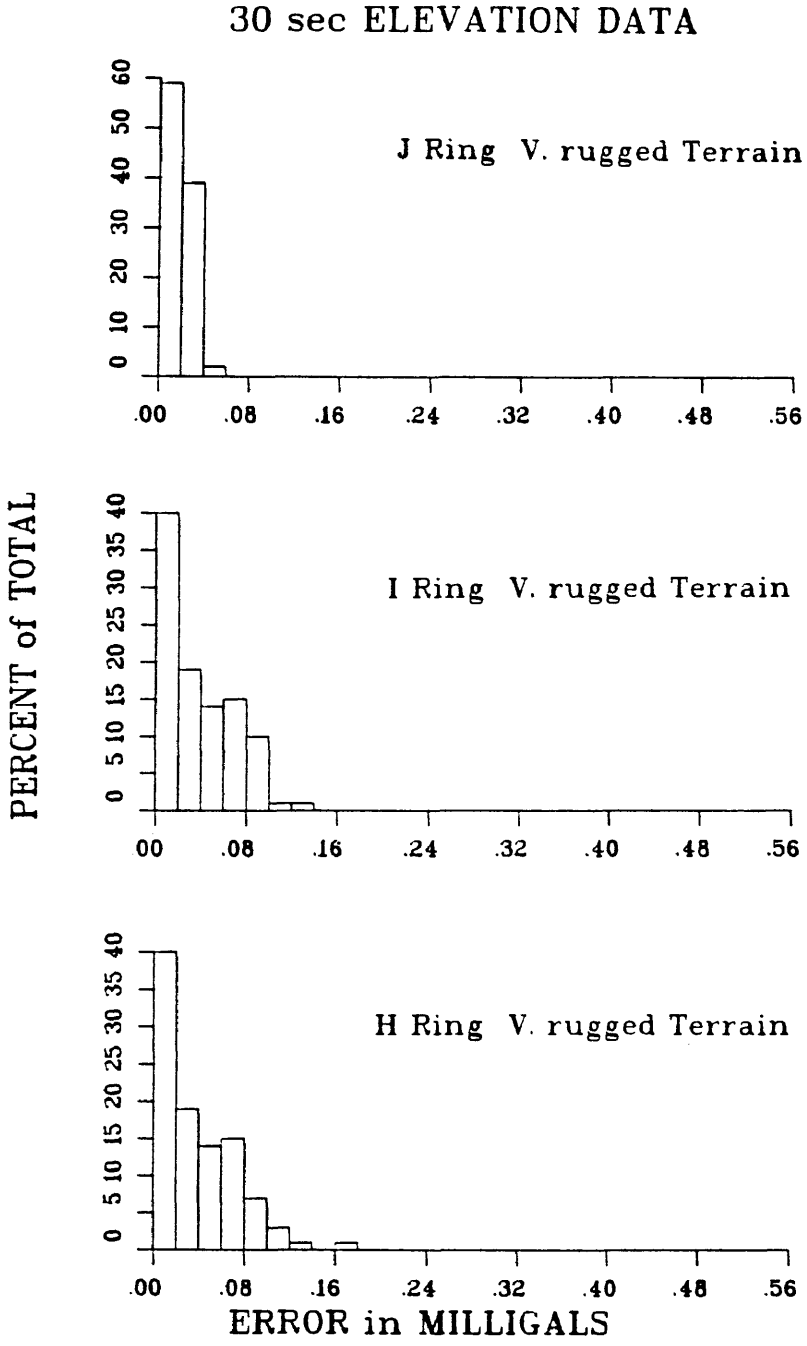

Figure A-5. Frequency versus error distribution of gravity effects associated with elevation errors occurring within a given ring. Average elevations per ring are 1) 1,750 feet in the H ring, 2) 2,400 feet in the I ring, and 3) 2,500 feet in the J ring.

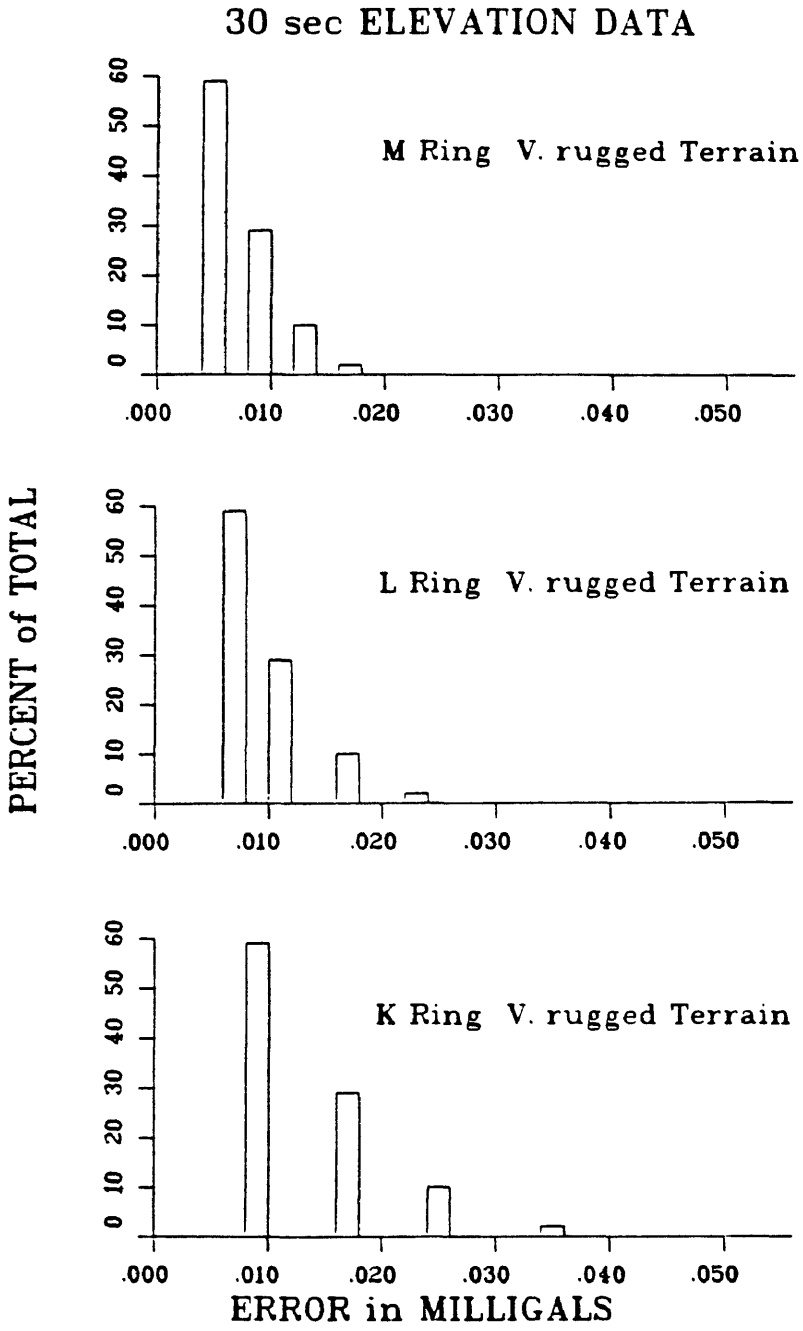

Figure A-6. Frequency versus error distribution of gravity effects associated with elevation errors occurring within a given ring. Average elevations per ring are 1) 2,500 feet in the K ring, 2) 2,500 feet in the L ring, and 3) 2,600 feet in the M ring.

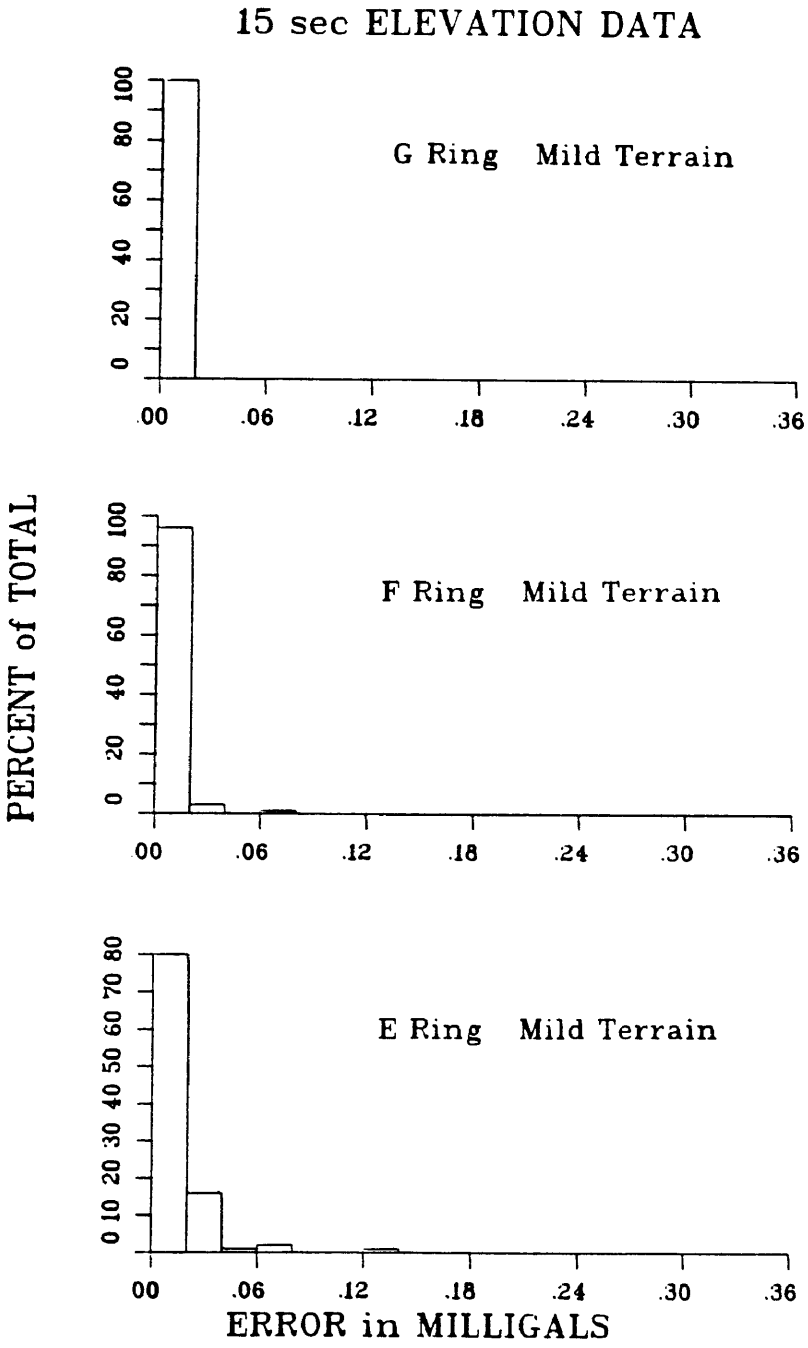

Figure A-7. Frequency versus error distribution of gravity effects associated with elevation errors occurring within a given ring. Average elevations per ring are 1) 15 feet in the E ring, 2) 20 feet in the F ring, and 3) 30 feet in the G ring.

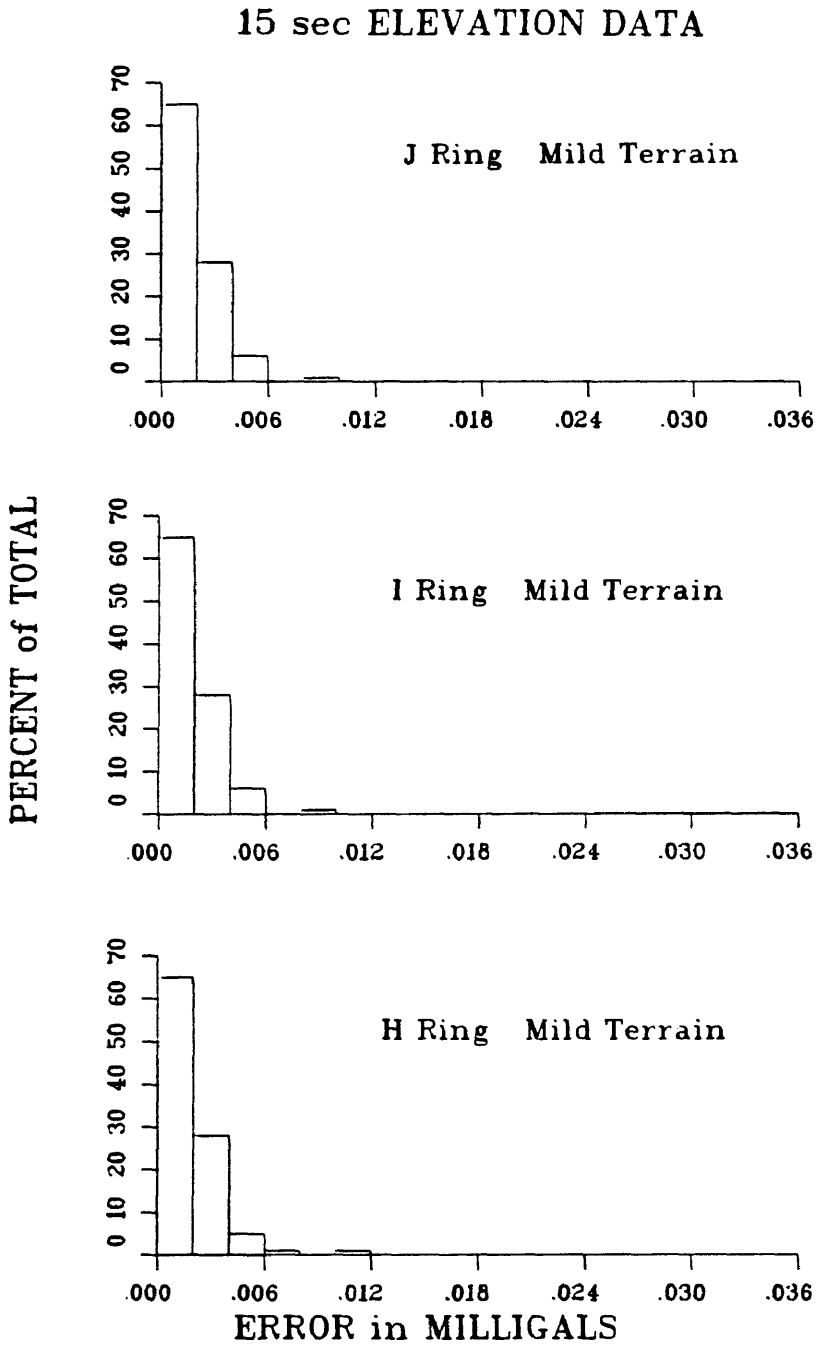

Figure A-8. Frequency versus error distribution of gravity effects associated with elevation errors occurring within a given ring. Average elevations per ring are 1) 50 feet in the H ring, 2) 100 feet in the I ring, and 3) 400 feet in the J ring.

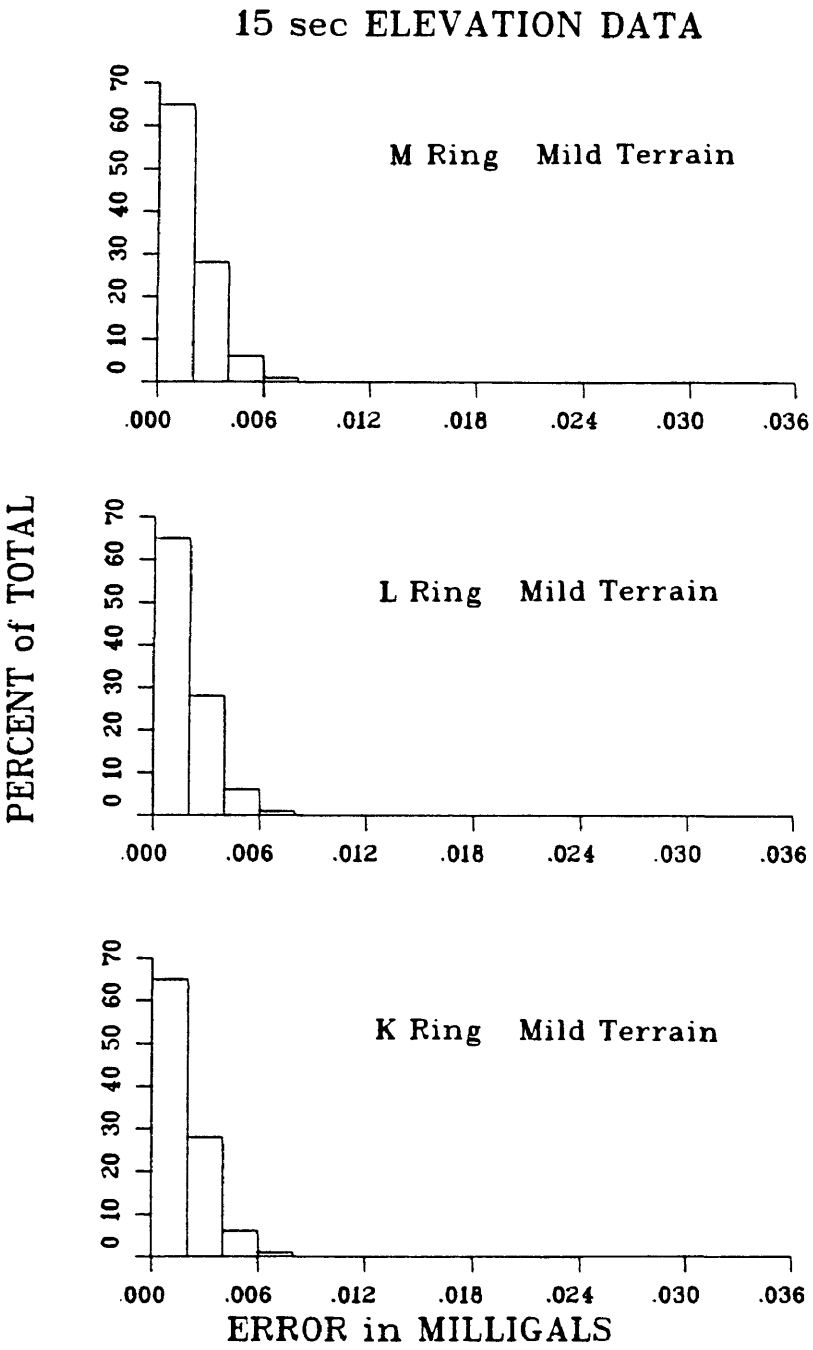

Figure A-9. Frequency versus error distribution of gravity effects associated with elevation errors occurring within a given ring. Average elevations per ring are 1) 600 feet in the K ring, 2) 1,000 feet in the L ring, and 3) 1,100 feet in the M ring.

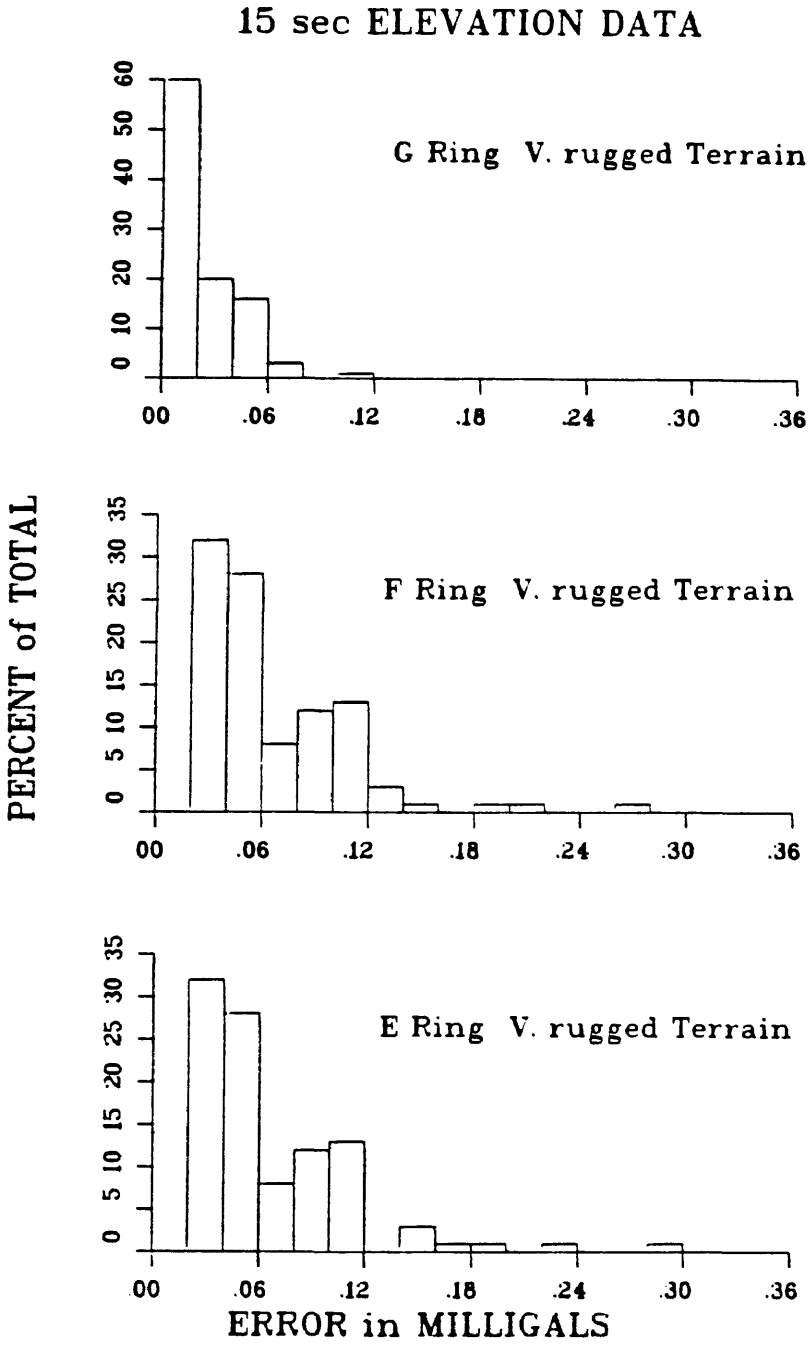

Figure A-10. Frequency versus error distribution of gravity effects associated with elevation errors occurring within a given ring. Average elevations per ring are 1) 330 feet in the E ring, 2) 710 feet in the F ring, and 3) 1,200 feet in the G ring.

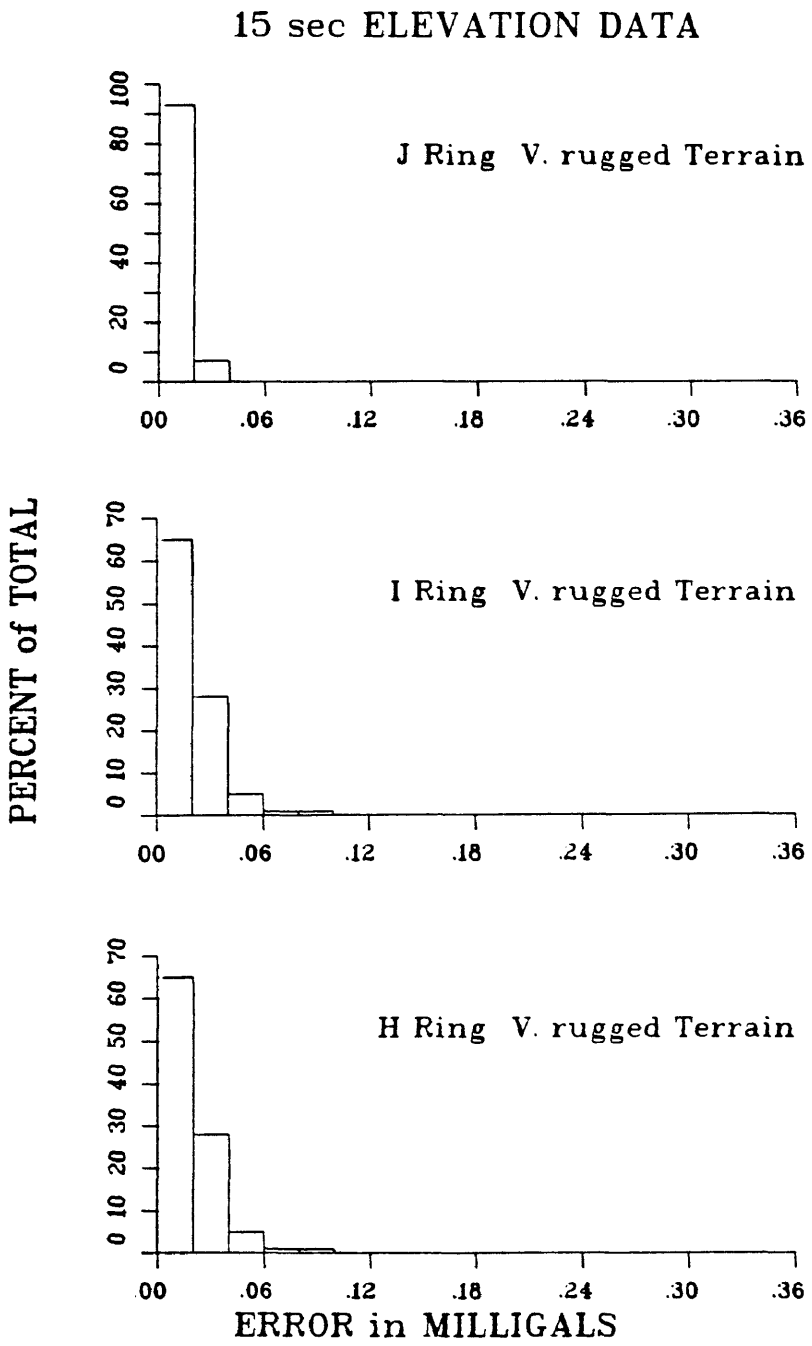

Figure A-11. Frequency versus error distribution of gravity effects associated with elevation errors occurring within a given ring. Average elevations per ring are 1) 1,750 feet in the H ring, 2) 2,400 feet in the I ring, and 3) 2,500 feet in the J ring.

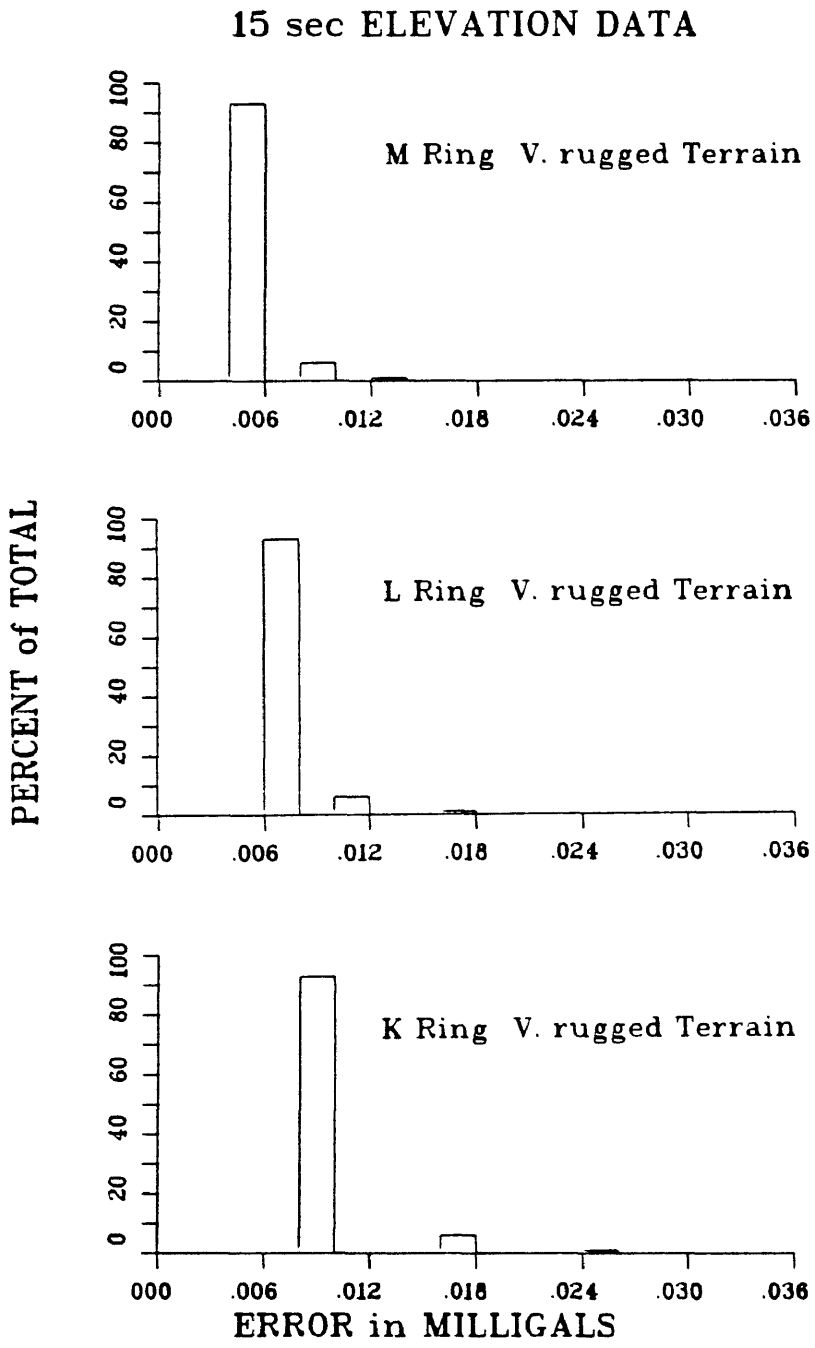

Figure A-12. Frequency versus error distribution of gravity effects associated with elevation errors occurring within a given ring. Average elevations per ring are 1) 2,500 feet in the K ring, 2) 2,500 feet in the L ring, and 3) 2,600 feet in the M ring.

APPENDIX B

PRINCIPAL FACTS FOR GRAVITY STATIONS

On the following pages, the principal facts for 191 gravity stations (located within the study area) are listed. The sources of these data are as follows:

1) the first 133 stations were acquired in this study,
2) all station identifications prefaced with an "L" are those occupied by LaFehr (1966),
3) all station identifications prefaced with a "W" are those occupied by Kim (1974),
4) all station identifications prefaced with an "E" are those occupied by Evernden (1963),
5) all station identifications prefaced with an "SH" are those occupied by Finn (1981) and Finn and Spydell (1982).

In the "Previous Geophysical Work" section, a total of 99 gravity stations were occupied by the outside sources listed above, whereas only 58 such stations are listed on the following pages. This discrepancy is entirely a result of editing, where 41 stations (common to more than one survey) were removed.

An explanation of the terms, used in the header of each listing, is given below.

STATION	station identification
LATITUDE	expressed in degrees, decimal minutes
LONGITUDE	expressed in degrees, decimal minutes
ELEV(Ft)	expressed in feet above sea level
OBS GRAV	the observed gravity, with tidal drift and instrument drift removed.
FAA	the free-air anomaly
SBA	the simple Bouguer anomaly, based upon a reduction density of 2.67 g/cc.
CC	the curvature correction
TC	the total terrain correction obtained by the methods of Hammer (other surveys) or Sandberg, and Krohn.
TER	the total terrain correction obtained by the computerized method of Plouff (all surveys)
TOT	the total terrain correction (TC + TER).
CBA	the complete Bouguer anomaly, based upon a reduction density of 2.67 g/cc

STATION	LATITUDE	LONGITUDE	ELEV(ft)	OBS GRAV	FAA	SBA	CC	TC	TER	TOT	CBA	STATION
1	41 29.21	122 26.56	2856.0	980020.45	-27.39	-110.34	1.01	0.07	1.97	2.04	-123.76	1
2	41 28.92	122 26.59	2866.3	980020.90	-25.53	-108.83	1.01	0.01	2.10	2.11	-122.19	2
3	41 26.63	122 26.54	3038.6	980013.34	-13.47	-102.65	1.05	0.00	3.20	3.20	-114.97	3
4	41 26.33	122 26.88	3068.5	980013.71	-9.84	-100.04	1.06	0.10	3.75	3.85	-111.71	4
5	41 26.30	122 27.34	3144.4	980011.60	-4.77	-97.56	1.08	0.19	3.98	4.17	-108.93	5
6	41 26.10	122 27.67	3149.7	980010.18	-5.40	-98.37	1.08	0.77	4.92	5.69	-108.21	6
7	41 27.10	122 21.65	3490.0	979974.68	-10.40	-114.97	1.16	0.02	3.01	3.03	-127.56	7
8	41 27.65	122 21.38	3482.0	979975.15	-11.51	-115.81	1.16	0.05	3.03	3.08	-128.35	8
9	41 28.20	122 21.13	3436.8	979979.01	-12.71	-115.47	1.15	0.09	3.13	3.22	-127.85	9
10	41 28.46	122 21.03	3461.0	979977.88	-11.97	-115.55	1.15	0.25	3.04	3.29	-127.87	10
11	41 28.85	122 21.75	3290.2	979988.25	-18.23	-115.99	1.11	0.07	2.59	2.66	-128.90	11
12	41 29.31	122 22.19	3099.4	980000.02	-25.09	-116.34	1.07	0.05	2.48	2.53	-129.34	12
13	41 29.64	122 22.89	2968.6	980008.21	-29.68	-116.47	1.04	0.04	2.25	2.29	-129.68	13
14	41 29.65	122 23.42	2942.4	980008.72	-31.65	-117.55	1.03	0.05	2.08	2.13	-130.91	14
15	41 29.67	122 24.43	3275.0	979983.04	-26.10	-123.34	1.11	4.22	1.94	6.16	-132.74	15
16	41 29.14	122 24.52	2876.5	980012.37	-33.44	-117.09	1.01	0.11	2.17	2.28	-130.28	16
17	41 28.56	122 24.65	2953.5	980008.27	-29.43	-115.70	1.03	0.30	2.20	2.50	-128.69	17
18	41 28.05	122 24.87	3021.7	980004.80	-25.73	-114.33	1.05	0.16	2.23	2.39	-127.45	18
19	41 28.14	122 25.66	3227.0	979992.27	-19.09	-114.69	1.10	1.74	2.03	3.77	-126.48	19
20	41 28.32	122 26.39	2903.5	980021.59	-20.46	-105.03	1.02	0.03	2.28	2.31	-118.21	20
21	41 26.10	122 28.16	3191.6	980009.77	-1.87	-96.27	1.09	0.39	5.48	5.87	-105.94	21
22	41 26.03	122 28.57	3277.0	980007.01	3.50	-93.81	1.11	0.93	5.87	6.80	-102.58	22
23	41 25.93	122 29.17	3406.4	980002.91	11.72	-90.00	1.14	1.60	6.45	8.05	-97.54	23
24	41 25.56	122 29.91	3623.8	979994.58	24.37	-84.77	1.19	1.57	8.01	9.58	-90.83	24
25	41 25.92	122 29.69	3486.3	980002.14	18.48	-85.97	1.16	0.71	7.18	7.89	-93.70	25
32	41 22.58	122 22.47	3869.6	979952.14	9.49	-108.02	1.24	0.04	3.33	3.37	-120.35	32
33	41 22.71	122 23.08	3829.5	979958.57	11.97	-104.18	1.23	0.38	3.13	3.51	-116.36	33
34	41 22.94	122 23.31	3947.3	979952.54	16.66	-103.51	1.25	0.14	2.83	2.97	-116.25	34
35	41 23.16	122 24.51	3769.8	979974.19	21.30	-92.81	1.22	0.07	3.48	3.55	-104.93	35
36	41 23.03	122 24.21	3797.1	979970.42	20.29	-94.76	1.22	0.10	3.32	3.42	-107.02	36
37	41 23.36	122 24.56	3757.7	979974.09	19.76	-93.94	1.21	0.08	3.38	3.46	-106.15	37
38	41 23.97	122 25.19	3445.7	979989.29	4.73	-98.34	1.15	0.13	4.10	4.23	-109.72	38
39	41 24.23	122 24.47	3573.3	979979.36	6.40	-101.01	1.18	0.34	3.09	3.43	-113.22	39
40	41 24.03	122 24.77	3550.9	979983.09	8.33	-98.32	1.17	0.32	3.43	3.75	-110.20	40
41	41 24.41	122 24.07	3587.2	979974.63	2.71	-105.18	1.18	0.28	2.90	3.18	-117.63	41
42	41 24.79	122 23.70	3571.5	979973.45	-0.51	-107.86	1.18	0.07	2.73	2.80	-120.69	42
43	41 23.89	122 22.75	3717.9	979963.98	5.12	-107.22	1.21	0.04	2.95	2.99	-119.90	43
44	41 23.52	122 22.73	4007.0	979943.53	12.40	-109.80	1.26	1.33	2.73	4.06	-121.46	44
45	41 24.09	122 22.84	3701.0	979964.35	3.61	-108.16	1.20	0.05	2.88	2.93	-120.89	45
46	41 23.76	122 21.54	3895.0	979946.10	4.09	-114.29	1.24	0.08	3.26	3.34	-126.65	46
47	41 23.64	122 22.16	3817.0	979953.59	4.43	-111.30	1.23	0.04	3.04	3.08	-123.90	47
B1	41 25.72	122 23.15	3465.6	979977.41	-7.90	-111.64	1.15	0.08	2.65	2.73	-124.53	B1
87	41 25.01	122 23.01	3533.5	979973.72	-4.15	-110.20	1.17	0.12	2.85	2.97	-122.86	87
103	41 24.50	122 25.95	3293.1	979998.92	-0.77	-98.63	1.11	0.04	4.73	4.77	-109.43	103
104	41 24.22	122 26.27	3358.7	979993.99	0.89	-99.21	1.13	0.07	5.57	5.64	-109.16	104

STATION	LATITUDE	LONGITUDE	ELEV(ft)	OBS GRAV	FAA	SBA	CC	TC	TER	TOT	CBA	STATION
105	41 24.08	122 26.93	3573.6	979981.03	8.33	-99.09	1.18	0.82	6.71	7.53	-107.19	105
106	41 23.96	122 27.62	3728.8	979972.21	14.27	-98.44	1.21	2.51	8.51	11.02	-103.09	106
107	41 23.88	122 27.92	3823.8	979967.91	19.02	-96.93	1.23	2.73	9.08	11.81	-100.81	107
108	41 23.55	122 28.69	4185.1	979947.99	33.56	-94.72	1.29	2.92	9.84	12.76	-97.71	108
109	41 23.35	122 28.92	4298.0	979940.88	37.36	-94.77	1.31	3.74	10.53	14.27	-96.28	109
110	41 22.95	122 29.46	4687.0	979919.82	53.45	-91.94	1.37	3.10	10.48	13.58	-94.19	110
88	41 23.01	122 23.77	3842.0	979964.40	18.52	-98.06	1.23	0.13	3.05	3.18	-110.56	88
91	41 26.11	122 23.79	3841.0	979950.44	-0.17	-116.71	1.23	3.57	2.94	6.51	-125.89	91
92	41 26.00	122 25.43	3166.0	979999.46	-14.43	-107.95	1.08	0.15	3.03	3.18	-120.31	92
93	41 25.88	122 24.56	3267.9	979991.51	-12.62	-109.62	1.11	0.37	2.77	3.14	-122.04	93
94	41 25.79	122 23.87	3365.5	979984.67	-10.16	-110.49	1.13	0.16	2.63	2.79	-123.29	94
89	41 26.12	122 26.15	3072.8	980008.40	-14.44	-104.78	1.06	0.03	3.48	3.51	-116.80	89
90	41 26.77	122 25.51	3056.0	980004.83	-20.55	-110.32	1.06	0.45	2.78	3.23	-122.61	90
98	41 28.63	122 28.66	2918.4	980029.05	-12.05	-97.13	1.02	0.01	2.98	2.99	-109.62	98
97	41 28.44	122 29.03	2961.9	980029.18	-7.56	-94.12	1.03	0.03	3.66	3.69	-105.92	97
96	41 28.37	122 29.44	3025.7	980029.33	-1.31	-90.04	1.05	0.11	4.27	4.38	-101.18	96
95	41 28.11	122 29.72	3174.9	980022.80	6.58	-87.24	1.09	0.53	5.03	5.56	-97.23	95
S1	41 21.81	122 18.29	4730.0	979883.10	22.49	-124.37	1.38	0.25	5.17	5.42	-134.78	S1
S2	41 21.85	122 17.69	4987.0	979866.25	29.74	-125.88	1.41	0.38	6.08	6.46	-135.29	S2
S3	41 21.83	122 17.11	5216.0	979849.93	34.98	-128.46	1.43	0.60	7.08	7.68	-136.67	S3
S4	41 22.30	122 17.12	5418.0	979836.25	39.58	-130.75	1.45	0.50	7.57	8.07	-138.60	S4
S5	41 22.70	122 17.13	5562.0	979826.52	42.77	-132.47	1.47	0.41	7.99	8.40	-139.99	S5
S6	41 23.13	122 17.14	5688.0	979819.27	46.72	-132.81	1.48	0.29	8.50	8.79	-139.96	S6
S7	41 23.57	122 17.15	5808.0	979810.12	48.20	-135.44	1.48	0.60	9.06	9.66	-141.72	S7
S8	41 21.82	122 16.00	5876.0	979803.53	50.62	-135.33	1.49	0.93	9.62	10.55	-140.73	S8
S9	41 21.78	122 15.53	6206.0	979780.43	58.59	-138.62	1.51	1.76	10.38	12.14	-142.45	S9
S10	41 21.87	122 15.65	6201.0	979781.26	58.82	-138.22	1.51	1.56	10.42	11.98	-142.20	S10
S11	41 21.81	122 14.84	6830.0	979739.74	76.49	-142.00	1.52	1.20	11.89	13.09	-144.89	S11
26	41 25.69	122 30.22	3948.4	979980.22	40.33	-79.87	1.25	1.82	6.08	7.90	-87.68	26
31	41 25.19	122 30.16	3868.7	979977.19	30.55	-86.93	1.24	2.84	8.57	11.41	-91.22	31
30	41 24.81	122 30.64	4098.0	979966.43	41.93	-83.37	1.28	4.13	9.86	13.99	-85.12	30
27	41 25.57	122 30.96	4212.0	979969.62	54.68	-74.51	1.30	1.48	6.93	8.41	-81.86	27
99	41 27.85	122 30.11	3427.8	980009.75	17.69	-84.76	1.14	0.98	5.92	6.90	-93.47	99
100	41 27.56	122 30.34	3638.9	979998.54	26.76	-82.89	1.19	1.96	6.56	8.52	-90.01	100
PARK	41 26.84	122 32.51	6887.0	979798.93	133.52	-86.92	1.52	4.66	21.70	26.36	-76.53	PARK
101	41 29.72	122 30.61	2841.0	980046.51	-3.50	-85.94	1.00	0.03	3.16	3.19	-98.21	101
DFALL	41 20.63	122 30.68	7904.0	979722.97	162.38	-92.74	1.48	4.25	17.00	21.25	-87.43	DFALL
54	41 29.64	122 33.06	2957.1	980057.56	18.58	-67.81	1.03	0.13	3.89	4.02	-79.29	54
55	41 29.39	122 33.70	3068.0	980055.43	27.26	-62.92	1.06	0.29	4.10	4.39	-74.05	55
56	41 28.72	122 34.35	3131.1	980052.66	31.41	-60.92	1.08	0.49	5.62	6.11	-70.35	56
57	41 28.35	122 34.99	3234.3	980047.75	36.76	-59.09	1.10	0.83	5.79	6.62	-68.03	57
58	41 28.15	122 35.53	3268.0	980046.04	38.52	-58.48	1.11	1.59	5.99	7.58	-66.46	58
59	41 28.04	122 36.05	3333.4	980041.73	40.52	-58.71	1.12	1.21	5.93	7.14	-67.15	59
60	41 27.87	122 36.45	3407.0	980035.74	41.69	-60.05	1.14	0.76	5.85	6.61	-69.04	60
61	41 27.78	122 37.20	3485.4	980028.87	42.33	-62.09	1.16	0.92	5.59	6.51	-71.19	61

STATION	LATITUDE	LONGITUDE	ELEV(ft)	OBS GRAV	FAA	SBA	CC	TC	TER	TOT	CBA	STATION
62	41 27.46	122 37.75	3647.0	980014.42	43.55	-66.37	1.19	1.53	5.41	6.94	-75.09	62
63	41 27.39	122 38.24	3778.8	980003.38	45.02	-69.40	1.22	3.55	5.32	8.87	-76.21	63
64	41 27.26	122 38.51	4372.7	979967.69	65.36	-69.32	1.32	2.25	3.26	5.51	-79.60	64
65	41 26.62	122 38.51	4751.8	979941.52	75.77	-71.84	1.38	3.21	3.06	6.27	-81.41	65
66	41 25.94	122 38.22	4921.2	979933.01	84.19	-69.19	1.40	0.55	2.90	3.45	-81.61	66
67	41 25.37	122 37.99	4796.5	979941.33	81.65	-67.49	1.39	0.31	2.91	3.22	-80.12	67
68	41 24.70	122 37.83	4575.8	979953.19	73.76	-67.84	1.35	0.28	3.45	3.73	-79.93	68
69	41 24.32	122 38.16	4354.6	979962.20	62.55	-71.51	1.32	0.73	3.87	4.60	-82.69	69
70	41 24.15	122 38.84	4218.2	979968.12	55.92	-73.49	1.30	0.66	3.64	4.30	-84.95	70
71	41 23.96	122 39.66	4118.5	979970.16	48.86	-77.15	1.28	0.22	3.20	3.42	-89.47	71
72	41 23.43	122 40.34	4031.5	979969.60	40.91	-82.13	1.27	0.13	2.88	3.01	-94.84	72
73	41 23.12	122 40.99	3948.2	979972.46	36.41	-83.79	1.25	0.15	2.77	2.92	-96.58	73
74	41 22.65	122 41.71	3835.3	979976.06	30.09	-86.26	1.23	0.16	2.94	3.10	-98.85	74
75	41 22.34	122 42.37	3771.7	979978.30	26.83	-87.35	1.22	0.12	2.79	2.91	-100.11	75
76	41 21.97	122 42.94	3731.4	979977.05	22.35	-90.45	1.21	0.15	2.65	2.80	-103.32	76
77	41 21.29	122 43.45	3698.9	979971.87	15.12	-96.58	1.20	0.17	2.59	2.76	-109.48	77
86	41 33.52	122 28.19	2634.1	980045.31	-29.85	-105.23	0.95	0.18	1.36	1.54	-119.11	86
85	41 33.19	122 28.48	2708.0	980039.59	-28.13	-106.03	0.97	0.06	1.23	1.29	-120.17	85
84	41 33.28	122 28.88	2717.0	980040.63	-26.37	-104.58	0.97	0.11	1.23	1.34	-118.68	84
83	41 33.02	122 29.42	2675.6	980045.41	-25.09	-101.89	0.96	0.07	1.40	1.47	-115.84	83
82	41 32.63	122 29.88	2708.8	980044.37	-22.44	-100.37	0.97	0.13	1.44	1.57	-114.23	82
81	41 32.25	122 30.19	2718.3	980045.05	-20.28	-98.54	0.97	0.02	1.53	1.55	-112.41	81
80	41 32.06	122 30.58	2728.6	980046.93	-17.15	-95.75	0.97	0.00	1.62	1.62	-109.56	80
79	41 32.05	122 31.03	2726.2	980050.06	-14.23	-92.75	0.97	0.09	1.71	1.80	-106.38	79
78	41 32.31	122 31.39	2721.5	980053.10	-12.03	-90.39	0.97	0.00	1.71	1.71	-104.11	78
102	41 33.31	122 31.49	2706.0	980054.58	-13.50	-91.34	0.97	0.01	1.51	1.52	-105.24	102
51	41 31.24	122 31.34	2771.2	980054.34	-4.50	-84.56	0.98	0.01	2.08	2.09	-97.92	51
50	41 30.91	122 31.45	2794.8	980055.23	-0.92	-81.78	0.99	0.03	2.30	2.33	-94.90	50
49	41 30.66	122 31.64	2840.8	980054.49	3.05	-79.38	1.00	0.14	2.43	2.57	-92.28	49
48	41 30.50	122 32.03	2940.7	980052.27	10.46	-75.38	1.03	0.39	2.44	2.83	-88.04	48
52	41 30.35	122 32.47	2932.1	980055.16	12.76	-72.78	1.03	0.14	2.80	2.94	-85.33	52
53	41 30.21	122 32.87	2958.5	980056.24	16.54	-69.91	1.03	0.03	3.01	3.04	-82.36	53
112	41 32.29	122 32.02	2749.5	980056.55	-5.91	-85.23	0.98	0.00	1.86	1.86	-98.81	112
113	41 32.32	122 32.62	2796.4	980058.32	0.23	-80.69	0.99	0.01	2.00	2.01	-94.13	113
114	41 32.29	122 33.20	2843.0	980059.32	5.65	-76.86	1.00	0.01	2.24	2.25	-90.07	114
115	41 32.32	122 33.70	2896.6	980059.48	10.81	-73.53	1.02	0.10	2.38	2.48	-86.53	115
116	41 32.34	122 34.38	2962.7	980058.48	15.99	-70.60	1.03	0.63	2.66	3.29	-82.80	116
117	41 32.33	122 34.98	3008.1	980058.05	19.84	-68.29	1.05	0.40	2.97	3.37	-80.43	117
118	41 32.53	122 35.36	3048.7	980057.65	22.96	-66.56	1.06	0.06	2.91	2.97	-79.11	118
119	41 32.66	122 36.06	3112.2	980055.04	26.11	-65.58	1.07	0.46	3.44	3.90	-77.21	119
120	41 32.81	122 36.44	3216.5	980049.67	30.32	-64.92	1.10	0.26	3.60	3.86	-76.61	120
121	41 33.09	122 32.59	2792.0	980056.49	-3.19	-83.95	0.99	0.01	1.70	1.71	-97.69	121
122	41 33.09	122 33.19	2830.0	980059.11	3.00	-79.06	1.00	0.01	1.88	1.89	-92.62	122
W0194	41 21.17	122 32.35	7127.0	979782.58	148.19	-80.43	1.51	6.62	7.67	14.29	-82.11	W0194
W0195	41 22.97	122 35.54	7624.0	979756.51	166.12	-79.45	1.49	12.65	13.91	26.56	-68.84	W0195

STATION	LATITUDE	LONGITUDE	ELEV(ft)	OBS GRAV	FAA	SBA	CC	TC	TER	TOT	CBA	STATION
W0339	41 20.26	122 24.06	5020.0	979895.19	64.15	-92.61	1.41	4.10	4.24	8.34	-100.14	W0339
W0340	41 27.81	122 17.13	5008.0	979869.31	25.84	-130.51	1.41	1.28	5.82	7.10	-139.28	W0340
L0038	41 28.72	122 29.40	2964.0	980032.24	-4.72	-91.35	1.03	0.26	3.27	3.53	-103.32	L0038
L0049	41 34.48	122 32.70	2704.0	980066.08	-3.94	-81.71	0.97	0.20	1.76	1.96	-95.17	L0049
L0061	41 32.03	122 14.80	3979.0	979948.88	2.40	-118.85	1.26	0.24	3.09	3.33	-131.23	L0061
L0410	41 27.68	122 23.10	3267.0	979990.29	-16.62	-113.59	1.11	0.08	2.28	2.36	-126.80	L0410
L0412	41 28.09	122 26.10	2921.0	980015.98	-24.08	-109.24	1.02	0.04	2.29	2.33	-122.40	L0412
L0413	41 29.24	122 27.30	2856.0	980020.49	-27.40	-110.35	1.01	0.03	2.01	2.04	-123.78	L0413
L0414	41 31.95	122 28.10	2673.0	980035.75	-33.40	-110.10	0.96	0.20	1.47	1.67	-123.86	L0414
L0419	41 33.16	122 27.80	2732.0	980032.43	-32.99	-111.71	0.97	0.00	1.15	1.15	-125.99	L0419
L0422	41 28.28	122 17.80	4462.0	979906.18	10.70	-127.03	1.34	1.67	4.81	6.48	-136.35	L0422
L0424	41 20.93	122 18.80	4243.0	979916.93	11.86	-118.39	1.30	0.40	3.88	4.28	-129.87	L0424
L0720	41 32.42	122 35.20	3013.0	980057.84	19.96	-68.34	1.05	0.59	2.55	3.14	-80.70	L0720
L0721	41 34.06	122 41.10	3440.0	980027.15	26.95	-75.91	1.15	1.79	2.22	4.01	-87.51	L0721
L0764	41 21.15	122 43.90	3783.0	979966.76	18.11	-96.45	1.22	0.45	2.19	2.64	-109.48	L0764
E0678	41 26.09	122 21.60	3489.6	979974.40	-9.21	-113.77	1.16	0.10	3.34	3.44	-125.95	E0678
L0035	41 29.96	122 19.70	3562.0	979972.54	-10.05	-117.08	1.17	0.28	2.80	3.08	-129.64	L0035
L0597	41 31.44	122 17.10	3740.0	979962.82	-5.26	-118.36	1.21	0.44	2.93	3.37	-130.65	L0597
L0711	41 25.15	122 21.40	3725.0	979957.23	-2.85	-115.44	1.21	0.28	3.32	3.60	-127.51	L0711
L0821	41 20.36	122 43.10	3591.0	979971.90	6.39	-101.62	1.18	0.46	3.17	3.63	-113.63	L0821
L0833	41 33.22	122 36.80	3886.0	980009.32	52.30	-65.78	1.24	3.55	1.83	5.38	-76.10	L0833
L0834	41 31.73	122 38.00	5156.0	979926.20	90.79	-70.61	1.43	5.18	4.48	9.66	-76.83	L0834
L0835	41 32.68	122 38.50	5209.0	979923.72	91.86	-71.34	1.43	5.47	4.77	10.24	-77.00	L0835
L0837	41 34.49	122 38.40	5414.0	979910.39	95.10	-75.09	1.45	6.47	6.03	12.50	-78.51	L0837
L0866	41 33.01	122 41.00	3523.0	980022.72	31.90	-73.80	1.16	2.55	2.23	4.78	-84.65	L0866
L0867	41 31.75	122 41.30	3627.0	980016.26	37.10	-72.15	1.19	4.81	2.41	7.22	-80.58	L0867
L0868	41 33.12	122 44.50	3558.0	980010.44	22.74	-84.16	1.17	2.49	1.82	4.31	-95.48	L0868
L0869	41 32.37	122 44.80	3700.0	980000.25	27.03	-84.71	1.20	4.56	1.86	6.42	-93.95	L0869
L1074	41 28.86	122 27.30	2930.0	980021.02	-19.34	-104.81	1.03	0.09	2.06	2.15	-118.15	L1074
L1075	41 28.25	122 26.80	2945.0	980021.49	-16.56	-102.54	1.03	0.05	2.26	2.31	-115.72	L1075
L1076	41 27.53	122 26.20	2943.0	980016.61	-20.54	-106.46	1.03	0.16	2.55	2.71	-119.24	L1076
L1077	41 26.62	122 22.30	3554.0	979970.73	-7.62	-114.37	1.17	0.22	2.59	2.81	-127.19	L1077
E0607	41 27.50	122 25.75	2953.2	980012.90	-23.26	-109.52	1.03	0.16	2.51	2.67	-122.34	E0607
E0608	41 25.38	122 23.20	3420.6	979980.60	-8.43	-110.64	1.14	0.42	2.78	3.20	-123.04	E0608
E0594	41 34.12	122 31.45	2668.0	980059.20	-13.67	-90.20	0.96	0.09	1.28	1.37	-104.25	E0594
E0595	41 31.57	122 31.23	2753.0	980051.50	-9.56	-88.99	0.98	0.14	1.64	1.78	-102.65	E0595
L0041	41 21.22	122 21.30	3915.0	979944.63	8.29	-110.78	1.24	3.50	0.35	3.85	-122.63	L0041
L0060	41 30.04	122 30.90	2828.0	980048.63	-3.10	-85.09	1.00	2.10	0.25	2.35	-98.20	L0060
L0068	41 33.82	122 15.80	3554.0	979980.11	-9.01	-115.76	1.17	2.50	0.15	2.65	-128.75	L0068
L0069	41 34.77	122 17.10	3225.0	980004.06	-17.41	-112.94	1.10	2.30	0.11	2.41	-126.10	L0069
L0425	41 19.91	122 14.50	5679.0	979822.82	54.23	-125.00	1.48	6.60	1.36	7.96	-132.97	L0425
L0428	41 21.83	122 19.30	4320.0	979911.58	12.41	-120.47	1.32	3.30	0.50	3.80	-132.45	L0428
L0712	41 24.45	122 20.70	4037.0	979934.74	5.05	-118.18	1.27	3.70	0.36	4.06	-129.85	L0712
L0713	41 24.51	122 18.40	5153.0	979856.23	31.35	-129.94	1.43	6.20	0.89	7.09	-138.74	L0713
L0715	41 21.81	122 22.60	3801.0	979956.58	8.65	-106.53	1.22	3.10	0.32	3.42	-118.79	L0715

STATION	LATITUDE	LONGITUDE	ELEV(ft)	OBS GRAV	FAA	SBA	CC	TC	TER	TOT	CBA	STATION
L0717	41 22.16	122 26.30	4310.0	979944.41	43.80	-88.74	1.31	6.70	0.56	7.26	-97.25	L0717
L0817	41 26.28	122 32.90	6546.0	979830.32	133.69	-75.11	1.51	13.50	2.35	15.85	-75.24	L0817
L0818	41 26.63	122 31.70	5866.0	979869.65	108.60	-77.01	1.49	12.30	1.64	13.94	-79.02	L0818
L0820	41 22.68	122 34.50	8542.0	979692.54	188.83	-88.05	1.42	31.30	5.35	36.65	-67.28	L0820
L0836	41 30.64	122 38.40	6093.0	979861.03	115.30	-78.05	1.50	16.30	1.87	18.17	-75.84	L0836
L0870	41 31.62	122 43.50	6039.0	979842.06	89.80	-101.71	1.50	25.70	1.92	27.62	-90.05	L0870
L0758	41 29.85	122 33.00	2953.0	980058.24	18.57	-67.69	1.03	3.60	0.31	3.91	-79.27	L0758
SH009	41 28.90	122 14.50	5670.0	979818.55	50.13	-143.08	1.48			8.22	-136.34	SH009
SH016	41 25.80	122 14.78	8593.0	979600.71	111.57	-181.08	1.41			26.52	-155.97	SH016
SH017	41 24.23	122 14.89	9084.0	979562.89	122.23	-187.12	1.35			39.15	-149.32	SH017
SH039	41 31.22	122 18.28	3471.0	979966.51	-12.07	-130.40	1.15			3.45	-128.16	SH039